Università degli Studi di Napoli Federico II

Scuola Politecnica e delle Scienze di Base
Dipartimento di Ingegneria Elettrica e Tecnologie dell'Informazione
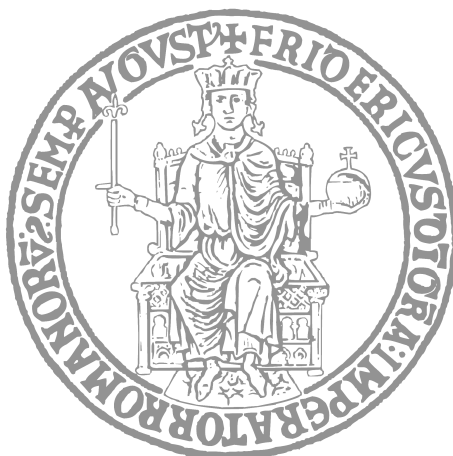
Doctoral Thesis

Analysis and Control of Piecewise-Smooth Systems and Networks

Author:
Marco Coraggio

Tutor:
Prof. Mario di Bernardo

31 January 2020

A Franco, Matilde e Luca,
che sempre sono stati
e sempre saranno con me.

Abstract

Piecewise-smooth systems are common in applications, ranging from dry friction oscillators in mechanics, to power converters in electrical engineering, to neuron cells in biology. While the theory of stability and the control of such dynamical systems have been studied extensively, the conditions that trigger specific collective dynamics when many of such systems are interconnected in a network are not fully understood. The study of emergent behaviour, and in particular synchronization, has applicability in seismology, for what concerns the dynamics of neighbouring faults, in determining frequency consensus in power grids, in operating multi-body mechanical systems, and more. In the first part of this work we provide a series of sufficient conditions to assess global asymptotic state synchronization. Most notably, when the agents' dynamics satisfy the QUAD condition, an ordinary diffusive coupling is sufficient to achieve synchronization, even if the dynamics is discontinuous. In the case of more generic dynamics, we found that a further discontinuous coupling layer can be added to enforce convergence. Moreover, we show that the minimum threshold on the coupling gain associated to the new discontinuous communication protocol depends on the density of the sparsest cut in the graph. This quantity, which we named minimum density, plays a role very similar to that of the algebraic connectivity in the case of networks of smooth systems, in describing the relation between synchronizability and topology. In the second part of the thesis, we focus on specific applications of single PWS systems, and the unique challenges that emerge when particular domains are considered. In particular, we dealt with the design of control strategies to suppress undesired oscillations in the landing gear of an aeroplane and in a robotic set-up in contact with a moving belt. In addition, we expand the tools available to design observers for PWS systems through the use of contraction theory.

Acknowledgements

I wish to deeply thank Mario di Bernardo, who not only greatly contributed to this work with careful technical comments, ingenious insights and thorough revisions, but most importantly, motivated me: he pushed me to achieve the best I could do and fostered my growth as a researcher and as an engineer. I also wish to thank Pietro De Lellis for the valuable collaboration we had on many of the matters in this thesis. His technical skills were as valuable as his spontaneous willingness to help, which is not common. I know how time is a precious resource for a scientist, hence I am deeply grateful to them for the time they chose to allocate reviewing this work. I would also like to thank the people I had the pleasure to collaborate with when preparing the papers cited in this thesis, Daniel A. Burbano-L., Davide Fiore, Franco Garofalo, S. John Hogan, Davide Marchese, and Michele Pugliese. Last but not least, I am profoundly grateful to all the loving people that supported me during these beautiful years.

Contents

1 Introduction

1.1 Nature and applications of piecewise-smooth dynamical systems

A great variety of real-world systems exhibit behaviour that can be better captured by means of *piecewise-smooth* (*PWS*) dynamical systems (also known as *Filippov systems*), i.e., sets of ordinary differential equations (ODEs) with discontinuous right-hand side [56, 43, 34, 87, 29]. Examples are found in multiple domains of Science and Engineering. In Mechanics, rigid bodies that are subject to dry-friction, backlash, or impacts experience instantaneous changes in their acceleration [85] that can be modelled on a macroscopic time-scale using differential equations with discontinuous right-hand sides. This is the case of gears, cam-followers, positioning systems using lead screws, or robotic arms manipulating objects or performing cuts [84, 1]. PWS systems are also used to model dry friction in earthquake models [22, 96]. In Electrical Engineering, diodes and other switching components (e.g. those used in power converters), together with some nonlinear resistors, are all modelled through sets of PWS differential equations [135]. PWS systems are also common in control theory, where bang-bang, switched, or hybrid controllers are often used [136]. Also, in Medicine and Biology, neurons display slow changes in their electrical potential, interrupted by abrupt large variations, named "spikes". In some cases, this twofold fast-slow dynamics is modelled through PWS ODEs [31, 30]. Furthermore, non-smooth models are also used to describe the dynamics of cardiac cells [9, 43] and gene regulatory networks [23]. Other applications include the modelling of transmission control protocols (TCP) in computer science [121, 91], social consensus formation in opinion dynamics [79, 143], and disease spreading in epidemiology [63] and more [41, 78]

In many domains of application, it is possible to think of groups of interconnected PWS systems. These ensembles, where each agent is a dynamical system and one or more graphs are used to describe communication between the systems goes by the name of *complex networks* [141, 130, 140, 6, 124, 98]. Examples include a series of interconnected faults in earthquake engineering, networks of cardiac cells, the driveline in a vehicle, electronic devices in power grids, and so on. Complex networks can exhibit many different types of collective behaviour; examples include various kinds of synchronous behaviour such as complete synchronization, cluster synchronization, and partial-state synchronization

[112, 113, 10, 131]. Understanding the occurrence of synchronization (i.e., the states of all the nodes converging towards a common trajectory) for PWS networks is crucial in many applications. To give only a few examples, synchronization of the generators' frequencies in power grids—where there can be switching components like diodes—translates to an efficient operating condition, and spike synchronization in neurons has a crucial role in activities such as vision and motor coordination [52, 134]. In mechanical engineering, synchronization may be useful when a series of robot manipulators or mobile robots must achieve a cooperative task in the presence of impacts or other discontinuities [26], or to transfer kinetic energy avoiding losses in multi-body systems [65].

1.2 Key research questions

Aspects of the theory concerning PWS dynamical systems, such as stability analysis, bifurcations and control are mostly understood [43, 87]. Nonetheless typically, when applications are concerned, the design of the best control scheme for a specific system and a certain control goal is a unique problem, that requires special ad-hoc considerations, depending on the nature of the system and the limitations of the control environment. One of the emerging phenomena that discontinuity in the vector field can give birth to are undesired oscillations. Moreover, not all of the theory that is complementary to control is completely mature. An example of this is state observation for PWS systems, which does not yet encompass all the design tools available in the case of smooth systems.

Moreover, the analysis and control of collective behaviour emerging in ensembles of discontinuous agents still poses some significant challenges. The reason is that many common mathematical tools and assumptions used to prove convergence in networks of dynamical systems (e.g., Lyapunov approaches or the *master stability function* (*MSF*) technique [113]), in their standard form, require some degree of smoothness in the agents' vector fields. By the same token, hypotheses on the vector fields, like the QUAD hypothesis [39], commonly used when dealing with synchronization problems, although being useful in some cases, cannot always be exploited. Therefore, extensions need to be found to the available analysis and control approaches. Up to now, conditions for the local stability of the synchronization manifold, or for bounded global convergence have been presented. However, criteria cannot be found in the existing literature that guarantee global asymptotic synchronization of a network of PWS systems in the absence of an external control acting on all of the nodes.

Summing up, the big questions that motivate this work are the following.

1. **What conditions guarantee global asymptotic convergence and synchronization in a network of piecewise-smooth systems?**
2. **How to control emergent phenomena such as oscillations in piecewise-smooth systems, and how to estimate the state of these systems?**

We give an answer to the first question in Part I, whereas the second question will find an answer in Part II.

1.3   Contributions of this work

The contributions of this thesis can be grouped in two areas, those concerning synchronization and convergence of complex networks of PWS dynamical systems and those related to the analysis and control of emergent complex behaviour in individual PWS systems.

Concerning the former topic, we present findings also reported in [33] and [32] (the latter currently under peer review), where we advance the current state of the art as follows:

- We give simple conditions for global asymptotic convergence of the class of PWS systems that satisfy to the QUAD condition, which is a regularity assumption on the vector field of the systems, presented in Section 2.2. Specifically, we allow for a large variety of coupling laws, including nonlinear ones and linear diffusion where the inner coupling matrix is not positive definite. In all cases we provide analytical expressions for the critical thresholds of the coupling gains required for synchronization.
- We propose a multiplex control approach where diffusive coupling among the nodes is extended via an additional discontinuous coupling layer whose topology might differ from that of the diffusive one. We show that this communication protocol can be used to guarantee global asymptotic synchronization for a much wider class of PWS systems. Furthermore, we give analytical estimates of the critical values of both the coupling gains associated to the diffusive coupling and the discontinuous coupling, sufficient to enforce convergence.
- We shed light on the dependence of the analytically computed threshold values of the gains upon the properties of the vector fields of the nodes, and more importantly the structural properties of the network control layers. More specifically, we show that their value is dependent on a quantity we name *minimum density of a graph*, which is tightly related to its *sparsest cut*, a widely used concept in graph theory. In simple terms, this relation shows that the presence of a severe bottleneck in the communication graph undermines the chance of achieving synchronization.

Regarding the analysis and control of PWS systems, we describe here the following results, which we reported in [19, 102, 57].

- *Shimmy* is a dangerous phenomenon that occurs when aircraft's nose landing gears oscillate in a rapid and uncontrollable fashion. We propose the use of two nonlinear control approaches (zero average control and model reference adaptive control based on minimal control synthesis) as simple yet effective strategies to suppress undesired oscillations, even in the presence of uncertainties and partial state measurements.
- The *Painlevé paradox* is a phenomenon that causes instability in mechanical systems subjects to unilateral constraints. We investigate the manifestation of this phenomenon in a two-links robot in contact with a moving belt, through a bifurcation study. Then, we use the results of this analysis to inform the design of

two control strategies (a PID and a hybrid force/motion control) to keep the robot sliding on the belt and avoid the onset of undesired lift-off.

• We show that by using a recent extension of contraction theory to nondifferentiable vector fields, it is possible to design observers for a large class of nonlinear bimodal piecewise-smooth systems, resulting in increased flexibility in the design process.

1.4 Thesis structure and outline

This thesis is organised into two parts. Part I is concerned with synchronization and convergence in networks of piecewise-smooth systems, while Part II deals with the analysis and control of single PWS systems.

In Part I, Chapter 2 presents the problem statement, while Chapter 3 illustrates the state of the art on synchronization in piecewise-smooth complex networks. After that, Chapter 4 introduces some mathematical preliminaries. Then, in Chapter 5, the theoretical convergence results are given, together with numerical simulations to validate the findings; part of the proofs are postponed to Chapter 6. Finally, Chapter 7 reviews the content of Part I.

In Part II, Chapter 8 details the control design of strategies to suppress undesired oscillations in landing gears. After that, in Chapter 9, we discuss the occurrence of the Painlevé paradox in a two-link planar robot, presenting a structural stability analysis and validating two control schemes to stabilize vibrations occurring in the system. Then, in Chapter 10, we show how recent results on the contraction of PWS systems can be used to synthesise observers for Filippov systems.

Conclusions are drawn in Chapter 11. After that, three appendices follow. Appendix A reviews various regularity conditions that are applied to the PWS vector fields in order to study synchronization. Appendix B presents some analytical expressions concerning the concept of minimum density (a topological connectivity measure for graphs introduced in Section 4.3). Finally, Appendix C contains an early extension of the techniques presented in Part I to enforce asymptotic synchronization in networks of non-identical systems.

1.5 Notation

In this section, we expound the general notation we will use throughout the thesis. We encourage the reader to to feel free to skip this section and to return to it in case they encounter some symbols whose meaning is not clear.

Notation concerning sets is as follows, Q being a generic set:

• $\mathbb{N}$ is the set of natural numbers including zero, and $\mathbb{N}_{>0}$ is the set of natural numbers excluding zero,
• $\mathbb{Z}$ is the set of integers,
• $\mathbb{R}$ is the set of real numbers, $\mathbb{R}_{\geq 0}$ excludes negative numbers, and $\mathbb{R}_{>0}$ excludes non-positive numbers,
• $\mathbb{C}$ is the set of complex numbers,
• $\varnothing$ is the empty set,

- if Q is finite, $|Q|$ is its cardinality.
- If $Q \subset \mathbb{R}$, the notation $Q \leq 0$ means that $\forall s \in Q$, $s \leq 0$ (analogously for $\geq$, $=$, etc.),
- $\mathcal{F}[f]$ is the *Filippov set-valued function* associated to the function f (see Section 4.2,
- $C^p(Q_1, Q_2)$, with $p \in \mathbb{N}$, is the set of functions from Q_1 to Q_2 that are continuous and continuously differentiable p times.

Notation concerning operators is as follows:

- the dot diacritic $\dot{}$ represents total derivative with respect to time,
- $\frac{\partial a}{\partial b}$ is the partial derivative of a with respect to b,
- ∇ is the gradient and is a row vector,
- $\otimes$ denotes the Kronecker product,
- $\times$ is the Cartesian product,
- $^\top$ is the transpose,
- $\approx$ means "approximately equal",
- $\triangleq$ means "is defined as",
- when considering a one-sided limit, $a \searrow b$ means that a approaches b from the right (or from above), and $a \nearrow b$ means approaching from the left (or below).
- the right vertical bar with a subscript means "evaluated with the subscript as a constraint". For example, "$f(x, y)|_{x=1}$" is the same as "$f(1, y)$".

Notation concerning scalars is as follows, $s \in \mathbb{R}$ being a generic scalar:

- $|s|$ is the absolute value of s (although if $s \in \mathbb{C}$, then $|s|$ is the module of s),
- $\text{sign}(s)$ is its sign (with $\text{sign}(0) = 0$),
- $\lfloor s \rfloor$ is the largest integer r such that $r \leq s$,
- $\lceil s \rceil$ is the smallest integer r such that $r \geq s$.
- e is Euler's number.

Notation concerning vectors is as follows, $\mathbf{v} \in \mathbb{R}^n$ being a generic vector:

- normally we will denote a vector by a lower-case bold letter; if not specified differently, we assume it is a column vector,
- v_i is the i-th element of $\mathbf{v}$; in the presence of a set $\{\mathbf{v}_1, \ldots, \mathbf{v}_N\}$ of N vectors, $v_{k,i}$ is the i-th element of the k-th vector in the set,
- $|\mathbf{v}| = [|v_1| \ |v_2| \ \cdots \ |v_n|]^\top$,
- $\text{sign}(\mathbf{v}) = [\text{sign}(v_1) \ \text{sign}(v_2) \ \cdots \ \text{sign}(v_n)]^\top$,
- $\mathbf{i}_i \in \mathbb{N}^n$ is the column vector having 1 in position i and 0 elsewhere,
- $\text{diag}(\mathbf{v}) \in \mathbb{R}^{n \times n}$ is the diagonal matrix having the elements of vector $\mathbf{v}$ on its diagonal,
- $\|\mathbf{v}\|_p$ is the p-norm of $\mathbf{v}$, with p being equal to 2 if it is omitted; we recall that $\|\mathbf{v}\|_1 \triangleq \sum_{i=1}^n |v_i|$.

Notation concerning matrices is as follows, $\mathbf{A} \in \mathbb{R}^{n \times m}$ being a generic matrix:

- normally we will denote a matrix by an upper-case bold letter,
- A_{ij} is the (i, j)-th element of $\mathbf{A}$.

- $\text{sym}(\mathbf{A}) = \left(\mathbf{A} + \mathbf{A}^\mathsf{T}\right)/2$ is the symmetric part of $\mathbf{A}$,
- $\lambda_i(\mathbf{A})$ is its i-th eigenvalue, with the eigenvalues being sorted in an increasing fashion if they are all real ($\lambda_{\min}(\mathbf{A}) \triangleq \lambda_1(\mathbf{A})$ is the smallest one),
- $\|\mathbf{A}\|_p$ is the p-norm of $\mathbf{A}$, with p being equal to 2 if it is omitted; we recall that $\|\mathbf{A}\|_\infty \triangleq \max\limits_{i=1,\ldots,n} \left(\sum_{j=1}^{n} |A_{ij}|\right)$,
- $\mu_p(\mathbf{A})$ is the matrix measure of $\mathbf{A}$ induced by the p-norm (see Section 4.1), with p being equal to 2 if it is omitted,
- The notation $\mathbf{A} > 0$ indicates that $\mathbf{A}$ is positive definite (analogously for semi- and negative definiteness),
- $\mathbf{I}_n$ is the $n \times n$ identity matrix; we will omit the subscript when not necessary,
- $\mathbf{0}_{n \times m}$ is the $n \times m$ null matrix, and $\mathbf{0}_n$ is the null column vector with n entries; we will omit the subscripts when not necessary.

Part I

Synchronization and convergence in networks of piecewise-smooth systems

2 Background

In this chapter we state the goal of Part II and expound, for the sake of clarity, a small number of formal preliminaries that are preparatory to the following Chapters.

2.1 Problem description

We consider $N \in \mathbb{N}_{>0}$ identical piecewise-smooth systems (also called *agents* or *nodes*, in the context of complex networks), whose internal dynamics are given by

$$\begin{cases} \dot{\mathbf{x}}_i(t) = \mathbf{f}(\mathbf{x}_i; t), \\ \mathbf{x}_i(0) = \mathbf{x}_{0,i}, \end{cases} \quad i = 1, \dots, N,$$

where

- $\mathbf{x}_i \in \mathbb{R}^n$ is the *state* vector of the i-th agent,
- $t \in \mathbb{R}_{\geq 0}$ is time,
- the vector field $\mathbf{f} : \mathbb{R}^n \times \mathbb{R}_{\geq 0} \to \mathbb{R}^n$ can be discontinuous with respect to $\mathbf{x}_i$ and might possibly exhibit sliding mode dynamics [43].
- $\mathbf{x}_{0,i} \in \mathbb{R}^n$ is the *initial condition* of the i-th agent; below we will omit to explicitly state the initial conditions.

The lack of continuity in $\mathbf{f}$ (or at least one of its derivatives) with respect to $\mathbf{x}_i$ is what characterises *piecewise-smooth systems*, in contrast to *smooth systems*, that feature a continuous $\mathbf{f}$. Moreover, systems where $\mathbf{f}$ is discontinuous are also called *Filippov systems* [56], whereas systems where $\mathbf{f}$ is continuous but its Jacobian is not are called *piecewise-smooth continuous (PWSC) systems*. For the sake of completeness, we mention that further notable cases are those of *hybrid systems*, where there exist some maps that make $\mathbf{x}(t)$ discontinuous, and *time-switching systems*, where $\mathbf{f}$ is discontinuous with respect to time t.

When two or more PWS systems are coupled in a network, they form a *complex piecewise-smooth network*, whose dynamics is given by

$$\dot{\mathbf{x}}_i(t) = \mathbf{f}(\mathbf{x}_i; t) + \mathbf{u}_i(\mathbf{x}_1, \dots, \mathbf{x}_N; t), \quad i = 1, \dots, N, \tag{2.1}$$

where the functions $\mathbf{u}_i$ represent the effects of coupling. The information of which agents communicate with whom is encompassed in one or more graphs [17]. Assume that

communication between agents in (2.1) takes place over $K \in \mathbb{N}_{>0}$ *coupling layers* (a graphical representation with $K = 2$ layers is portrayed in Figure 5.1). Each layer is represented by a *graph* $\mathcal{G}_k = (\mathcal{V}, \mathcal{E}_k)$, $k = 1, \ldots, K$, where $\mathcal{V}$ is the set of *vertices* (or *nodes*) and $\mathcal{E}_k$ is the set of *edges* (or *links*) in the graph. Each vertex in $\mathcal{V}$ corresponds to one of the agents, and an edge exists in $\mathcal{E}_k$ between two agents if and only if some communication exists between the two over the k-th layer. Important properties of the edges are to be *undirected* or *directed*, *unweighted* or *weighted*, and constant or not constant [17]; Unless specified differently, we always assume that edges are undirected, unweighted and constant. A fairly generic expression for the terms $\mathbf{u}_i$ is

$$\mathbf{u}_i(\mathbf{x}_1, \ldots, \mathbf{x}_N; t) = \sum_{k=1}^{K} \left(c_k \sum_{j=1}^{N} L_{ij}^k \mathbf{g}_k(\mathbf{x}_i, \mathbf{x}_j; t) \right), \quad i = 1, \ldots, N,$$

where

- $c_k \in \mathbb{R}$ is the *coupling strength* or *coupling gain* in the k-th layer,
- L_{ij}^k is the (i, j)-th element of the *Laplacian matrix* $\mathbf{L}_k \in \mathbb{R}^{N \times N}$ [6] of graph $\mathcal{G}_k$,
- $\mathbf{g}_k : \mathbb{R}^n \times \mathbb{R}^n \times \mathbb{R}_{\geq 0} \to \mathbb{R}^n$ are *coupling functions*.

Of course, different and much more complicated structures exist for the coupling terms $\mathbf{u}_i$, e.g., accounting for stochastic variations, inter-layer communication, time-delays and more. However, that will not be relevant to the theory described in this thesis.

Our goal is to find sufficient conditions on the internal vector field $\mathbf{f}$ and on the coupling laws $\mathbf{u}_i$, $i = 1, \ldots, N$, so that all the agents converge asymptotically towards a common evolution, regardless of the initial conditions. In more formal terms, we seek conditions such that *global asymptotic synchronization* is achieved.

> **Definition 2.1** (Asymptotic synchronization). *Network* (2.1) *achieves asymptotic synchronization in* $\Omega \subseteq \mathbb{R}^{nN}$ *if, for all initial conditions in* Ω,
>
> $$\lim_{t \to +\infty} \left\| \mathbf{x}_i(t) - \mathbf{x}_j(t) \right\| = 0, \quad \forall i, j = 1, \ldots, N.$$

In some papers, asymptotic synchronization is called *complete synchronization*.

> **Definition 2.2** (Bounded synchronization). *Network* (2.1) *achieves bounded synchronization in* $\Omega \subseteq \mathbb{R}^{nN}$ *if there exists* $\varepsilon \in \mathbb{R}_{>0}$ *such that, for all initial conditions in* Ω,
>
> $$\lim_{t \to +\infty} \left\| \mathbf{x}_i(t) - \mathbf{x}_j(t) \right\| \leq \varepsilon, \quad \forall i, j = 1, \ldots, N.$$

As far as Definitions 2.1 and 2.2 are concerned, we say that synchronization is *global* if $\Omega = \mathbb{R}^{nN}$. Differently, if Ω is a neighbourhood of the synchronous trajectory(-ies) in the state space of the network, then we say that synchronization is *local*. Note that in general the meaning of *convergence* is more general than that of synchronization, as it indicates that the trajectories of the agents *converge* towards some specific attractor, which needs not be a synchronous solution. Also, convergence is a term often used in control

theory when describing the fact that some error goes to zero, typically in stabilization, regulation and tracking problems. In this work, when we talk about convergence we refer in particular to synchronization, and to the fact that synchronization errors[1] become zero.

2.2 Regularity properties of vector fields

Here we give two mathematical assumptions that are used to characterise the internal dynamics of the agents. These, along with the other assumptions mentioned in this Section are preparatory to compare the different results present in the literature and described in Chapter 3. A condition that is widely used in the field of complex networks is the so-called *QUAD* (quadratic) condition [39, 38].

Definition 2.3 (QUADness). *A function* $\mathbf{f} : \mathbb{R}^n \times \mathbb{R}_{\geq 0} \to \mathbb{R}^n$ *is* QUAD($\mathbf{P}, \mathbf{Q}$) *if, there exist* $\mathbf{P}, \mathbf{Q} \in \mathbb{R}^{n \times n}$ *such that, for all* $\boldsymbol{\xi}_1, \boldsymbol{\xi}_2 \in \mathbb{R}^n$, $t \in \mathbb{R}_{\geq 0}$, *it holds that*

$$(\boldsymbol{\xi}_1 - \boldsymbol{\xi}_2)^\top \mathbf{P} [\mathbf{f}(\boldsymbol{\xi}_1; t) - \mathbf{f}(\boldsymbol{\xi}_2; t)] \leq (\boldsymbol{\xi}_1 - \boldsymbol{\xi}_2)^\top \mathbf{Q} (\boldsymbol{\xi}_1 - \boldsymbol{\xi}_2).$$

To have a broader picture of how QUADness compare to other regularity conditions typically used in the literature, like Lipschitz continuity, we refer the reader to Appendix A. In particular, it is useful to consider that if some not too strict bounds hold on the Jacobian of a function, then it is QUAD, as illustrated in Proposition A.4. There is the possibility for QUAD functions to display a limited kind of jump discontinuities, but the vast majority is left out. Therefore, to use a framework flexible enough to fit a large variety of piecewise-smooth functions, we introduce the following definition, where σ stands for "signum".

Definition 2.4 (σ-QUADness). *A function* $\mathbf{f} : \mathbb{R}^n \times \mathbb{R} \to \mathbb{R}^n$ *is* σ-QUAD($\mathbf{P}, \mathbf{Q}, \mathbf{M}$) *if, there exists* $\mathbf{P}, \mathbf{Q}, \mathbf{M} \in \mathbb{R}^{n \times n}$ *such that, for all* $\boldsymbol{\xi}_1, \boldsymbol{\xi}_2 \in \mathbb{R}^n$, $t \in \mathbb{R}$, *it holds that*

$$(\boldsymbol{\xi}_1 - \boldsymbol{\xi}_2)^\top \mathbf{P} [\mathbf{f}(\boldsymbol{\xi}_1; t) - \mathbf{f}(\boldsymbol{\xi}_2; t)] \leq (\boldsymbol{\xi}_1 - \boldsymbol{\xi}_2)^\top \mathbf{Q} (\boldsymbol{\xi}_1 - \boldsymbol{\xi}_2)$$
$$+ (\boldsymbol{\xi}_1 - \boldsymbol{\xi}_2)^\top \mathbf{M} \mathrm{sign} (\boldsymbol{\xi}_1 - \boldsymbol{\xi}_2).$$

Note that, in the case that $\mathbf{M} = \mathbf{0}_{n \times n}$, Definition 2.4 becomes equivalent to Definition 2.3. However, differently from the QUAD condition, the σ-QUAD property includes cases where $\mathbf{f}$ has any number of arbitrary finite jumps discontinuities. As an illustrative example of what the σ-QUAD property implies, consider the functions $f_1, f_2 : \mathbb{R} \to \mathbb{R}$, given by $f_1(\xi) = \xi - \mathrm{sign}(\xi)$ and $f_2(\xi) = \xi + \mathrm{sign}(\xi)$, represented in Figure 2.1. f_1 is σ-QUAD with $\mathbf{P} = 1$, $\mathbf{Q} = 1$, $\mathbf{M} = 0$, and thus is also QUAD; differently, f_2 is σ-QUAD with $\mathbf{P} = 1$, $\mathbf{Q} = 1$, $\mathbf{M} = 2$, and can be proved not to be QUAD.

Definition 2.4 can be seen as a slight extension of a similar condition in [146] (see Assumption A.7), where $\mathbf{M}$ is constrained to be a diagonal matrix. A related concept is the *QUAD-affine* condition defined in [38] (see Definition A.6), where an affine term is

---

[1]One such error is the difference between the state of a node and the average of the others.
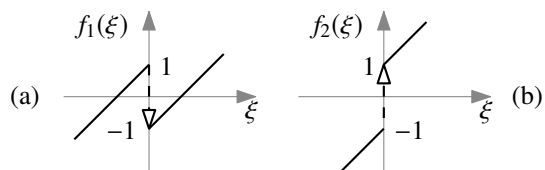
Figure 2.1: (a) f_1 is QUAD and σ-QUAD; (b) f_2 is not QUAD, but is σ-QUAD.

added to the right-hand side of (2.3) to account for the presence of finite jumps. Moreover, in [90], the notion of a non-autonomous vector field being *semi-QUAD* is introduced (see Definition A.5). Specifically, a vector field, say $\mathbf{f}(\boldsymbol{\xi};t)$, is said to be semi-QUAD if its difference with respect to another vector field $\mathbf{g}(\boldsymbol{\xi};t)$, known to be QUAD, tends asymptotically to zero as time increases. Finally, another related concept is the *growth condition* for a vector field, defined in [92] (see Definition A.8).

3   State of the art on piecewise-smooth networks

Since the 2010's the Control Theory and Applied Mathematics scientific communities have shown greater and greater interest towards the study of synchronization in networks of PWS systems. In order to start tackling this difficult problem, the various scientists that have taken on this research area have focused on a small series of simplifying assumptions or selected scenarios. In particular, some focused their study on *local* synchronization, for which an extension of the master stability function approach was developed. Others have investigated *bounded* convergence, in which case common Lyapunov functions are to be used. On the other hand, fairly generic criteria to assess *global asymptotic* synchronization have not been published; the exception being when using centralised switching controllers on all the nodes. However, such a control system is rather difficult to implement, because there is some information that an entity needs to pass to all the nodes, and in a way frustrates the beneficial effect of communication, that is what is typically used to enforce convergence in networks. As we show in Chapter 5, also in the case of PWS network a suitable coupling action is sufficient to enforce synchronization and no costly centralised controllers are needed. It is worth to point out that, at the current state, enough evidence suggests that some kind of discontinuous action is required to prove global asymptotic convergence in PWS networks; we chose to incorporate such action in the coupling terms between the agents.

In Tables 3.1 and 3.2 we summarise the results contained in the main works we cite in this chapter and the examples contained therein. Note that Table 3.1 also contain a time-line that can be used to trace how knowledge in this field has progressed through the years.

Table 3.1: Primary references in chronological order. The regularity conditions on the dynamics are explained in Section 2.2 and Appendix A. The meaning of the acronyms are as follows. A: adaptive, ASS: assumption A.7, ASY: asymptotic, BOU: bounded, CHA: chaotic, Conv.: convergence, DEL: delayed, DFO: dry-friction oscillators, DIS: discontinuous, GC: growth condition, GLO: global, HOM: homogeneous (identical systems), HET: heterogeneous (non-identical systems), LIN: linear, LOC: local, NN: neural network, N-LIN: nonlinear, OTH: other, PWA: piecewise-affine, QUAD-A: QUAD affine, Ref.: reference SEQ: semi-QUAD, SYN: synchronization, TRA: tracking.

Year	Ref.	Agents	Dynamics	Coupling	Problem	Conv.	Region
2011	[93]	2HOM	NN, GC	LIN	SYN, TRA	BOU	GLO
2012	[90]	HOM	SEQ, OTH	LIN	SYN	ASY	GLO
2012	[92]	HET	GC	LIN+DEL	SYN	BOU	GLO
2013	[145]	2HOM	NN, GC	A LIN+DIS	SYN, TRA	ASY	GLO
2013	[146]	HET	CHA+ASS	LIN+DIS	TRA	ASY	GLO
2015	[38]	HET	QUAD-A	N-LIN	SYN	BOU	GLO
2016	[31, 30]	HOM	PWA	LIN	SYN	ASY	LOC
2017	[103, 104]	HOM	DFO	LIN	SYN	ASY	LOC
2018	[33]	HOM	QUAD	LIN	SYN	ASY	GLO
2019	[32]	HOM	σ-QUAD	LIN+DIS	SYN	ASY	GLO

3.1 Local stability of the synchronization manifold

One of the first papers where sufficient conditions for the occurrence of local synchronization between coupled PWS systems are discussed is [37], where the case of two interconnected discontinuous systems is studied, although the specific case of coupled friction oscillators was discussed earlier in [64, 65, 66].

More recently, alternative criteria for local stability of the synchronization manifold were presented in [31, 30, 80], where synchronization of limit cycles in bimodal piecewise-affine models of neurons was investigated via the extension of the *master stability function* technique to a class of PWS systems [113]. Most commonly, the systems considered are in the form[1]

$$\dot{\mathbf{x}}_i = \mathbf{f}(\mathbf{x}_i) - c \sum_{j=1}^{N} L_{ij}\mathbf{\Gamma}(\mathbf{x}_j - \mathbf{x}_i), \quad i = 1, \ldots, N, \quad \mathbf{f}(\mathbf{x}_i) = \begin{cases} \mathbf{A}^+\mathbf{x}_i + \mathbf{b}^+, & \sigma(\mathbf{x}_i) > 0, \\ \mathbf{A}^-\mathbf{x}_i + \mathbf{b}^-, & \sigma(\mathbf{x}_i) < 0. \end{cases}$$

Initially, a known extension of Floquet theory is used to assess the stability of limit cycles of PWS systems. This theory requires the explicit form of the solution which can be obtained by "gluing" together the smooth parts of the solutions. In turn, it is possible to write these smooth parts in a closed form, because the dynamics is piecewise-affine. Next, the master stability function method is applied in order to get a series of differential

---

[1]$\mathbf{A}^+, \mathbf{A}^- \in \mathbb{R}^{n \times n}, \mathbf{b}^+, \mathbf{b}^- \in \mathbb{R}^n, \sigma : \mathbb{R}^n \to \mathbb{R}$.

Table 3.2: Examples used in primary references, listed in chronological order.

Ref.	Examples
[93]	delayed neural network
[90]	abstract systems, variant of Lorenz
[92]	Chua circuit, abstract systems
[145]	delayed neural network
[146]	Sprott, Chua, and Chen circuits
[38]	Ikeda system, Chua circuit, chaotic relay, Kuramoto network
[31]	McKean, absolute, and homoclinic neuron models
[30]	Piecewise-linear and Heaviside Wilson–Cowan neural mass models
[103, 104]	dry-friction oscillators
[33]	relay, Sprott circuit, hierarchical oscillator, energy harvester
[32]	chaotic relay, hierarchical oscillator

equations describing the piecewise-smooth dynamics of small perturbations in the network. At that point, the theory on *monodromy matrices* (comprising *saltation matrices* [43]) is used to account for the discontinuity in the dynamics. In conclusion, N n-dimensional monodromy matrices $\mathbf{\Phi}_i$ are obtained, with the expression of each containing at least two saltation matrices, say $\mathbf{S}_k$ with different k's. If $\mathbf{\Phi}_i$, $i = 2, \ldots, N$, have stable eigenvalues (module less than 1), then it is possible to conclude that the synchronous limit cycle is locally stable. Note that if the agent dynamics is piecewise-smooth continuous (i.e., $\mathbf{f}$ is continuous, but not differentiable), then all $\mathbf{S}_k = \mathbf{I}$, and the outlined method is easily applicable, as the eigenvalues of the $\mathbf{\Phi}_i$'s are computable without great effort. Unfortunately tough, as remarked in [80], the computation of the $\mathbf{\Phi}_i$'s becomes practically infeasible if the internal node dynamics is not piecewise-smooth continuous. The reason is that the ordering by which the agents cross their switching manifold becomes crucial in computing the $\mathbf{S}_k$'s (which appear in the $\mathbf{\Phi}_i$'s). However, it is not easy to determine such ordering a priori.

Local synchronizability was also the main focus of the work on coupled dry-friction oscillators presented in [103, 104], in the form[2]

$$\dot{\mathbf{x}}_i = \left[\begin{matrix} x_{i,2} \\ -x_{i,1} + f_{df}(x_{i,2}) + \frac{U}{x_{i,1(t=0)}} \cos(\omega t) \end{matrix} \right] - c \sum_{j=1}^{N} L_{ij} \begin{bmatrix} 0 & 0 \\ 1 & 0 \end{bmatrix} (\mathbf{x}_j - \mathbf{x}_i), \quad i = 1, \ldots, N.$$

$$f_{df}(\xi) = \left(\mu_k + (\mu_s - \mu_k) e^{-k|v - \xi|} \right) \text{sign}(v - \xi).$$

The method used is that of the *two-probe-oscillator*. In a simple two-agents network, a series of numerical simulation are run, with initial conditions close to the synchronization manifold. All values of the coupling strength c such that synchronization is achieved

---

[2] $\mathbf{x}_i \in \mathbb{R}^2$, $U, \omega, \mu_s, \mu_k, k \in \mathbb{R}_{>0}$, $v \in \mathbb{R}$.

are recorded, $C \in \mathbb{R}$ being the set of such values. Then, $A \triangleq \{\alpha \in \mathbb{R} \mid \alpha = c\lambda_2(\mathbf{L}) = 2c, c \in C\}$ is defined. After that, for different and larger networks (thus with a different Laplacian $\mathbf{L}$) to display local stability of the synchronization manifold, it is just required that $c\lambda_i(\mathbf{L}) \in A$, for $i = 2, \ldots, N$. The justification of this method lies in the master stability function approach. However, in their study, the authors approximate the sign function present in f_{dc} with the arc tangent function, thus making f_{dc} continuous and the systems smooth, and without taking any special precaution to properly extend the theory of master stability function to the case of discontinuous agents. Therefore, it cannot be taken for granted that the results still hold when the agents really are discontinuous.

3.2 Global bounded convergence

Sufficient conditions for global bounded convergence to a synchronous solution are given in [38], where the case of complex network systems with non-identical, possibly PWS, nodes is investigated in the case of either linear or nonlinear, possibly discontinuous, diffusive coupling functions. The network model used is

$$\dot{\mathbf{x}}_i = \mathbf{f}_i(\mathbf{x}_i; t) - c \sum_{j=1}^{N} L_{ij} \mathbf{g}_{ij}(\mathbf{x}_j - \mathbf{x}_i; t), \quad i = 1, \ldots, N.$$

Exploiting the notion of Filippov solutions and common Lyapunov functions, it is shown that, in the case of linear coupling (i.e., $\mathbf{g}_{ij}(\mathbf{x}_j - \mathbf{x}_i; t) = \mathbf{\Gamma}(\mathbf{x}_j - \mathbf{x}_i)$), if the agents are *QUAD affine* (see Definition A.6 and Section 2.2), then there exists a minimum coupling gain $c^* > 0$ such that bounded synchronization is achieved and the synchronization error converges to a ball of finite radius that depends on the coupling gain; a conservative estimate of this critical gain is also provided. In addition, if the agents' dynamics satisfy to the QUAD affine condition with $\mathbf{Q} < 0$—which can be read as an intrinsic non divergence of the internal dynamics of the nodes—then a further different bound on the synchronization error is given. Such a bound is independent of the coupling gain, which in this case can be simply non negative in order to have bounded synchronization. While a large variety of settings are considered, conditions are only obtained for bounded rather than asymptotic convergence to the synchronization manifold.

Also, the bounded synchronization of two neural networks (each one being modelled as a single dynamical system) is investigated in [93], considering a linear feedback term acting on only one of the two agents. The proofs employ dissipativity and the Halanay inequality. Moreover, importantly, the authors claim that the two systems cannot synchronize asymptotically even if they are identical, because a discontinuous action is missing either in the coupling or as a control term. This is in accordance with our findings, that in general asymptotic synchronization is not obtainable without some added discontinuous action. In [92], results on bounded synchronization are expanded to the framework of heterogeneous PWS networks controlled with a linear feedback control on all the nodes, in the presence of linear coupling, and with the possibility of having delays in the communication protocol. The proofs exploit the Filippov notion of solution, Lyapunov functions and the generalised Halanay inequality. The article also contains

conditions for the boundedness of the solutions of the network. Finally, the case of networks with switching topology or time-switching dynamics is considered, giving conditions for bounded synchronization.

3.3 Global asymptotic synchronization

A step towards the achievement of asymptotic synchronization in a pair of coupled PWS systems can be found in [145], where the authors exploited a state-feedback control plus a discontinuous action to make one chaotic neural network track the state of another identical one. Both the cases of constant gains and adaptive gains are studied. When the gains are constant, an estimate of the convergence time is given, which is instead missing for the case of adaptive gains, with the benefit however of saving energy. The two scenarios are investigated with both increasing activation functions and with more general ones. The theoretical framework used in the proof is that of Filippov solutions and Lyapunov functions.

In [146], the authors expand the analysis to a network of generic size of chaotic non-identical PWS nodes, using again a state-feedback control with a discontinuous action, applied to all the nodes:[3]

$$\dot{\mathbf{x}}_i = \mathbf{f}_i(\mathbf{x}_i) + \mathbf{u}_{c,i}(\mathbf{x}_i - \mathbf{s}) - c \sum_{j=1}^{N} L_{ij} \boldsymbol{\Gamma}(\mathbf{x}_j - \mathbf{x}_i), \quad i = 1, \ldots, N.$$

$$\mathbf{u}_{c,i}(\mathbf{x}_i - \mathbf{s}) = -k_{1,i}(\mathbf{x}_i - \mathbf{s}) - k_{2,i}\text{sign}(\mathbf{x}_i - \mathbf{s}).$$

The first main assumption in this paper is that a certain regularity condition on the internal dynamics $\mathbf{f}$ holds (see Assumption A.7); such condition can be seen as a slightly simpler (but earlier) version of σ-QUADness (in Definition 2.4). Secondly, it is mandatory to be able to exert a centralised control action on all the systems and that the uncontrolled coupled network (i.e., with $\mathbf{u}_{c,i} = \mathbf{0}$) and the reference trajectory $\mathbf{s}$ are chaotic. This last fact is used to infer that the trajectories of the agents in the controlled network are bounded. Then, it is showed that if the control gains $k_{1,i}, k_{2,i}$ are large enough, the trajectories $\mathbf{x}_i(t)$ of the agents will be steered towards the desired one, $\mathbf{s}(t)$, in a finite time. A similar approach was employed in [144] to synchronize time-delayed neural networks with discontinuous activation functions. While this is an interesting take on the problem at hand, the main drawback of these findings resides in the need of a centralised controller, able to communicate to all the nodes. Furthermore, injecting a control input on all the agents from the same controller trivialises the effect and structure of the network, de facto degrading the coupling to not much more than a (possibly helpful) disturbance. In reality, the beneficial effect of the discontinuous term in $\mathbf{u}_{c,i}$ can be more efficiently and meaningfully implemented in the coupling, as we show in Section 5.4 and Chapter 6.

So far, the only attempt we found in the literature at finding conditions to ensure global asymptotic convergence in a network of generic PWS nodes without a centralised

---

[3]$\mathbf{u}_{c,i}$ is the control input, $\mathbf{s}$ is the target synchronous trajectory; $k_{1,i}, k_{2,i} \in \mathbb{R}$, $i = 1, \ldots, N$.

control action is presented in [90], using the network model[4]

$$\dot{\mathbf{x}}_i = \mathbf{f}(\mathbf{x}_i) - c \sum_{j=1}^{N} L_{ij} \mathbf{\Gamma}(\mathbf{x}_j - \mathbf{x}_i), \quad i = 1, \dots, N.$$

Therein, a set of sufficient conditions for convergence are given, under the assumption that the internal agent dynamics verifies a specific, and rather convoluted, regularity condition, that is [90, (6)]. This condition is satisfied if (i) the agents' dynamics are continuous (thus making the systems smooth) and QUAD or (ii) the agents are PWS but with semi-QUAD dynamics (i.e., QUAD asymptotically; see Section 2.2 and Appendix A). However, if these are not the cases, as remarked by the authors, it is particularly difficult to verify formally whether condition [90, (6)] holds for generic discontinuous dynamics. Therefore, the results are not easily applicable to fairly generic PWS systems.

3.4   Our contribution to the literature

Recently in [33], exploiting Filippov theory and common Lyapunov functions, we gave sufficient conditions for global asymptotic synchronization in the case that the agents are PWS but also satisfy the QUAD assumption, employing only a diffusive (not necessarily linear) coupling protocol. In that work, we also accounted for the troublesome case where the inner coupling matrix in a linear diffusive coupling law is not positive definite. We also presented extensive numerical simulations to preliminarily validate a framework that we only later proved formally in [32], which at the time of the writing of this thesis is ongoing the revision process in order to be accepted for publication. Namely, since many PWS functions do not fulfil the QUAD assumption (See for example [38, 146, 92]), we showed that a discontinuous coupling protocol can be added to the typical diffusive layer to enforce synchronization. With respect to the previous literature, one notable benefit of this theory is that the discontinuous coupling law, which could be seen as a control action, is decentralised. The results we mentioned in this Section, contained in both [33, 32], are expounded in detail in Chapter 5.

3.5   Other related papers

For the sake of completeness, we briefly mention a handful of other related works. Given that these papers do not deal directly with synchronization of PWS systems, we do not discuss them extensively, but we report them here, as they may be of inspiration in the design of new analytical tools for synchronization problems and contain relevant insights about ensembles of discontinuous systems.

In [116], convergence of piecewise-linear maps was investigated in a semi-analytical fashion; consensus for PWS systems was studied in [142]; tracking for piecewise-affine systems was investigated in [138]; in [152], passivity of two interlaced PWS systems was defined and analysed; finally, in [123] synchronization of hybrid systems was studied.

---

[4]The coupling graph can be directed and weighted.

4 Mathematical preliminaries and definitions

Here we give a series of definitions and properties that are instrumental to the theoretical results and the proofs in Chapters 5 and 6.

4.1 Matrices

Definition 4.1 (Diagonalisability). *A matrix* $\mathbf{A} \in \mathbb{R}^{n \times n}$ *is* diagonalisable *if there exists an invertible matrix* $\mathbf{T} \in \mathbb{R}^{n \times n}$ *such that* $\mathbf{A} = \mathbf{T}^{-1} \boldsymbol{\Delta}_\mathbf{A} \mathbf{T}$, *where* $\boldsymbol{\Delta}_\mathbf{A}$ *is a diagonal matrix containing the eigenvalues of* $\mathbf{A}$.

Note that if $\mathbf{A}$ is diagonalisable and symmetric, then $\mathbf{T}^\mathsf{T} = \mathbf{T}^{-1}$.

Definition 4.2 (Simultaneous diagonalisability). *Two matrices* $\mathbf{A}, \mathbf{B} \in \mathbb{R}^{n \times n}$ *are* simultaneously diagonalisable *if there exists an invertible matrix* $\mathbf{T} \in \mathbb{R}^{n \times n}$ *such that* $\mathbf{A}$ *and* $\mathbf{B}$ *are both diagonalisable using* $\mathbf{T}$.

We highlight that $\mathbf{A}$ and $\mathbf{B}$ are simultaneously diagonalisable if they are diagonalisable and they *commute*, i.e., $\mathbf{AB} = \mathbf{BA}$.

The *matrix measure* [42, 36, 139, 148] of $\mathbf{A} \in \mathbb{R}^{n \times n}$ induced by the given norm $\|\cdot\|$ is the function $\mu : \mathbb{R}^{n \times n} \to \mathbb{R}$ defined as

$$\mu(\mathbf{A}) \triangleq \lim_{h \searrow 0} \frac{(\|\mathbf{I} + h\mathbf{A}\| - 1)}{h}.$$

The most commonly used matrix measures are those associated to the ℓ^1-norm, the Euclidean norm and the uniform norm, given by the following expressions

$$\mu_1(\mathbf{A}) = \max_{j=1,\ldots,n} \left(A_{jj} + \sum_{i=1,\ldots,n, i \neq j} |A_{ij}| \right),$$

$$\mu_2(\mathbf{A}) = \lambda_{\max} \left(\frac{\mathbf{A} + \mathbf{A}^\mathsf{T}}{2} \right),$$

$$\mu_\infty(\mathbf{A}) = \max_{i=1,\ldots,n} \left(A_{ii} + \sum_{j=1,\ldots,n, j \neq i} |A_{ij}| \right).$$

Definition 4.3. *The function* $\mu_\infty^- : \mathbb{R}^{n \times n} \to \mathbb{R}$*, for all* $\mathbf{A} \in \mathbb{R}^{n \times n}$*, is given by*

$$\mu_\infty^-(\mathbf{A}) \triangleq \min_{i=1,\ldots,n} \left(A_{ii} - \sum_{j=1, j \neq i}^{n} |A_{ij}| \right). \tag{4.1}$$

The symbol μ_∞^- was chosen to highlight the algebraic similarity between this quantity and the matrix measure μ_∞ induced by the infinite-norm. We also note that $\mu_\infty^-(\mathbf{I}_m \otimes \mathbf{A}) = \mu_\infty^-(\mathbf{A})$, for any $m \in \mathbb{N}_{>0}$.

Definition 4.4 (Z- and M-matrices). *Let* $\mathbf{A} \in \mathbb{R}^{n \times n}$ *be a matrix.*

- $\mathbf{A}$ *is a* Z*-matrix if* $A_{ij} \leq 0$ *for* $i \neq j$.
- $\mathbf{A}$ *is an* M*-matrix if it is a Z-matrix and it is possible to write* $\mathbf{A} = \alpha\mathbf{I} - \mathbf{B}$, *where* $B_{ij} \geq 0$ *for all* i, j, *and* $\alpha \geq |\lambda_i(\mathbf{B})|$ *for all* i.

4.2   Filippov vector fields and solutions

In Definitions 4.5–4.8, we briefly recall the main concepts introduced by Filippov to characterise solutions of PWS systems [56, 34]. In this subsection we use the following notation:

- $\overline{\text{co}}(\cdot)$ is a function that gives the convex closure of a set,
- $\mathcal{P}(\mathbb{R}^n)$ is the power set of $\mathbb{R}^n$,
- $\hat{N} \subset \mathcal{P}(\mathbb{R}^n)$ is the set of all sets in $\mathbb{R}^n$ that have null Lebesgue measure,
- $\boldsymbol{\xi}$ is a vector in $\mathbb{R}^n$,
- $\mathcal{A}_\delta^{\text{o}}(\boldsymbol{\xi})$ is an open ball centred in $\boldsymbol{\xi}$ with radius $\delta > 0$,
- $t \in \mathbb{R}_{\geq 0}$ represents time,
- $\mathbf{f} : \mathbb{R}^n \times \mathbb{R}_{\geq 0} \to \mathbb{R}^n$ is a not necessarily continuous vector field,
- $V : \mathbb{R}^n \to \mathbb{R}$ is a locally Lipschitz function, which is differentiable everywhere but in a zero-measure set $\mathcal{N}_V$.

Definition 4.5 (Filippov set-valued function). *The* Filippov set-valued function *associated to* $\mathbf{f}$ *is* $\mathcal{F}[\mathbf{f}] : \mathbb{R}^n \times \mathbb{R}_{\geq 0} \to \mathcal{P}(\mathbb{R}^n)$*, and is given by*

$$\mathcal{F}[\mathbf{f}](\boldsymbol{\xi}; t) \triangleq \bigcap_{\delta : \delta > 0} \bigcap_{N \in \hat{N}} \overline{\text{co}} \left\{ \mathbf{f}(\mathcal{A}_\delta^{\text{o}}(\boldsymbol{\xi}) \setminus N; t) \right\}.$$

Note that if $\mathbf{f}$ is continuous, then $\mathcal{F}[\mathbf{f}] = \mathbf{f}$.

Definition 4.6 (Filippov solution). *A* Filippov solution *is an absolutely continuous curve $\xi(t) : \mathbb{R}_{\geq 0} \to \mathbb{R}^n$ satisfying, for almost all $t \in \mathbb{R}_{\geq 0}$, the differential inclusion $\dot{\xi} \in \mathcal{F}[\mathbf{f}](\xi; t)$.*

Definition 4.7 (Generalised gradient). *The* generalised gradient *of V is $\partial V : \mathbb{R}^n \to \mathcal{P}(\mathbb{R}^n)$, and is given by*

$$\partial V(\xi) \triangleq \overline{\text{co}} \left\{ \left(\lim_{k \to +\infty} \frac{\partial}{\partial \xi} V(\xi_k) \right) \in \mathbb{R}^n \,\middle|\, (\xi_k)_{k \in \mathbb{N}_{>0}} : \xi_k \to \xi, \, (\xi_k) \cap \mathcal{N}_V = \varnothing \right\}.$$

Definition 4.8 (Set-valued Lie derivative). *The* set-valued Lie derivative $\mathcal{L}_{\mathcal{F}[\mathbf{f}]}(V) : \mathbb{R}^n \to \mathcal{P}(\mathbb{R})$ *of V with respect to $\mathcal{F}[\mathbf{f}]$ is given by*

$$\mathcal{L}_{\mathcal{F}[\mathbf{f}]} V(\xi) \triangleq \left\{ \ell \in \mathbb{R} \mid \exists \mathbf{a} \in \mathcal{F}[\mathbf{f}](\xi; t) : \forall \mathbf{v} \in \partial V(\xi), \, \mathbf{v}^{\mathsf{T}} \mathbf{a} = \ell \right\}.$$

When we give regularity conditions like QUADness or similar on a vector field $\mathbf{f}$ that must hold in a set or globally, for all points ξ where $\mathbf{f}(\xi)$ is discontinuous, we assume the implicit reformulation that the condition must hold for all $\phi \in \mathcal{F}[\mathbf{f}(\xi)]$.

4.3 Minimum density

Consider a graph $\mathcal{G} = (\mathcal{V}, \mathcal{E})$, with $|\mathcal{V}| = N$. We introduce the following:

- a *cut* C is a partition of $\mathcal{V}$ in two subsets $\mathcal{V}_1, \mathcal{V}_2$, with $N_1 = |\mathcal{V}_1|$, and $N_2 = |\mathcal{V}_2|$,
- $\hat{C}_{\mathcal{G}}$ is the set of all possible cuts on $\mathcal{G}$,
- b is the number of edges that connect a vertex in $\mathcal{V}_1$ with one in $\mathcal{V}_2$, for a given cut,
- the *density* of a cut is the ratio $b/N_1 N_2$.

Definition 4.9 (Minimum density). *Given a graph $\mathcal{G}$, its* minimum density *is*

$$\delta_{\mathcal{G}} \triangleq \frac{N}{2} \min_{C \in \hat{C}_{\mathcal{G}}} \frac{b}{N_1 N_2}. \tag{4.2}$$

The minimum density can be seen as a measure of connectivity in a graph; in simple terms, the smaller the quantity, the more pronounced is the worst bottleneck in the graph. The optimal cut $\arg\min_{C \in \hat{C}_{\mathcal{G}}} \frac{b}{N_1 N_2}$ associated to $\delta_{\mathcal{G}}$ is known as the *sparsest cut* [105], and is here denoted by C_{sc} (despite the name, it could be not unique). The problem of finding such a cut is called the *sparsest cut problem*, which is a special kind of graph partitioning problem [18]. The sparsest cut problem is NP-hard and is normally solved algorithmically, as discussed below and in [7, 8].

The minimum density of a graph can be computed using the free software METIS [77], which can solve the generic *graph partitioning* problem, i.e., given a graph, it finds
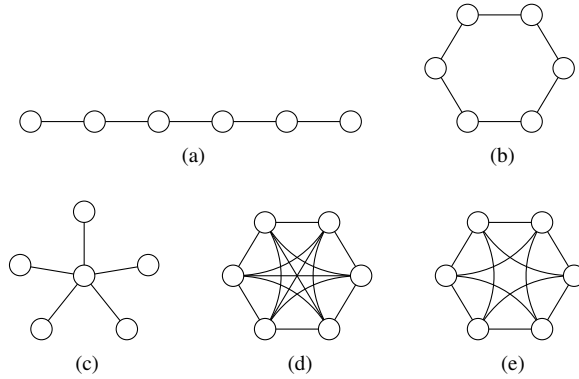
Figure 4.1: Example of well-known graphs, assuming they all contain $N = 6$ vertices. (a) is a path graph, (b) is a ring graph, (c) is a star graph, (d) is a complete graph, and (e) is a l-nearest neighbours graph with $l = 2$.

a partition of the vertices in two subsets of roughly equal size, such that the fewest edges exist among them, so that the resulting cut is

$$C_{\mathrm{gp}} = \arg \min_{C \in \hat{C}_{\mathcal{G}}} b, \quad N_1 \approx N_2.$$

For our purpose, we need to solve the sparsest cut problem and find

$$C_{\mathrm{sc}} = \arg \min_{C \in \hat{C}_{\mathcal{G}}} \frac{b}{N_1 N_2}.$$

This can be done by running METIS iteratively, constraining the sizes N_1 and N_2 of the two subsets resulting from the cut. Specifically, we run METIS $\lfloor N/2 \rfloor$ times, so that

$$
\begin{aligned}
\text{in run 1,} \quad & (N_1, N_2) = (1, N - 1), \\
\text{in run 2,} \quad & (N_1, N_2) = (2, N - 2), \\
& \cdots \\
\text{in run } \lfloor N/2 \rfloor, \quad & (N_1, N_2) = (\lfloor N/2 \rfloor, \lceil N/2 \rceil).
\end{aligned}
$$

At each run, we compute the value of the quantity $\frac{N}{2} \frac{b}{N_1 N_2}$ and eventually choose the smallest one as the minimum density of the graph, according to Definition 4.9. For the sake of completeness, we mention the Arora-Rao-Vazirani (ARV) algorithm [8, 7] as an alternative way of computing the sparsest cut.

Note that the minimum density of some selected graph topologies, represented in Figure 4.1, can be computed analytically by relatively simple algebra (see Appendix B). We summarise these findings in Table 4.1.

Table 4.1: Values of the minimum density $\delta_{\mathcal{G}}$, the algebraic connectivity $\lambda_2(\mathbf{L})$, and the number of edges $N_{\mathcal{E}}$ for selected topologies. "l-near.-n." stands for "l-nearest-neighbours"; $c_1 \triangleq \cos(\pi/N)$, $c_2 \triangleq \cos(2\pi/N)$. The values of the algebraic connectivity are taken from [55].

Topology	$\delta_{\mathcal{G}}$		$\lambda_2(\mathbf{L})$	$N_{\mathcal{E}}$
Complete	$N/2$		N	$\frac{N^2-N}{2}$
Star	$N/(2(N-1))$		1	$N-1$
Path	$\begin{cases} 2/N, & \text{if } N \text{ is even} \\ 2N/(N^2-1), & \text{if } N \text{ is odd} \end{cases}$		$2(1-c_1)$	$N-1$
Ring	$\begin{cases} 4/N, & \text{if } N \text{ is even} \\ 4N/(N^2-1), & \text{if } N \text{ is odd} \end{cases}$		$2(1-c_2)$	N
l-near.-n.	$\begin{cases} \frac{4\sum_{k=0}^{l-1}(l-k)}{N}, & \text{if } N \text{ is even} \\ \frac{4N\sum_{k=0}^{l-1}(l-k)}{N^2-1}, & \text{if } N \text{ is odd} \end{cases}$		$-$	Nl

5 Convergence results

Firstly, in Theorems 5.2 and 5.3 in Section 5.2, we provide sufficient conditions to assess global synchronization of piecewise-smooth networks, applicable to the case that the internal agent dynamics $\mathbf{f}$ is a QUAD function (see Definition 2.3). A certain number of discontinuous functions fall into this category, e.g. Coulomb friction, some relay functions, continuous but not differentiable functions like the characteristics of nonlinear resistors and more. The difference between the two theorems is that the latter allows for more generality in the coupling law, but contains more restricting conditions on the dynamics. Secondly, for the case that the internal dynamics $\mathbf{f}$ fails to satisfy the QUAD condition, but is σ-QUAD (see Definition 2.4), in Theorems 5.5 and 5.6 in Section 5.4, we give further sufficient conditions that can be used to ensure synchronization. Again, the difference between these two theorems is that the latter allows for the coupling laws to have positive semi-definite inner coupling matrices (rather than positive definite), but requires the inner dynamics of the agents to satisfy stricter assumptions. The theoretical results are illustrated by examples.

5.1 Coupling laws

We will consider two specific kinds of coupling, that is, two expressions for the functions $\mathbf{u}_i$ in (2.1).

1. The first one is a nonlinear single-layer coupling, associated to an undirected unweighted graph $\mathcal{G} = (\mathcal{V}, \mathcal{E})$. The dynamics of the network is given by

$$\dot{\mathbf{x}}_i(t) = \mathbf{f}(\mathbf{x}_i; t) - \sum_{j=1}^{N} L_{ij} \mathbf{g}(\mathbf{x}_i, \mathbf{x}_j; t), \quad i = 1, \ldots, N, \tag{5.1}$$

   where L_{ij} is the (i, j)-th element of the symmetric *Laplacian matrix* $\mathbf{L} \in \mathbb{R}^{N \times N}$ [6] of $\mathcal{G}$, and $\mathbf{g} : \mathbb{R}^n \times \mathbb{R}^n \times \mathbb{R}_{\geq 0} \to \mathbb{R}^n$ is a *coupling function*. In conjunction with (5.1) we will also make the following assumption.

   Assumption 5.1. *The coupling function* $\mathbf{g} : \mathbb{R}^n \times \mathbb{R}^n \times \mathbb{R}_{\geq 0} \to \mathbb{R}^n$ *in* (5.1) *is such that, for all* $\boldsymbol{\xi}_1, \boldsymbol{\xi}_2 \in \mathbb{R}^n$, $t \in \mathbb{R}_{\geq 0}$, *it holds that*

   (i) $\mathbf{g}(\boldsymbol{\xi}_1, \boldsymbol{\xi}_1; t) = \mathbf{0}$,
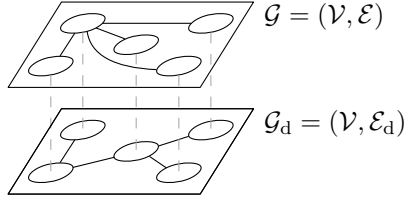
Figure 5.1: A multilayer network with $N = 5$ vertices and two coupling layers.

(ii) **g** *is antisymmetric with respect to its first two arguments, i.e.,* $\mathbf{g}(\boldsymbol{\xi}_1, \boldsymbol{\xi}_2; t) = -\mathbf{g}(\boldsymbol{\xi}_2, \boldsymbol{\xi}_1; t)$*, and*

(iii) there exist $c \in \mathbb{R}_{\geq 0}$*,* $\mathbf{P}, \mathbf{G} \in \mathbb{R}^{n \times n}$*, with* $\mathbf{G} = \mathbf{G}^{\mathsf{T}}$ *such that*

$$(\boldsymbol{\xi}_2 - \boldsymbol{\xi}_1)^{\mathsf{T}} \mathbf{P}\mathbf{g}(\boldsymbol{\xi}_1, \boldsymbol{\xi}_2; t) \geq (\boldsymbol{\xi}_1 - \boldsymbol{\xi}_2)^{\mathsf{T}} c\mathbf{G} (\boldsymbol{\xi}_1 - \boldsymbol{\xi}_2).$$

Clearly, a special case that satisfies Assumption 5.1 is that of linear diffusive coupling, where

$$\mathbf{g}(\mathbf{x}_i, \mathbf{x}_j; t) = c\boldsymbol{\Gamma}(\mathbf{x}_j - \mathbf{x}_i), \tag{5.2}$$

with $\boldsymbol{\Gamma} \in \mathbb{R}^{n \times n}$, $\mathbf{P} = \mathbf{I}$ and $\mathbf{G} = \text{sym}(\boldsymbol{\Gamma})$.

2. The second communication protocol is a multiplex one [20], combination of a linear diffusive layer and a discontinuous layer. The two layers are associated to two graphs, say $\mathcal{G} = (\mathcal{V}, \mathcal{E})$ and $\mathcal{G}_{\mathrm{d}} = (\mathcal{V}, \mathcal{E}_{\mathrm{d}})$, both being undirected and unweighted (see Figure 5.1). Thus, the dynamics of the network is

$$\dot{\mathbf{x}}_i(t) = \mathbf{f}(\mathbf{x}_i; t) - c \sum_{j=1}^{N} L_{ij}\boldsymbol{\Gamma}(\mathbf{x}_j - \mathbf{x}_i) - c_{\mathrm{d}} \sum_{j=1}^{N} L_{ij}^{\mathrm{d}}\boldsymbol{\Gamma}_{\mathrm{d}}\text{sign}(\mathbf{x}_j - \mathbf{x}_i), \quad i = 1, \ldots, N, \tag{5.3}$$

where $L_{ij}, L_{ij}^{\mathrm{d}}$ are the (i, j)-th elements of the symmetric *Laplacian matrices* $\mathbf{L}, \mathbf{L}_{\mathrm{d}} \in \mathbb{R}^{N \times N}$ associated to $\mathcal{G}, \mathcal{G}_{\mathrm{d}}$, respectively; $\boldsymbol{\Gamma}, \boldsymbol{\Gamma}_{\mathrm{d}} \in \mathbb{R}^{n \times n}$ are the *inner coupling matrices* describing how the coupling actions affect the dynamics of the nodes.

The coupling protocol in (5.1) with Assumption 5.1 can be used to describe a large variety of communication laws occurring in natural phenomena and Engineering. Indeed, diffusive couplings can be used to describes the effect of springs, resistors, and chemical diffusion processes. However, as illustrated in [38, 93, 92], a purely diffusive protocol does not suffice to achieve asymptotic synchronization in all cases. Therefore, in (5.3) we consider an additional discontinuous coupling layer, which could be seen as a control term, that is able to enforce synchronization in a much wider range of scenarios.

Finally, with reference to (2.1), we list here a series of symbols that will be employed in this and the next chapter.

- $\tilde{\mathbf{x}} \triangleq \sum_{i=1}^{N} \mathbf{x}_i / N \in \mathbb{R}^n$ is the *average of the states* of the nodes,

- $\mathbf{e}_i \triangleq \mathbf{x}_i - \tilde{\mathbf{x}} \in \mathbb{R}^n$, $i = 1, \ldots, N$ are the *synchronization errors*, and we denote the h-th element of $\mathbf{e}_i$ by $e_{i,h}$,
- $\bar{\mathbf{x}} \triangleq [\mathbf{x}_1^\mathsf{T} \ \cdots \ \mathbf{x}_N^\mathsf{T}]^\mathsf{T} \in \mathbb{R}^{nN}$ is the *stack of the states* of the nodes,
- $\bar{\mathbf{e}} \triangleq [\mathbf{e}_1^\mathsf{T} \ \cdots \ \mathbf{e}_N^\mathsf{T}]^\mathsf{T} \in \mathbb{R}^{nN}$ is the *stack of the errors*,
- $\mathbf{e}^h \triangleq [e_{1,h} \ \cdots \ e_{N,h}]^\mathsf{T} \in \mathbb{R}^N$ groups the h-th components of all the errors $\mathbf{e}_i$, $i = 1, \ldots, N$,
- $e_{\text{tot}} \triangleq \frac{1}{N} \sum_{i=1}^N \|\mathbf{e}_i\|_2$ is the *total synchronization error*.

5.2 Convergence of QUAD piecewise-smooth systems

Here, we present results appeared in [33] that extend [38, 117, 39] and give conditions for the global complete synchronization of PWS agents whose dynamics is QUAD, accounting for the generic nonlinear diffusive coupling function (5.1). Namely, considering Assumption 5.1, Theorem 5.2 can be used when $\mathbf{G} > 0$ (resp. $\mathbf{\Gamma} > 0$ if (5.2) holds), whereas Theorem 5.3 is to be employed when no assumptions on the definiteness of $\mathbf{G}$ (resp. $\mathbf{\Gamma}$) can be made.

Theorem 5.2. *Network* (5.1) *achieves global asymptotic synchronization if*

(a) *there exist* $c \in \mathbb{R}$, $\mathbf{P}, \mathbf{Q}, \mathbf{G} \in \mathbb{R}^{n \times n}$ *such that:*

- **f** *is QUAD(***P**, **Q***), with* **P** > 0,
- **g** *verifies Assumption 5.1 with c,* **P** *and* **G***, and with* **G** > 0,

(b) $\mathcal{G}$ *is a connected graph, and*

(c) $c > c^*$, *with*

$$c^* \triangleq \frac{\|\mathbf{Q}\|_2}{\lambda_2(\mathbf{L})\lambda_{\min}(\mathbf{G})}. \tag{5.4}$$

Proof. First, Note that

$$\dot{\mathbf{e}}_i \triangleq \boldsymbol{\phi}_i(\mathbf{x}_1, \ldots, \mathbf{x}_N; t) = \dot{\mathbf{x}}_i - \dot{\tilde{\mathbf{x}}} =$$

$$\mathbf{f}(\mathbf{x}_i; t) - \sum_{j=1}^N L_{ij}\mathbf{g}(\mathbf{x}_i, \mathbf{x}_j; t) - \frac{1}{N}\sum_{i=1}^N \left(\mathbf{f}(\mathbf{x}_i; t) - \sum_{j=1}^N L_{ij}\mathbf{g}(\mathbf{x}_i, \mathbf{x}_j; t) \right). \tag{5.5}$$

Then, consider the candidate set-valued Lyapunov function $V(\mathbf{e}) \triangleq \frac{1}{2}\sum_{i=1}^N \mathbf{e}_i^\mathsf{T}\mathbf{P}\mathbf{e}_i$. The fact that **f** is not continuous causes V to not be differentiable. However, employing Filippov formalism we can state that $\dot{V}(\mathbf{x}) \in \mathcal{V}$, where[1]

$$\mathcal{V} \triangleq \mathcal{L}_{\mathcal{F}[\boldsymbol{\phi}_i]}\left(\frac{1}{2}\sum_{i=1}^N \mathbf{e}_i^\mathsf{T}\mathbf{P}\mathbf{e}_i \right) = \frac{1}{2}\sum_{i=1}^N \mathcal{L}_{\mathcal{F}[\boldsymbol{\phi}_i]}\left(\mathbf{e}_i^\mathsf{T}\mathbf{P}\mathbf{e}_i \right).$$

Hence, if $\forall v \in \mathcal{V}, v < 0$, then $\lim_{t \to +\infty} V = 0$ and the network achieves synchronization globally. Note that, in (5.5), the facts that **L** is symmetric and **g** is antisymmetric (with

---

[1]The *sum rule* [34] is used to apply the set-valued Lie derivative operator separately to each addend in V.

respect to $\mathbf{x}_i$ and $\mathbf{x}_j$) imply that $\sum_{i=1}^{N} \sum_{j=1}^{N} \left(L_{ij} \mathbf{g}(\mathbf{x}_i, \mathbf{x}_j; t) \right) = 0$. Then, from Definition 4.8 and (5.5) we can write

$$\mathcal{V} = \sum_{i=1}^{N} \mathbf{e}_i^\mathsf{T} \mathbf{P} \left(\mathcal{F}[\mathbf{f}(\mathbf{x}_i; t)] - \mathcal{F} \left[\sum_{i=1}^{N} \frac{\mathbf{f}(\mathbf{x}_i; t)}{N} \right] \right) - \sum_{i=1}^{N} \sum_{j=1}^{N} L_{ij} \mathbf{e}_i^\mathsf{T} \mathbf{P} \mathcal{F} \left[\mathbf{g}(\mathbf{x}_i, \mathbf{x}_j; t) \right].$$

As $\sum_{i=1}^{N} \mathbf{e}_i = 0$, we have $\sum_{i=1}^{N} \mathbf{e}_i^\mathsf{T} \mathbf{P} \mathcal{F} \left[\sum_{i=1}^{N} \mathbf{f}(\mathbf{x}_i; t)/N \right] = 0$ and $\sum_{i=1}^{N} \mathbf{e}_i^\mathsf{T} \mathbf{P} \mathcal{F}[\mathbf{f}(\tilde{\mathbf{x}}; t)] = 0$. Thus, we can rewrite

$$\mathcal{V} = \sum_{i=1}^{N} \mathbf{e}_i^\mathsf{T} \mathbf{P} \left(\mathcal{F}[\mathbf{f}(\mathbf{x}_i; t)] - \mathcal{F} [\mathbf{f}(\tilde{\mathbf{x}}; t)] \right) - \sum_{i=1}^{N} \sum_{j=1}^{N} L_{ij} \mathbf{e}_i^\mathsf{T} \mathbf{P} \mathcal{F} \left[\mathbf{g}(\mathbf{x}_i, \mathbf{x}_j; t) \right].$$

Focusing on a generic element $v \in \mathcal{V}$ and exploiting the hypotheses on $\mathbf{f}$ and $\mathbf{g}$, we get[2]

$$v \leq \sum_{i=1}^{N} \mathbf{e}_i^\mathsf{T} \mathbf{Q} \mathbf{e}_i - c \sum_{i=1}^{N} \sum_{j=1}^{N} L_{ij} \mathbf{e}_i^\mathsf{T} \mathbf{G} \mathbf{e}_j.$$

This inequality can be rewritten in terms of the stack of the errors $\bar{\mathbf{e}}$ as

$$v \leq \bar{\mathbf{e}}^\mathsf{T} \left(\mathbf{I}_N \otimes \mathbf{Q} - c\mathbf{L} \otimes \mathbf{G} \right) \bar{\mathbf{e}} \leq \bar{\mathbf{e}}^\mathsf{T} \left(\|\mathbf{Q}\| \mathbf{I}_N \otimes \mathbf{I}_n - c\mathbf{L} \otimes \mathbf{G} \right) \bar{\mathbf{e}}$$
$$= \|\bar{\mathbf{e}}\|^2 \|\mathbf{Q}\| - \bar{\mathbf{e}}^\mathsf{T} \left(c\mathbf{L} \otimes \mathbf{G} \right) \bar{\mathbf{e}}. \tag{5.6}$$

Since $\sum_{i=1}^{N} \mathbf{e}_i = \mathbf{0}$, that is

$$\forall h = 1, \ldots, n, \quad \sum_{i=0}^{N-1} \bar{e}_{(i-1)n+h} = 0,$$

we can apply Corollary 13.4.2 in [68] and get[3]

$$v \leq \|\bar{\mathbf{e}}\|^2 \left(\|\mathbf{Q}\| - c\lambda_2(\mathbf{L})\lambda_{\min}(\mathbf{G}) \right).$$

Therefore, if $c > c^*$, $\dot{V}(\bar{\mathbf{e}}) < -\alpha \|\bar{\mathbf{e}}\|^2$ with $\alpha > 0$, and the network achieves synchronization globally. □

Theorem 5.3. *Network* (5.1) *achieves global asymptotic synchronization if*

(a) *there exist* $c \in \mathbb{R}$, $\mathbf{P}, \mathbf{Q}, \mathbf{Q}^-, \mathbf{Q}', \mathbf{G} \in \mathbb{R}^{n \times n}$ *such that:*
  - $\mathbf{f}$ *is QUAD(*$\mathbf{P}$, $\mathbf{Q}$*), with* $\mathbf{P} > 0$,
  - $\mathbf{g}$ *verifies Assumption* 5.1 *with* c, $\mathbf{P}$ *and* $\mathbf{G}$, *with* $\mathbf{G} \geq 0$,

---

[2]Recalling that $\mathbf{L} = \mathbf{L}^\mathsf{T}$, and using (i), (ii), (iii) in Assumption 5.1, we get

$$-\sum_{i=1}^{N} \sum_{j=1}^{N} L_{ij} \mathbf{e}_i^\mathsf{T} \mathbf{P} \mathbf{g}(\mathbf{x}_i, \mathbf{x}_j; t) = -\sum_{i=1}^{N} \sum_{j>i}^{N} L_{ij} (\mathbf{x}_i - \mathbf{x}_j)^\mathsf{T} \mathbf{P} \mathbf{g}(\mathbf{x}_i, \mathbf{x}_j; t)$$
$$\leq -c \sum_{i=1}^{N} \sum_{j>i}^{N} L_{ij} (\mathbf{x}_i - \mathbf{x}_j)^\mathsf{T} \mathbf{G} (\mathbf{x}_j - \mathbf{x}_i) = -c \sum_{i=1}^{N} \sum_{j=1}^{N} L_{ij} \mathbf{e}_i^\mathsf{T} \mathbf{G} \mathbf{e}_j.$$

[3]If (5.2) holds, with $\mathbf{\Gamma}$ being an M-matrix (see Definition 4.4), then a diagonal matrix $\mathbf{M}$ exists (that is $\mathbf{P}$) such that $\mathrm{sym}(\mathbf{M}\mathbf{\Gamma}) = \mathrm{sym}(\mathbf{G}) = \mathbf{G} > 0$ [40].

- $\mathbf{Q} = \mathbf{Q}^- + \mathbf{Q}'$, $\mathbf{Q}^- < 0$, $\mathbf{Q}' = (\mathbf{Q}')^{\mathsf{T}}$,
- $\mathbf{Q}'$ and $\mathbf{G}$ are simultaneously diagonalisable,
- $\lambda_h(\mathbf{G}) > 0$ if $\lambda_h(\mathbf{Q}') > 0$, with $h = 1, \ldots, n$.

(b) $\mathcal{G}$ is a connected graph, and

(c) $c \geq c^*$, with

$$c^* \triangleq \begin{cases} \dfrac{1}{\lambda_2(\mathbf{L})} \max\limits_{h=1,\ldots,n} \dfrac{\lambda_h(\mathbf{Q}')}{\lambda_h(\mathbf{G})}, & \text{if } \exists h \in \{1,\ldots,n\} : \lambda_h(\mathbf{Q}') > 0, \\ 0, & \text{otherwise.} \end{cases} \tag{5.7}$$

Proof. The first part of the proof is identical to that of Theorem 5.2 until (5.6), then we can write

$$\begin{aligned} v &\leq \bar{\mathbf{e}}^{\mathsf{T}} \left(\mathbf{I}_N \otimes \mathbf{Q} - c\mathbf{L} \otimes \mathbf{G} \right) \bar{\mathbf{e}} \\ &= \bar{\mathbf{e}}^{\mathsf{T}} \left(\mathbf{I}_N \otimes \mathbf{Q}^- \right) \bar{\mathbf{e}} + \bar{\mathbf{e}}^{\mathsf{T}} \left(\mathbf{I}_N \otimes \mathbf{Q}' \right) \bar{\mathbf{e}} - c v_{\mathbf{G}}, \end{aligned} \tag{5.8}$$

where $v_{\mathbf{G}} \triangleq \bar{\mathbf{e}}^{\mathsf{T}} (\mathbf{L} \otimes \mathbf{G}) \bar{\mathbf{e}}$. Now, given that $\mathbf{Q}'$ and $\mathbf{G}$ are simultaneously diagonalisable, there exists an invertible matrix $\mathbf{T} \in \mathbb{R}^{n \times n}$ such that $\mathbf{Q}' = \mathbf{T}^{-1} \boldsymbol{\Delta}_{\mathbf{Q}'} \mathbf{T}$ and $\mathbf{G} = \mathbf{T}^{-1} \boldsymbol{\Delta}_{\mathbf{G}} \mathbf{T}$, where $\boldsymbol{\Delta}_{\mathbf{Q}'}$ and $\boldsymbol{\Delta}_{\mathbf{G}}$ are diagonal matrices containing the real eigenvalues of $\mathbf{Q}'$ and $\mathbf{G}$, respectively (note that $\mathbf{Q}' = (\mathbf{Q}')^{\mathsf{T}}$ and $\mathbf{G} = \mathbf{G}^{\mathsf{T}}$ imply that $\mathbf{T}^{\mathsf{T}} = \mathbf{T}^{-1}$). Let us also define the transformed synchronization errors $\mathbf{y}_i \triangleq \mathbf{T}\mathbf{e}_i \in \mathbb{R}^n$ and their stack $\bar{\mathbf{y}} \triangleq (\mathbf{I}_N \otimes \mathbf{T}) \bar{\mathbf{e}} \in \mathbb{R}^{nN}$. Therefore, we can rewrite $v_{\mathbf{G}}$ as

$$\begin{aligned} v_{\mathbf{G}} &= \bar{\mathbf{e}}^{\mathsf{T}} (\mathbf{L} \otimes \mathbf{G}) \bar{\mathbf{e}} = \bar{\mathbf{e}}^{\mathsf{T}} \left[\mathbf{L} \otimes \left(\mathbf{T}^{-1} \boldsymbol{\Delta}_{\mathbf{G}} \mathbf{T} \right) \right] \bar{\mathbf{e}} \\ &= \bar{\mathbf{e}}^{\mathsf{T}} \left[\left(\mathbf{L} \otimes \mathbf{T}^{-1} \right) (\mathbf{I}_N \otimes (\boldsymbol{\Delta}_{\mathbf{G}} \mathbf{T})) \right] \bar{\mathbf{e}} \\ &= \bar{\mathbf{e}}^{\mathsf{T}} \left[\left(\mathbf{L} \otimes \mathbf{T}^{-1} \right) (\mathbf{I}_N \otimes \boldsymbol{\Delta}_{\mathbf{G}}) (\mathbf{I}_N \otimes \mathbf{T}) \right] \bar{\mathbf{e}} \\ &= \bar{\mathbf{e}}^{\mathsf{T}} \left[\left(\mathbf{I}_N \otimes \mathbf{T}^{\mathsf{T}} \right) \left(\mathbf{I}_N \otimes \mathbf{T}^{\mathsf{T}} \right)^{-1} \left(\mathbf{L} \otimes \mathbf{T}^{-1} \right) (\mathbf{I}_N \otimes \boldsymbol{\Delta}_{\mathbf{G}}) \right] \bar{\mathbf{y}} \\ &= \bar{\mathbf{y}}^{\mathsf{T}} \left[\left(\mathbf{I}_N \otimes \mathbf{T}^{\mathsf{T}} \right)^{-1} \left(\mathbf{L} \otimes \mathbf{T}^{-1} \right) (\mathbf{I}_N \otimes \boldsymbol{\Delta}_{\mathbf{G}}) \right] \bar{\mathbf{y}} \\ &= \bar{\mathbf{y}}^{\mathsf{T}} \left[\left(\mathbf{L} \otimes \left(\mathbf{T}\mathbf{T}^{-1} \right) \right) (\mathbf{I}_N \otimes \boldsymbol{\Delta}_{\mathbf{G}}) \right] \bar{\mathbf{y}} = \bar{\mathbf{y}}^{\mathsf{T}} (\mathbf{L} \otimes \boldsymbol{\Delta}_{\mathbf{G}}) \bar{\mathbf{y}}. \end{aligned}$$

Applying the same steps to $\bar{\mathbf{e}}^{\mathsf{T}} (\mathbf{I}_N \otimes \mathbf{Q}') \bar{\mathbf{e}}$, we rewrite (5.8) as

$$v \leq \bar{\mathbf{e}}^{\mathsf{T}} (\mathbf{I}_N \otimes \mathbf{Q}^-) \bar{\mathbf{e}} + \bar{\mathbf{y}}^{\mathsf{T}} (\mathbf{I}_N \otimes \boldsymbol{\Delta}_{\mathbf{Q}'} - c\mathbf{L} \otimes \boldsymbol{\Delta}_{\mathbf{G}}) \bar{\mathbf{y}}.$$

Now, let us define $\mathbf{y}^h \triangleq [y_{1,h} \ y_{2,h} \ \cdots \ y_{N,h}]^{\mathsf{T}} \in \mathbb{R}^N$, with $h = 1, \ldots, n$, as the vector of all the h-th components of the N transformed synchronization errors $\mathbf{y}_i$. Since $\boldsymbol{\Delta}_{\mathbf{Q}'}$ and $\boldsymbol{\Delta}_{\mathbf{G}}$ are diagonal matrices, it is possible to write

$$v \leq \bar{\mathbf{e}}^{\mathsf{T}} (\mathbf{I}_N \otimes \mathbf{Q}^-) \bar{\mathbf{e}} + \sum_{h=1}^{n} \left(\mathbf{y}^h \right)^{\mathsf{T}} (\lambda_h(\mathbf{Q}')\mathbf{I}_N - c\lambda_h(\mathbf{G})\mathbf{L}) \, \mathbf{y}^h,$$

and, using again Corollary 13.4.2 in [68], we have

$$v \le \bar{\mathbf{e}}^\mathsf{T} \left(\mathbf{I}_N \otimes \mathbf{Q}^- \right) \bar{\mathbf{e}} + \sum_{h=1}^{n} \left\| \mathbf{y}^h \right\|^2 \left(\lambda_h(\mathbf{Q}') - c \lambda_h(\mathbf{G}) \lambda_2(\mathbf{L}) \right).$$

In order to have $v \le \bar{\mathbf{e}}^\mathsf{T} \left(\mathbf{I}_N \otimes \mathbf{Q}^- \right) \bar{\mathbf{e}} < 0$, and thus prove synchronization, it is required that $\lambda_h(\mathbf{Q}') - c \lambda_h(\mathbf{G}) \lambda_2(\mathbf{L}) \le 0$, $h = 1, \ldots, n$. Note that if $\lambda_h(\mathbf{Q}') \le 0$, then $\lambda_h(\mathbf{G})$ can be null. Differently, if $\lambda_h(\mathbf{Q}') > 0$, then it is required that $\lambda_h(\mathbf{G}) > 0$. The value of c^* in (5.7) stems trivially from the last consideration. $\qquad\square$

As a handy simplification of Theorem 5.3, we give the following corollary. With reference to (5.2), assume that

$$\boldsymbol{\Gamma} = \mathrm{diag}\left(\begin{bmatrix} \gamma_1 & \cdots & \gamma_n \end{bmatrix} \right), \quad \text{where } \gamma_h \ge 0 \ \forall h = 1, \ldots, n. \tag{5.9}$$

Corollary 5.4. *Network* (5.1) *with linear diffusive coupling* (5.2)-(5.9), *achieves global asymptotic synchronization if*

(a) *there exist* $\mathbf{Q}, \mathbf{Q}^-, \mathbf{Q}' \in \mathbb{R}^{n \times n}$ *such that:*
- $\mathbf{f}$ *is QUAD*$(\mathbf{I}_n, \mathbf{Q})$,
- $\mathbf{Q} = \mathbf{Q}^- + \mathbf{Q}'$, $\mathbf{Q}^- < 0$, *and* $\mathbf{Q}' = \mathrm{diag}\left(\begin{bmatrix} q_1 & \cdots & q_n \end{bmatrix} \right)$,
- $\gamma_h > 0$ *if* $q_h > 0$, *with* $h = 1, \ldots, n$.

(b) $\mathcal{G}$ *is a connected graph, and*
(c) $c \ge c^*$, *with*

$$c^* \triangleq \begin{cases} \dfrac{1}{\lambda_2(\mathbf{L})} \max_{h=1,\ldots,n} \dfrac{q_h}{\gamma_h}, & \text{if } \exists h \in \{1 \ldots, n\} : q_h > 0, \\ 0, & \text{otherwise.} \end{cases} \tag{5.10}$$

Proof. The proof follows immediately from the application of Theorem 5.3. $\qquad\square$

5.3 Examples of convergence of QUAD piecewise-smooth systems

5.3.1 Example 1: Positive definite coupling term

As an application of Theorem 5.2, consider the relay system

$$\mathbf{f}(\mathbf{x}_i) = \begin{bmatrix} -1 & -1 \\ 2 & 3 \end{bmatrix} \mathbf{x}_i - \begin{bmatrix} 0 \\ 2\mathrm{sign}(x_{i,1} + x_{i,2}) \end{bmatrix}.$$

Such a system can either reach an equilibrium point in the set $\{\mathbf{x}_i \in \mathbb{R}^2 \mid x_{i,1} = -x_{i,2}, \ x_{i,2} \in [-2,2]\}$ or diverge, and is QUAD with $\mathbf{P} = \mathbf{I}_n$ and $\mathbf{Q} = 3.06\mathbf{I}_n$. We coupled $N = 50$ of these relays through an Erdös-Rényi random graph built with wiring probability
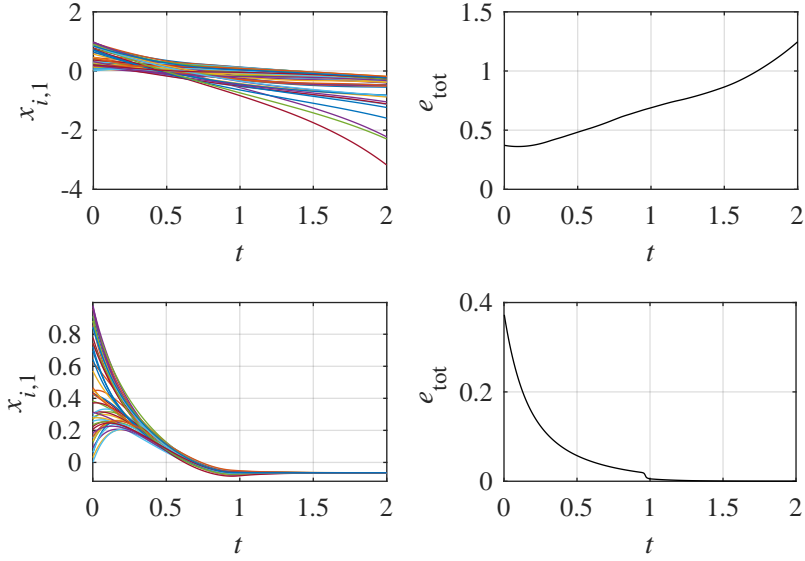
Figure 5.2: State dynamics and global synchronization error e_{tot} for coupled relay systems. Top panels: $c = 0.05$; bottom panels: $c = 0.25$.

$p = 0.5$ [54], resulting in a topology with $\lambda_2(\mathbf{L}) = 14.80$; in addition, we considered a linear diffusive coupling (5.2) with $\mathbf{\Gamma} = \mathbf{I}_n$. The critical value of the coupling gain computed using Theorem 5.2 is $c^* = \|\mathbf{Q}\| / \lambda_2(\mathbf{L}) = 0.21$. Figure 5.2 shows the absence and the emergence of synchronization in the cases $c = 0.05 < c^*$ and $c = 0.25 > c^*$.

5.3.2 Example 2: Positive semi-definite coupling term

To illustrate Theorem 5.3 and Corollary 5.4, consider the following PWS oscillator as a representative example:

$$\mathbf{f}(\mathbf{x}_i; t) = \begin{bmatrix} -x_{i,1} + 2x_{i,2}\sin(t) \\ f_2(x_{i,2}) \end{bmatrix}, \quad \text{where } f_2(x_{i,2}) = \begin{cases} -x_{i,2} - 2, & \text{if } x_{i,2} \leq -1, \\ x_{i,2}, & \text{if } -1 < x_{i,2} < 1, \\ -x_{i,2} + 2, & \text{if } x_{i,2} \geq 1. \end{cases}$$

This is a cascaded system, as $\dot{x}_{i,2}$ depends only on $x_{i,2}$. Moreover the state variable $x_{i,2}$ has two stable equilibria in -2 and $+2$; $x_{i,1}$ displays a sinusoidal behaviour, whose amplitude and phase are dependant on $x_{i,2}$. Notice that $\mathbf{f}$ is continuous but not differentiable, and QUAD with $\mathbf{P} = \mathbf{I}_n$ and $\mathbf{Q} = \begin{bmatrix} -1 & 2 \\ 0 & 1 \end{bmatrix}$; then we take $\mathbf{Q}^- = \begin{bmatrix} -1 & 2 \\ 0 & -3 \end{bmatrix}$ and $\mathbf{Q}' = \begin{bmatrix} 0 & 0 \\ 0 & 4 \end{bmatrix}$. As in the previous example, we deploy a random network with $N = 50$ nodes, and again $\lambda_2(\mathbf{L}) = 14.80$, but this time $\mathbf{\Gamma} = \begin{bmatrix} 0 & 0 \\ 0 & 1 \end{bmatrix}$ (note that $\mathbf{\Gamma} \not\succ 0$). Applying Theorem 5.3 with $\mathbf{T} = \mathbf{I}_n$ we get $c^* = \lambda_2(\mathbf{Q}')/(\lambda_2(\mathbf{L})\lambda_2(\mathbf{\Gamma})) = 4/(14.80 \cdot 1) = 0.27$. Figure 5.3 shows the results of two simulations, with $c = 0.02 < c^*$, and $c = 0.28 > c^*$; only the latter case displays synchronization.
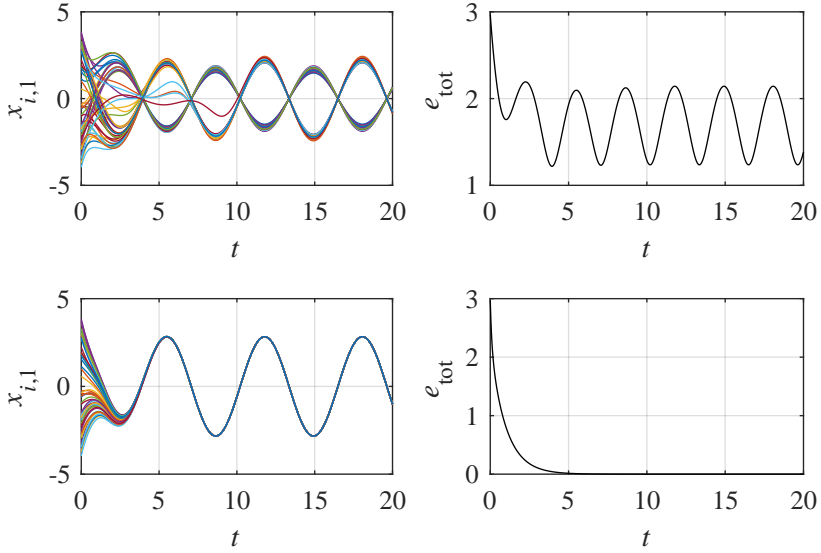
Figure 5.3: State dynamics and global synchronization error e_{tot} for coupled oscillating systems. Top panels: $c = 0.02$; bottom panels: $c = 0.28$.

5.4 Convergence of generic PWS systems through distributed discontinuous coupling

Next, we expound results contained in [32], which is under revision at the time of the writing of this thesis. In particular, assuming the σ-QUAD condition to hold for the piecewise-smooth dynamics $\mathbf{f}$, we show that convergence towards a common synchronous solution can be enforced when a discontinuous coupling layer is added on top of the diffusive one (see (5.3)). In addition, we provide expressions for the values of the critical coupling gains c^* and c_{d}^* of the diffusive and discontinuous coupling layers, respectively, required for synchronization.

Theorem 5.5. *Network* (5.3) *achieves global asymptotic synchronization if*

(a) *there exist* $\mathbf{P}, \mathbf{Q}, \mathbf{M} \in \mathbb{R}^{n \times n}$ *such that:*

- $\mathbf{f}$ *is σ-QUAD*($\mathbf{P}$, $\mathbf{Q}$, $\mathbf{M}$), *with* $\mathbf{P} > 0$,
- $\text{sym}(\mathbf{P}\Gamma) > 0$,
- $\mu_\infty^-(\mathbf{P}\Gamma_{\text{d}}) > 0$,[a]

(b) $\mathcal{G}$ *and* $\mathcal{G}_{\text{d}}$ *are connected graphs, and*

(c) $c > c^*$, and $c_d \geq c_d^*$ with

$$c^* \triangleq \frac{\|\mathbf{Q}\|_2}{\lambda_2(\mathbf{L})\lambda_{\min}(\text{sym } \mathbf{P\Gamma})}, \quad c_d^* \triangleq \frac{\|\mathbf{M}\|_\infty}{\delta_{\mathcal{G}_d}\mu_\infty^-(\mathbf{P\Gamma}_d)}. \tag{5.11}$$

---

[a]We recall that the expression of the function μ_∞^- is given in Definition 4.3.

A proof of this theorem is given later in Chapter 6. Here, we wish to emphasise that the critical coupling gains depend on the internal node dynamics through the matrices $\mathbf{Q}, \mathbf{P}, \mathbf{M}$, the inner coupling matrices $\mathbf{\Gamma}, \mathbf{\Gamma}_d$, and the structure of the control layers $\mathbf{L}, \mathbf{L}_d$ through the algebraic connectivity $\lambda_2(\mathbf{L})$ and the minimum density of the discontinuous coupling layer $\delta_{\mathcal{G}_d}$ (see Section 4.3). Hence, the convergence theorem above can be effectively used to design the network control layers as illustrated via representative examples in Section 5.5.

Next, we provide an alternative condition for global synchronization to deal with the case in which the inner coupling matrices $\mathbf{\Gamma}$ and $\mathbf{\Gamma}_d$ do not fulfil the conditions $\text{sym}(\mathbf{P\Gamma}) > 0$ and $\mu_\infty^-(\mathbf{P\Gamma}_d) > 0$ in Theorem 5.5.

Theorem 5.6. *Network* (5.3) *achieves global asymptotic synchronization if*

(a) there exist $\mathbf{P}, \mathbf{Q}, \mathbf{Q}^-, \mathbf{Q}', \mathbf{M} \in \mathbb{R}^{n \times n}$ such that:

- $\mathbf{f}$ *is σ-QUAD($\mathbf{P}, \mathbf{Q}, \mathbf{M}$), with $\mathbf{P} > 0$, $\mathbf{M} = \text{diag}([m_1 \;\; \cdots \;\; m_n])$,*
- $\mathbf{Q} = \mathbf{Q}^- + \mathbf{Q}'$, $\mathbf{Q}^- < 0$, $\mathbf{Q}' = (\mathbf{Q}')^\mathsf{T}$,
- $\mathbf{P\Gamma} = (\mathbf{P\Gamma})^\mathsf{T}$, $\mathbf{Q}'$ *and* $\mathbf{P\Gamma}$ *are simultaneously diagonalisable, and* $\lambda_h(\mathbf{P\Gamma}) \geq 0 \; \forall h = 1, \ldots, n$, *but* $\lambda_h(\mathbf{P\Gamma}) > 0$ *if* $\lambda_h(\mathbf{Q}') > 0$,
- $\mathbf{P\Gamma}_d = \text{diag}([\gamma_1 \;\; \cdots \;\; \gamma_n])$, *and* $\gamma_h \geq 0 \; \forall h = 1, \ldots, n$, *but* $\gamma_h > 0$ *if* $m_h > 0$;

(b) $\mathcal{G}$ and $\mathcal{G}_d$ are connected graphs, and

(c) $c > c^*$ and $c_d \geq c_d^*$, with

$$c^* \triangleq \begin{cases} \dfrac{1}{\lambda_2(\mathbf{L})} \max\limits_{h=1,\ldots,n} \dfrac{\lambda_h(\mathbf{Q}')}{\lambda_h(\mathbf{P\Gamma})}, & \text{if } \exists h : \lambda_h(\mathbf{Q}') > 0, \\ 0, & \text{otherwise}, \end{cases} \tag{5.12}$$

$$c_d^* \triangleq \begin{cases} \dfrac{1}{\delta_{\mathcal{G}_d}} \max\limits_{h=1,\ldots,n} \dfrac{m_h}{\gamma_h}, & \text{if } \exists h : m_h > 0, \\ 0, & \text{otherwise}. \end{cases} \tag{5.13}$$

Note that the theorem above relaxes some of the assumptions on the inner coupling matrices, but requires other alternative structural hypothesis on these matrices that, although seemingly more restrictive, can be of use in some cases as shown in Section 5.5. The proof of the theorem is given later in Chapter 6.

Note that Theorems 5.5 and 5.6 give sufficient conditions on the threshold values of the coupling gain that scale with $\lambda_2(\mathbf{L})^{-1}$ for c^* and $\delta_{\mathcal{G}_d}^{-1}$ for c_d^*. Table 4.1 shows how these structural variables change for a set of paradigmatic network topologies of N nodes

together with their total number of links. The multiplex nature of the strategy proposed here allows to pick the structure of each layer so as to fulfil a trade-off between the values of the required coupling gains and the number of edges in each layer.

5.5 Examples of convergence of σ-QUAD piecewise-smooth systems

5.5.1 Example 1: Positive definite coupling terms

We consider the problem of achieving global asymptotic synchronization in a network of $N = 30$ relay systems whose vector field is given by $\mathbf{f}(\mathbf{x}_i) = \mathbf{A}\mathbf{x}_i - \mathbf{B}\mathrm{sign}(x_{i,1})$, with

$$\mathbf{A} = \begin{bmatrix} 1.51 & 1 & 0 \\ -99.922 & 0 & 1 \\ -5 & 0 & 0 \end{bmatrix}, \quad \mathbf{B} = \begin{bmatrix} 1 \\ -2 \\ 1 \end{bmatrix}.$$

As shown in [43], with these parameter values each relay system exhibits chaotic behaviour and therefore, when a group of such relays is considered, they will not synchronize unless appropriately coupled. In [38], it is shown that under some hypotheses a network of such relays can achieve bounded convergence to the synchronous manifold. We show below that using Theorem 5.5, we can prove instead global asymptotic convergence of this network of discontinuous systems towards each other.

Note that each relay can be shown to be σ-QUAD according to Definition 2.4 through simple algebraic manipulations with

$$\mathbf{P} = \mathbf{I}_3, \quad \mathbf{Q} = \mathbf{A}, \quad \mathbf{M} = \begin{bmatrix} 0 & 0 & 0 \\ 4 & 0 & 0 \\ 0 & 0 & 0 \end{bmatrix};$$

therefore $\|\mathbf{Q}\|_2 = 100.063$ and $\|\mathbf{M}\|_\infty = 4$. We assume that the relays are coupled via two layers as in (5.3) with the structure of the proportional layer, $\mathbf{L}$, corresponding to a ring graph, with $\lambda_2(\mathbf{L}) = 1$, while the structure of the discontinuous coupling layer, $\mathbf{L}_\mathrm{d}$, being chosen as the Erdős-Rényi-like graph [53] shown in Figure 5.4a. Figure 5.4b shows the sparsest cut of this latter graph obtained numerically, whose minimum density is computed to be $\delta_{\mathcal{G}_\mathrm{d}} = 1.290$. We assume all states are available for coupling so that $\mathbf{\Gamma} = \mathbf{\Gamma}_\mathrm{d} = \mathbf{I}_3$; hence, $\lambda_{\min}(\mathrm{sym}(\mathbf{P}\mathbf{\Gamma})) = \mu_\infty^-(\mathbf{P}\mathbf{\Gamma}_\mathrm{d}) = 1$. From Theorem 5.5, we can then compute the critical coupling gains as $c^* = 100.063$ and $c_\mathrm{d}^* = 3.102$ that are sufficient for global convergence.

Figures 5.5a and 5.5b show the evolution of the total synchronization error e_tot (defined in Section 1.5) when the coupling gains are chosen below and above the critical threshold values. As expected from the theoretical results, when the gains are above the thresholds, the synchronization error converges asymptotically to zero. Note that the analytical estimates of the critical coupling gains are very conservative as expected from a Lyapunov-based proof of convergence.
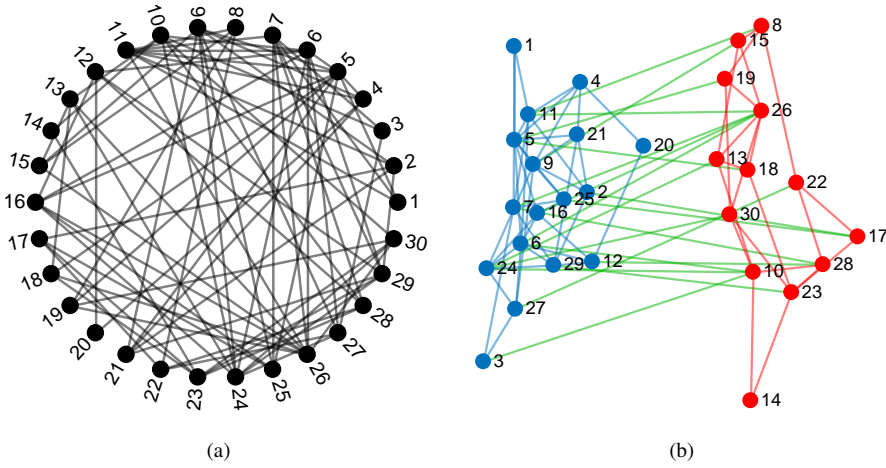
Figure 5.4: (a) Topology of the discontinuous coupling layer. The graph is an Erdős-Rényi-like one, with wiring probability $p = 0.2$. (b) Sparsest cut of the topology in (a); $N_1 = 17$, $N_2 = 13$. $b = 19$.

5.5.2 Example 2: Resilience to edge faults

Next, we show how the findings in Theorem 5.5 can be used to evaluate the resilience of the network with respect to structural changes in the communication layer. To this aim, consider the graph in Figure 5.4 which contains 82 edges. Now, assume that, due to some fault, 8 links (roughly 10% of the total) are removed. We investigate two possible scenarios.

A: 4 blue and 4 red links are removed from each cluster in the sparsest cut of the original graph; the minimum density of this new graph $\mathcal{G}_A$, shown in Figure 5.6a, will be called $\delta_{\mathcal{G}_A}$.

B: 8 green links interconnecting the two different clusters are removed, so that by $\delta_{\mathcal{G}_A}$ we refer to the minimum density of the perturbed graph $\mathcal{G}_B$ in Figure 5.6b.

The minimum densities of the perturbed graphs can be computed numerically as $\delta_{\mathcal{G}_A} = 1.080$ and $\delta_{\mathcal{G}_B} = 0.747$, respectively. Consequently, the threshold value c_d^* as obtained from (5.11) associated to $\mathcal{G}_B$ will be larger (thus worse) than that associated to $\mathcal{G}_A$. This shows that removing some links rather than others can be more impactful on the synchronizability of the network and hence on its resilience to intentional or unintentional perturbations. Specifically, we observe a greater loss of resilience when the inter-cluster links are removed, although a detailed analysis of this effect is beyond the scope of this paper and will be the subject of future work.

(a)

(b)
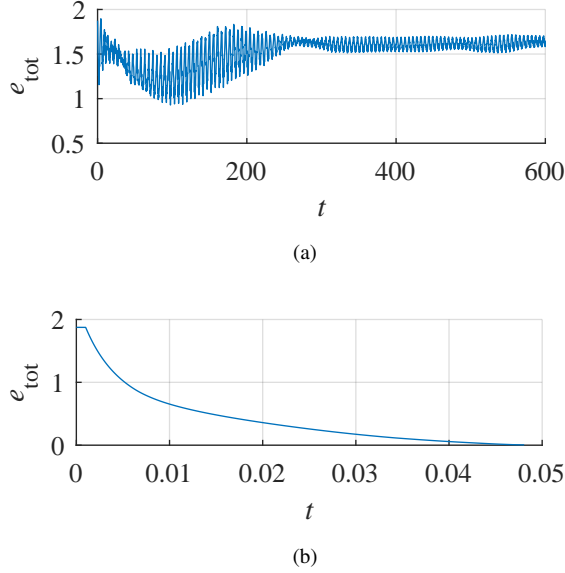
Figure 5.5: Error dynamics in a network of relay systems with (a) $c = 0.1$, $c_{\mathrm{d}} = 0.001$ and with (b) $c = 101$, $c_{\mathrm{d}} = 3.200$.

5.5.3 Example 3: Positive semi-definite coupling terms

To illustrate an application of Theorem 5.6 and the importance of the discontinuous coupling action, we present the following example. Consider the cascaded PWS oscillator whose vector field is

$$\mathbf{f}(\mathbf{x}_i; t) = \begin{bmatrix} -x_{i,1} + 2\sin(x_{i,2}\pi t) \\ f_2(x_{i,2}) \end{bmatrix}, \quad \text{with } f_2(x_{i,2}) = \begin{cases} +\cos(x_{i,2}), & \text{if } x_{i,2} > 0, \\ -\cos(x_{i,2}), & \text{if } x_{i,2} < 0. \end{cases}$$

The dynamics of the state variable $x_{i,2}$ is decoupled from that of $x_{i,1}$ and has infinite (stable and unstable) equilibrium values; $x_{i,1}$ instead displays a sinusoidal behaviour in time, whose amplitude and frequency depend on $x_{i,2}$.

It can be easily verified that $\mathbf{f}$ is not QUAD, but is σ-QUAD with $\mathbf{P} = \mathbf{I}_2$, $\mathbf{M} = \begin{bmatrix} 0 & 0 \\ 0 & 2 \end{bmatrix}$ and $\mathbf{Q} = \begin{bmatrix} -1 & 2 \\ 0 & 1 \end{bmatrix} = \mathbf{Q}^- + \mathbf{Q}'$, where we select $\mathbf{Q}^- = \begin{bmatrix} -1 & 2 \\ 0 & -3 \end{bmatrix}$ and $\mathbf{Q}' = \begin{bmatrix} 0 & 0 \\ 0 & 4 \end{bmatrix}$. Similarly to example 1, we deploy $N = 30$ nodes, with the same topologies for the coupling layers, having again $\lambda_2(\mathbf{L}) = 1$ and $\delta_{\mathcal{G}_{\mathrm{d}}} = 1.290$. However, this time $\mathbf{\Gamma} = \mathbf{\Gamma}_{\mathrm{d}} = \begin{bmatrix} 0 & 0 \\ 0 & 1 \end{bmatrix}$, and therefore sym($\mathbf{P\Gamma}$) and $\mu_\infty^-(\mathbf{P\Gamma})$ are not positive definite, thus not fulfilling the assumptions of Theorem 5.5. Applying Theorem 5.6 instead, we get $c^* = \lambda_2(\mathbf{Q}')/(\lambda_2(\mathbf{L})\lambda_2(\mathbf{\Gamma})) = 4$ and $c_{\mathrm{d}}^* = m_2/(\gamma_2 \delta_{\mathcal{G}_{\mathrm{d}}}) = 1.550$. Figure 5.7 shows the results of two simulations, with $c = 4.100 > c^*$, $c_{\mathrm{d}} = 0 < c_{\mathrm{d}}^*$, and with $c = 4.100 > c^*$, $c_{\mathrm{d}} = 1.600 > c_{\mathrm{d}}^*$. Convergence is observed only in the latter case, where both the coupling gains are above the thresholds found with Theorem 5.6; differently, in the former case, the diffusive action alone is not enough to guarantee synchronization, even though its coupling gain is selected above the
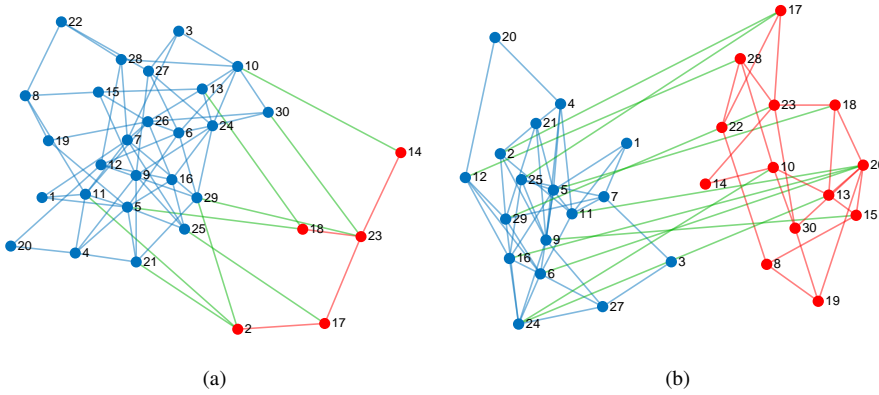
Figure 5.6: Topologies obtained removing links in the graph in Figure 5.4b and associated sparsest cuts. (a) 4 blue links (2-9, 5-9, 6-11, 6-16) and 4 red links (17-22, 18-26, 19-30, 23-28) from Figure 5.4b were removed; (b) 8 green links (3-10, 5-19, 6-10, 7-26, 7-28, 8-11, 22-27, 24-30) from Figure 5.4b were removed.

relative threshold.

5.5.4 Example 4: A numerical study of synchronizability

To provide a demonstration of the interplay between the two communication layers in (5.3), we consider a network of $N = 10$ identical Sprott circuits, whose dynamics is given by

$$\mathbf{f}(\mathbf{x}_i) = \begin{bmatrix} 0 & 1 & 0 \\ 0 & 0 & 1 \\ -1 & -1 & -0.5 \end{bmatrix} \mathbf{x}_i + \begin{bmatrix} 0 \\ 0 \\ \text{sign}(x_{i,1}) \end{bmatrix}.$$

In the network, $\mathbf{\Gamma} = \mathbf{\Gamma}_d = \mathbf{I}_n$, and the nodes are diffusively coupled via a graph with Laplacian matrix $\mathbf{L}$ associated to a 3-nearest neighbours topology. Differently, $\mathbf{L}_d$ is associated to 3 possible topologies, as portrayed in Figure 5.8, which displays the steady state value of the global synchronization error e_{tot} (defined in Section 1.5) for each different combination of the coupling layer structures. Initial conditions were selected randomly (with a uniform distribution), in the range of chaoticity of the Sprott circuit. We notice that the stability region depends on the relative choice of the structures of the two coupling layers. Obviously, the worst case is when the structure of the discontinuous layer is the sparsest (see Figure 5.8a). Surprisingly, to enhance stability it is sufficient to add a few long range links to the discontinuous coupling layer (see Figure 5.8b); the largest stability region being observed when the discontinuous coupling layer shares the same links as the underlying diffusive one.

Notice that applying Theorem 5.5, rather conservative results are obtained. Indeed, the hypotheses of the theorem hold with $\mathbf{P} = \mathbf{I}_3$, $\|\mathbf{Q}\|_2 = 1.70$ $\|\mathbf{M}\|_\infty = 2$,

(a)

(b)
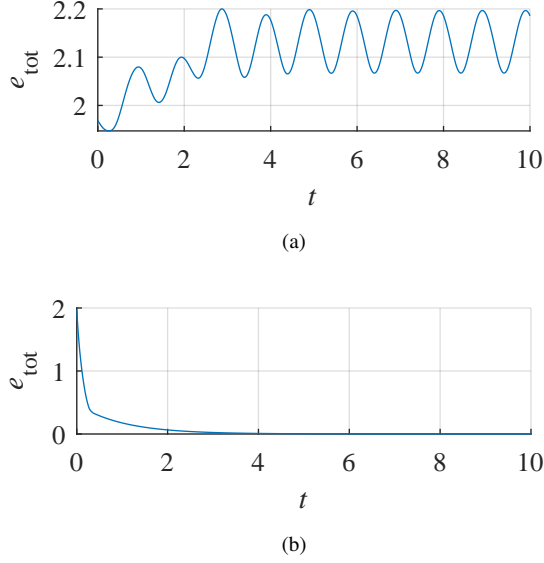
Figure 5.7: (a) Error dynamics in a network of cascaded systems with $c = 4.1$, $c_\mathrm{d} = 0$. (b) Error dynamics with $c = 4.1$, $c_\mathrm{d} = 1.6$.

$\lambda_{\min}\left(\mathrm{sym}(\mathbf{P\Gamma})\right) = \mu_\infty^-(\mathbf{P\Gamma_d}) = 1$, $\lambda_2(\mathbf{L}) = 4.382$, and $\delta_{\mathcal{G}_\mathrm{d}} \in (0.5, 0.714, 2.4)$, for the three different configurations (a), (b) and (c) of the discontinuous coupling layer in Figure 5.8. Therefore, we have $c^* = 0.388$ and $c_\mathrm{d}^* \in (4, 2.801, 0.833)$.

5.5.5   Example 5: The necessity of a discontinuous coupling term

To further illustrate the beneficial effect of the discontinuous layer, we consider a network of $N = 10$ PWS bistable systems, used to model energy harvesters [27] or simplified climatic models [82], and described by

$$\mathbf{f}(\mathbf{x}_i) = \begin{bmatrix} 0 & 1 \\ -1 & -1 \end{bmatrix} \mathbf{x}_i + \begin{bmatrix} 0 \\ \mathrm{sign}(x_{i,1}) \end{bmatrix}.$$

The system has two coexisting stable equilibria in $[1 \ \ 0]^\mathsf{T}$ and $[-1 \ \ 0]^\mathsf{T}$. The agents are coupled over a path graph, with $\mathbf{L} = \mathbf{L}_\mathrm{d}$ and $\mathbf{\Gamma} = \mathbf{\Gamma}_\mathrm{d} = \mathbf{I}_2$. We consider the particularly challenging case where five nodes are started at one of the equilibria, while the other five are at the other. In this case, as shown in Figure 5.9, the diffusive coupling layer alone is unable to synchronize the network for any value of c, when the discontinuous coupling layer is disconnected ($c_\mathrm{d} = 0$). In this case, synchronization is only achieved when both coupling layers are present.

(a)

(b)

(c)
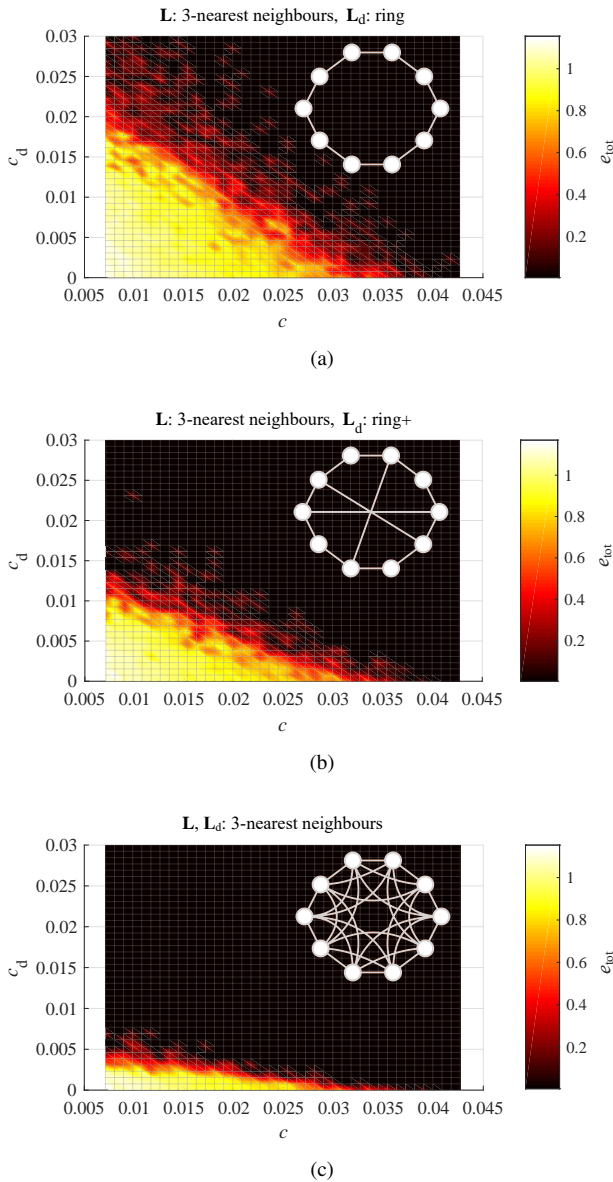
Figure 5.8: Characterization of synchronizability in a network of Sprott circuits. Five random initial conditions were used, with $\mathbf{x}_i(0) \in [[0,1] \ [0,0.5] \ [0,0.5]]^{\mathsf{T}}$, and, for each combination of c and c_d, e_{tot} is taken as the average of the five simulations. The diffusive layer is always associated to a 3-nearest neighbours; differently, the discontinuous coupling layer varies in each figure.
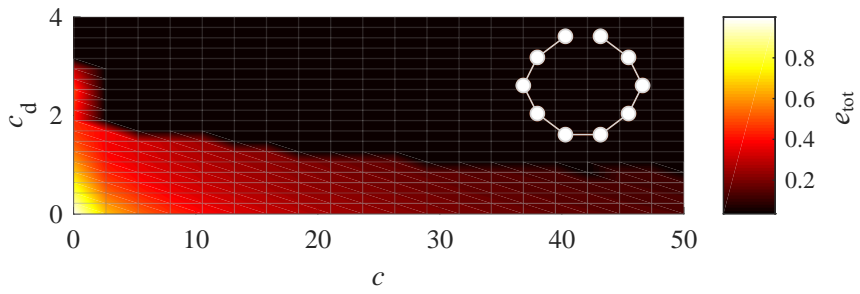
Figure 5.9: Characterization of synchronizability in a network of bistable systems.

6 Proofs of convergence with discontinuous coupling

We give here the proofs of Theorems 5.5 and 5.6 presented in Chapter 5. We start by giving some lemmas and definitions in Section 6.1, then we introduce the concept of star functions in Section 6.2 and show how such functions can be associated to a given graph in Section 6.3. In particular, we show that semi-negativity of the star function for a given graph can be studied by evaluating its value on the bipartitions of the graph, which will be crucial to prove the two theorems.

6.1 Preliminary lemmas and definitions

> **Definition 6.1** (Clusterization). *Given a vector $\boldsymbol{\xi} \in \mathbb{R}^n$, we define its* clusterization, *denoted by* $\mathrm{clus}(\boldsymbol{\xi})$, *as a partition of the set of indices* $\mathcal{I} = \{1, \ldots, n\}$, *say* $\{\mathcal{I}_1, \ldots, \mathcal{I}_Q\}$ *with $1 \le Q \le n$, such that, for all $i, j \in \mathcal{I}$, $\xi_i = \xi_j$ if and only if there exists q such that $i, j \in \mathcal{I}_q$.*

For example, according to this definition, the vector $\boldsymbol{\xi} = [1 \ \ 1 \ \ 6 \ \ 2 \ \ 2]^\mathsf{T}$ has a clusterization $\mathrm{clus}(\boldsymbol{\xi}) = \{\mathcal{I}_1, \mathcal{I}_2, \mathcal{I}_3\}$ with $\mathcal{I}_1 = \{1, 2\}, \mathcal{I}_2 = \{3\}, \mathcal{I}_3 = \{4, 5\}$. Clearly, the clusterization of a vector is unique up to a reordering of the clusters.

> **Lemma 6.2.** *Given $\boldsymbol{\xi} \in \mathbb{R}^n$ and $\mathbf{A} \in \mathbb{R}^{n \times n}$, it holds that*
>
> $$\boldsymbol{\xi}^\mathsf{T} \mathbf{A} \, \mathrm{sign}(\boldsymbol{\xi}) \le \|\mathbf{A}\|_\infty \|\boldsymbol{\xi}\|_1 \,.$$

Proof. We can write

$$
\begin{aligned}
\boldsymbol{\xi}^\mathsf{T} \mathbf{A} \, \mathrm{sign}(\boldsymbol{\xi}) &= \sum_{i=1}^n \left(A_{ii} |\xi_i| + \sum_{j=1, j \neq i}^n A_{ij} \xi_i \, \mathrm{sign}(\xi_j) \right) \\
&\le \sum_{i=1}^n \left(|A_{ii}| |\xi_i| + \sum_{j=1, j \neq i}^n |A_{ij}| |\xi_i| \right)
\end{aligned}
$$

$$\leq \max_{i=1,\dots,n} \left(\sum_{j=1}^{n} \left| A_{ij} \right| \right) \sum_{i=1}^{n} |\xi_i| \,.$$

$\square$

Lemma 6.3. *Given $\boldsymbol{\xi} \in \mathbb{R}^n$ and $\mathbf{A} \in \mathbb{R}^{n\times n}$, it holds that*

$$\boldsymbol{\xi}^{\mathsf{T}} \mathbf{A} \operatorname{sign}(\boldsymbol{\xi}) \geq \mu_{\infty}^{-}(\mathbf{A}) \, \|\boldsymbol{\xi}\|_1 \,,$$

with $\mu_{\infty}^{-}(\mathbf{A})$ defined as in ([4.1](#)).

Proof. We have

$$\boldsymbol{\xi}^{\mathsf{T}} \mathbf{A} \operatorname{sign}(\boldsymbol{\xi}) \geq \sum_{i=1}^{n} \left(A_{ii} - \sum_{j=1, j\neq i}^{n} \left| A_{ij} \right| \right) |\xi_i| \geq \min_{i=1,\dots,n} \left(A_{ii} - \sum_{j=1, j\neq i}^{n} \left| A_{ij} \right| \right) \sum_{i=1}^{n} |\xi_i| \,.$$

$\square$

Let $\mathbb{V}_d$ be a vector space in $\mathbb{R}^d$.

Definition 6.4 (Cones).

(i) *A set $\mathcal{K} \subseteq \mathbb{V}_d$ is a (convex) cone if, for any $\boldsymbol{\xi}_1, \boldsymbol{\xi}_2 \in \mathcal{K}$ and $\alpha_1, \alpha_2 \geq 0$, it holds that $\alpha_1 \boldsymbol{\xi}_1 + \alpha_2 \boldsymbol{\xi}_2 \in \mathcal{K}$.*

(ii) *A cone is* finitely generated *if it is the* conic combination *(i.e. a linear combination with non-negative coefficients) of a finite number of unit norm vectors, which we call* generators *of the cone.*

(iii) *A cone $\mathcal{K}$ is* polyhedral *if there exists a matrix $\mathbf{C} = [\mathbf{c}_1 \ \mathbf{c}_2 \ \cdots \ \mathbf{c}_q] \in \mathbb{R}^{d\times q}$ (with $q \geq d$ and $\mathbf{C}$ having rank d) such that $\mathbf{C}^{\mathsf{T}} \boldsymbol{\xi} \geq \mathbf{0}$, for all $\boldsymbol{\xi} \in \mathcal{K}$.*

A finitely generated cone in $\mathbb{R}^3$ is illustrated in Figure [6.1a](#). Note that a convex cone contains its boundary.

Lemma 6.5 (Equivalence of cones [16]). *A polyhedral cone is a finitely generated cone having p generators; the i-th generator $\hat{\boldsymbol{\xi}}_i$ is such that $\mathbf{c}_j^{\mathsf{T}} \hat{\boldsymbol{\xi}}_i = 0$ for $n-1$ indices $j \neq i$. A finitely generated cone is also a polyhedral cone.*

Definition 6.6 (Incidence matrix [68]). *Given a graph $\mathcal{G}$, the* incidence matrix $\mathbf{B} \in \mathbb{Z}^{N\times N_{\mathcal{E}}}$ *has columns $\mathbf{b}_i$, $i = 1, \dots, N_{\mathcal{E}}$, where $\mathbf{b}_i$ is associated to edge i connecting vertices v_j and v_k, and has all its elements equal to zero, except for positions j and k, where it has arbitrarily either 1 and -1, or -1 and 1.*
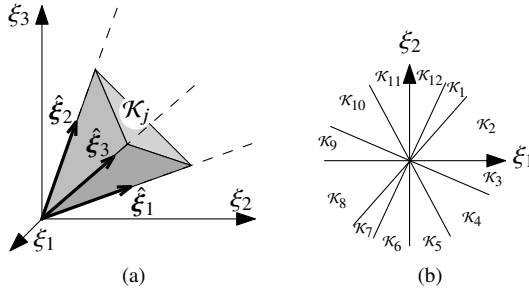
Figure 6.1: (a) A finitely generated cone $\mathcal{K}_j$ in $\mathbb{R}^3$; $\hat{\boldsymbol{\xi}}_1$, $\hat{\boldsymbol{\xi}}_2$, and $\hat{\boldsymbol{\xi}}_3$ are the generators of the cone. (b) Example of the domain of a star function with 12 cones $\mathcal{K}_j$, $j = 1, \ldots, 12$, in the case that $n = 2$.

Definition 6.7 (Bipartitions and tripartitions). *We term as* bipartitions $\hat{\mathcal{B}}$ *and* tripartitions $\hat{\mathcal{T}}$ *of a graph* $\mathcal{G}$ *the set of all the possible partitions of the vertices set* $\mathcal{V}$ *of the graph in two or three subsets (or clusters), respectively. We require that in both the bipartitions and the tripartitions there are at least two clusters made of connected vertices.*

As far as notation is concerned, we denote generic bipartitions and tripartitions by $\mathcal{B} = \{\mathcal{I}_1, \mathcal{I}_2\}$ and $\mathcal{T} = \{\mathcal{I}_1, \mathcal{I}_2, \mathcal{I}_3\}$, respectively, where $\mathcal{I}_i$ is the set of indices of the vertices belonging to the i-th cluster. Finally, we denote as $\hat{\mathcal{P}}$ the set of all bipartitions and tripartitions of a graph of interest, i.e. $\hat{\mathcal{P}} \triangleq \hat{\mathcal{B}} \cup \hat{\mathcal{T}}$. A partition that is either a bipartition or a tripartition is denoted by $\mathcal{P} \in \hat{\mathcal{P}}$.

6.2 Star functions

Definition 6.8 (Star function). *A continuous piecewise-linear function* $\phi : \mathbb{R}^n \to \mathbb{R}$ *is a* star function *if*

   (i) it is linear in a set of polyhedral convex cones $\mathcal{K}_j$, $j = 1, \ldots, J$, *with* $J \in \mathbb{N}_{>0}$,
   (ii) the cones can overlap only on their boundaries, and
   (iii) they are a cover for $\mathbb{R}^n$.

An example of the domain of a star function is illustrated in Figure 6.1b. We can now give the following Lemma, used to assess the semi-negativity of a star function.

Lemma 6.9. *Given a star function* $\phi : \mathbb{R}^n \to \mathbb{R}$, *if* $\phi(\boldsymbol{\xi}) \le 0$ *on the generators of the cones* $\mathcal{K}_j$, $j = 1, \ldots, J$ *over which it is defined, then* $\phi(\boldsymbol{\xi}) \le 0$ *for all* $\boldsymbol{\xi} \in \mathbb{R}^n$.

Proof. Without loss of generality, consider any cone $\mathcal{K}_j$ where ϕ is linear. Since by

definition $\mathcal{K}_j$ is a finitely generated cone, each of its points can be expressed as

$$\boldsymbol{\xi} = \alpha_1 \hat{\boldsymbol{\xi}}_1 + \alpha_2 \hat{\boldsymbol{\xi}}_2 + \ldots + \alpha_p \hat{\boldsymbol{\xi}}_p, \quad \boldsymbol{\xi} \in \mathcal{K}_j,$$

where $\hat{\boldsymbol{\xi}}_1, \ldots, \hat{\boldsymbol{\xi}}_p$ are the p generators of $\mathcal{K}_j$, and $\alpha_1, \ldots, \alpha_p \geq 0$. Then, exploiting linearity of ϕ, we have

$$\phi(\boldsymbol{\xi}) = \alpha_1 \phi(\hat{\boldsymbol{\xi}}_1) + \alpha_2 \phi(\hat{\boldsymbol{\xi}}_2) + \ldots + \alpha_n \phi(\hat{\boldsymbol{\xi}}_n), \quad \boldsymbol{\xi} \in \mathcal{K}_j.$$

Thus, since $\alpha_1, \ldots, \alpha_p \geq 0$, if ϕ is non-positive on all the generators $\hat{\boldsymbol{\xi}}_i$ of $\mathcal{K}_j$, then $\phi(\boldsymbol{\xi}) \leq 0$ for all $\boldsymbol{\xi} \in \mathcal{K}_j$. The same is true for any other $\mathcal{K}_j$.

$\square$

6.3   Star function associated to a graph

Next we give a set of results concerning a specific type of star function that can be associated to a graph $\mathcal{G}$. We also show that the properties of this function can be interpreted in a graph-theoretic manner and derive some results that will be useful later in Section 6.4 to prove Theorem 5.5.

We denote by $\mathcal{S} \subset \mathbb{R}^N$ the subspace

$$\mathcal{S} \triangleq \left\{ \mathbf{e} \in \mathbb{R}^N \ \middle| \ \sum_{i=1}^{N} e_i = 0 \right\}. \tag{6.1}$$

We associate to any graph $\mathcal{G}$ a function $\phi_{\mathcal{G}} : \mathcal{S} \to \mathbb{R}$, given by

$$\phi_{\mathcal{G}}(\mathbf{e}) = a_1 \sum_{i=1}^{N} \left| \mathbf{i}_i^{\mathsf{T}} \mathbf{e} \right| - a_2 \sum_{i=1}^{N_{\mathcal{E}}} \left| \mathbf{b}_i^{\mathsf{T}} \mathbf{e} \right|, \tag{6.2}$$

where N and $N_{\mathcal{E}}$ are the numbers of vertices and edges in $\mathcal{G}$, respectively, a_1, a_2 are positive scalars, $\mathbf{i}_i$ is the i-th vector of the canonical basis of $\mathbb{R}^N$, and $\mathbf{b}_i$ are the columns of the incidence matrix $\mathbf{B}$ of $\mathcal{G}$.

Lemma 6.10. *Given a graph $\mathcal{G}$, the function $\phi_{\mathcal{G}}$ constructed as in (6.2) is a star function.*

Proof. We prove that $\phi_{\mathcal{G}}$ is a star function by verifying that all the three conditions in Definition 6.8 are fulfilled.

(i)   From its definition, $\phi_{\mathcal{G}}$ is linear in the set of regions, which we name $\mathcal{K}_j$ with $j \in \mathbb{N}_{>0}$, where the argument of each of the absolute values in (6.2) has a certain sign. Next, we need to show that all $\mathcal{K}_j$ are polyhedral cones. Without loss of generality, assume

$\mathcal{K}_1$ is the set where the arguments of the absolute values have the following signs:[1]

$$\begin{cases} \mathbf{i}_1^\mathsf{T}\mathbf{e} \geq 0, \dots, \mathbf{i}_{N-1}^\mathsf{T}\mathbf{e} \geq 0, \\ \mathbf{i}_N^\mathsf{T}\mathbf{e} \leq 0, \\ \mathbf{b}_1^\mathsf{T}\mathbf{e} \geq 0, \dots, \mathbf{b}_{N_\mathcal{E}}^\mathsf{T}\mathbf{e} \geq 0. \end{cases} \tag{6.3}$$

$\mathcal{K}_1$ can be equivalently expressed as the locus where the vector constraint $\mathbf{C}^\mathsf{T}\mathbf{e} \geq \mathbf{0}$ holds, with

$$\mathbf{C} \triangleq \begin{bmatrix} \mathbf{i}_1 & \cdots & \mathbf{i}_{N-1} & -\mathbf{i}_N & \mathbf{b}_1 & \cdots & \mathbf{b}_{N_\mathcal{E}} \end{bmatrix}.$$

Given that $\mathbf{i}_1 \dots, \mathbf{i}_N$ are linearly independent, $\mathbf{C}$ has rank N; thus $\mathcal{K}_1$ is a polyhedral cone in $\mathcal{S}$; see Definition 6.4. Considering a different region $\mathcal{K}_j$ would only change the signs of the inequalities in (6.3), and thus the signs of the columns in $\mathbf{C}$, not affecting the validity of the argument. Therefore, all $\mathcal{K}_j$'s are polyhedral cones.

(ii) Since each $\mathcal{K}_j$ is defined by a specific combination of signs for the inequalities in (6.3), the intersection of any two $\mathcal{K}_j$'s can either be the origin or only contain points in their boundaries. In fact, a point $\mathbf{e}'$ such that $\mathbf{c}^\mathsf{T}\mathbf{e}' = 0$, for some $\mathbf{c} \in C_{\mathbf{i,b}} \triangleq \{\mathbf{i}_1, \dots, \mathbf{i}_N, \mathbf{b}_1, \dots, \mathbf{b}_{N_\mathcal{E}}\}$, belongs both to a region where $\mathbf{c}^\mathsf{T}\mathbf{e}' \geq 0$ and to one in which $\mathbf{c}^\mathsf{T}\mathbf{e}' \leq 0$, and is on the boundaries of both. Conversely, if another point $\mathbf{e}''$ is such that $\mathbf{c}^\mathsf{T}\mathbf{e}'' \neq 0$, for all $\mathbf{c} \in C_{\mathbf{i,b}}$, it can only belong to one region $\mathcal{K}_j$.

(iii) Finally, given that each value of $\mathbf{e} \in \mathcal{S}$ determines a combination of signs for the non-zero arguments in the absolute values in (6.2), each point $\mathbf{e}$ belongs to at least one $\mathcal{K}_j$; therefore, the family of all $\mathcal{K}_j$'s is a cover for $\mathcal{S}$. Hence, the thesis follows.

□

Lemma 6.11. *Let $\mathcal{G}$ be a connected graph and $\phi_\mathcal{G}$ its associated star function defined as in (6.2). Say $\hat{\mathbf{e}}$ any generator of $\phi_\mathcal{G}$, then the clusters of indexes in* clus($\hat{\mathbf{e}}$) *form either a bipartition or a tripartition of $\mathcal{G}$.*[a]

---

[a]Note that clus($\hat{\mathbf{e}}$) is a partition of $\{1, \dots, N\}$.

Proof. To prove the thesis, we need to show that (i) clus($\hat{\mathbf{e}}$) = $\{\mathcal{I}_1, \dots, \mathcal{I}_Q\}$ with $Q = 2$ or $Q = 3$; (ii) the partition of $\mathcal{G}$ contains at least two clusters of connected vertices.

(i) From the proof of Lemma 6.10 (step (i)) and Lemma 6.5, it follows that any generator $\hat{\mathbf{e}}$ of $\phi_\mathcal{G}$ is a vector in $\mathcal{S}$ with unit norm such that $N - 2$ independent constraints $\mathbf{c}_i^\mathsf{T}\hat{\mathbf{e}} = 0$ hold, with the vectors $\mathbf{c}_i$'s picked from the set $C_{\mathbf{i,b}} \triangleq \{\mathbf{i}_1, \dots, \mathbf{i}_N, \mathbf{b}_1, \dots, \mathbf{b}_{N_\mathcal{E}}\}$.

We term as p the number of constraints of the form $\mathbf{i}_i^\mathsf{T}\hat{\mathbf{e}} = 0$, so that those of the kind $\mathbf{b}_i^\mathsf{T}\hat{\mathbf{e}} = 0$ are $N - 2 - p$, with $0 \leq p \leq N - 2$.

According to the definition of $\mathbf{b}_i$, each of the constraints $\mathbf{b}_i^\mathsf{T}\hat{\mathbf{e}} = 0$ implies that two components of $\hat{\mathbf{e}}$ are equal, i.e. that $\hat{e}_j = \hat{e}_k$, for some pair of indices (j, k). Therefore, from the $N - 2 - p$ constraints of the form $\mathbf{b}_i^\mathsf{T}\hat{\mathbf{e}} = 0$, we can conclude that clus($\mathbf{e}$) contains at most $N - (N - 2 - p) = p + 2$ clusters. We need now to apply the remaining p constraints of the form $\mathbf{i}_i^\mathsf{T}\hat{\mathbf{e}} = 0$; we analyse separately the cases when $p = 0$ or $p > 0$.

---

[1]We set $\mathbf{i}_N^\mathsf{T}\mathbf{e} \leq 0$ because the sign of $\mathbf{i}_N^\mathsf{T}\mathbf{e}$ is automatically determined by the set of inequalities $\{\mathbf{i}_1^\mathsf{T}\mathbf{e} \geq 0, \dots, \mathbf{i}_{N-1}^\mathsf{T}\mathbf{e} \geq 0\}$, by virtue of $\sum_{i=1}^N e_i = 0$.
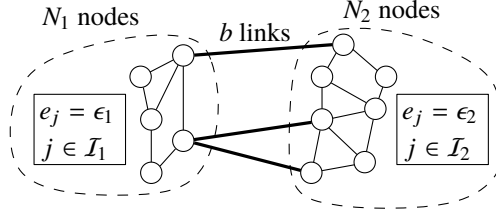
Figure 6.2: A bipartition $\mathcal{B} = \{\mathcal{I}_1, \mathcal{I}_2\}$ of a graph; N_1 and N_2 are the number of vertices in each cluster and b is the number of edges between the clusters.

- If $p = 0$, there are no constraints like $\mathbf{i}_i^{\mathsf{T}} \hat{\mathbf{e}} = 0$ to consider; thus, clus($\hat{\mathbf{e}}$) = $\{\mathcal{I}_1, \mathcal{I}_2\}$ with

$$
\begin{cases}
\hat{e}_j = \epsilon_1, & j \in \mathcal{I}_1, \\
\hat{e}_j = \epsilon_2, & j \in \mathcal{I}_2,
\end{cases}
\tag{6.4}
$$

for some $\epsilon_1, \epsilon_2 \in \mathbb{R}$, with $\epsilon_1, \epsilon_2 \neq 0$ and $\epsilon_1 \neq \epsilon_2$.

- If, on the other hand, $p > 0$, then we need to apply the additional p constraints of the form $\mathbf{i}_i^{\mathsf{T}} \hat{\mathbf{e}} = 0$. Each of these implies an element of $\hat{\mathbf{e}}$ is null. For example, if $p = 1$, we get that $e_i = 0$ for some i. Without loss of generality, assume $e_1 = 0$ then one cluster in clus($\hat{\mathbf{e}}$) will be characterised by all the null elements in $\hat{\mathbf{e}}$ and there will be $Q = p + 2 = 3$ clusters in total.

  Analogously, if $p > 1$, the p elements such that $e_i = 0$ will form one cluster in clus($\mathbf{e}$) so that out of the $p+2$ possible clusters in clus($\hat{\mathbf{e}}$) only $Q = p+2-(p-1) = 3$ will remain. Hence, clus($\hat{\mathbf{e}}$) = $\{\mathcal{I}_1, \mathcal{I}_2, \mathcal{I}_3\}$ with

$$
\begin{cases}
\hat{e}_j = \epsilon_1, & j \in \mathcal{I}_1, \\
\hat{e}_j = \epsilon_2, & j \in \mathcal{I}_2, \\
\hat{e}_j = 0, & j \in \mathcal{I}_3,
\end{cases}
\tag{6.5}
$$

for some $\epsilon_1, \epsilon_2 \in \mathbb{R}$, with $\epsilon_1, \epsilon_2 \neq 0$ and $\epsilon_1 \neq \epsilon_2$.

(ii)   To show that clus($\hat{\mathbf{e}}$) = $\{\mathcal{I}_1, \ldots, \mathcal{I}_Q\}$ contains at least two clusters that are clusters of connected vertices in $\mathcal{G}$ it suffices to notice that in our derivation there were at least two clusters induced by the constraints of the form $\mathbf{b}_i^{\mathsf{T}} \hat{\mathbf{e}} = 0$. Since, by construction, the vectors $\mathbf{b}_i$ represent edges in $\mathcal{G}$ then these clusters must correspond to connected vertices in $\mathcal{G}$.

$\qquad\qquad\qquad\qquad\qquad\qquad\qquad\qquad\qquad\qquad\qquad\qquad\qquad\qquad\qquad$ $\square$

Note that given a bipartition (or a tripartition) of $\mathcal{G}$ we can always find at least a generator $\hat{\mathbf{e}} \in \mathcal{S}$ such that clusters of indexes in clus($\hat{\mathbf{e}}$) corresponds to vertices of $\mathcal{G}$ in that bipartition (or tripartition) verifying (6.4) (or (6.5)). In what follows we will denote by $\phi_{\mathcal{G}}(\mathcal{B})$ the set of values that the function $\phi_{\mathcal{G}}$ takes over each of the vectors $\hat{\mathbf{e}} \in \mathcal{S}$ whose clusterization corresponds to the bipartition $\mathcal{B}$ (analogously for $\phi_{\mathcal{G}}(\mathcal{T})$, being $\mathcal{T}$ a tripartition). We will say that $\phi_{\mathcal{G}}(\mathcal{B}) \leq 0$ if this is true for all values of $\phi_{\mathcal{G}}$ in that set (and equivalently for $\phi_{\mathcal{G}}(\mathcal{T})$).
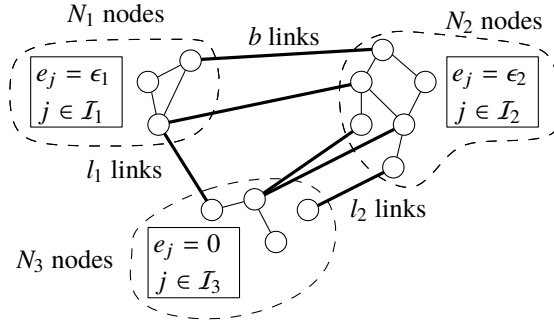
Figure 6.3: A tripartition $\mathcal{T} = \{\mathcal{I}_1, \mathcal{I}_2, \mathcal{I}_3\}$ of a graph; N_1, N_2, N_3 are the number of vertices in each cluster and b, l_1, l_2 are the number of edges between the clusters.
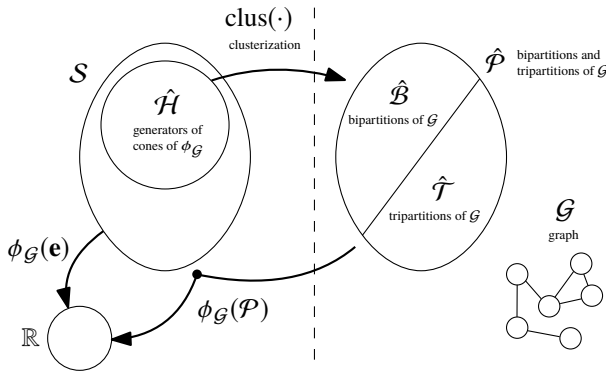
Figure 6.4: Relations between the sets and functions used in Section 6.3.

The relations between the sets $\mathcal{S}, \hat{\mathcal{H}}, \hat{\mathcal{B}}, \hat{\mathcal{T}}, \hat{\mathcal{P}}$ and the functions clus, $\phi_\mathcal{G}$ are summarised in Figure 6.4.

Lemma 6.12. *Given a connected graph $\mathcal{G}$ and its associated star function $\phi_\mathcal{G}$, if $\phi_\mathcal{G} \leq 0$ on all of the bipartitions of $\mathcal{G}$, then $\phi_\mathcal{G} \leq 0$ on all of the tripartitions of $\mathcal{G}$.*

Proof. The proof is composed of three steps. First, we determine what conditions must hold so that $\phi_\mathcal{G}(\mathcal{B}) \leq 0$ for any bipartition $\mathcal{B}$. Then, we do the same for a generic tripartition $\mathcal{T}$. Finally, we show that, for each $\mathcal{T}$, there exists a specific $\mathcal{B}'$ such that $\phi_\mathcal{G}(\mathcal{B}') \leq 0 \Rightarrow \phi_\mathcal{G}(\mathcal{T}) \leq 0$. Hence, if $\phi_\mathcal{G}(\mathcal{B}) \leq 0$ for all $\mathcal{B} \in \hat{\mathcal{B}}$, then also $\phi_\mathcal{G}(\mathcal{T}) \leq 0$ for all $\mathcal{T} \in \hat{\mathcal{T}}$, that is the thesis.

(i) Let us consider a generic bipartition $\mathcal{B} = \{\mathcal{I}_1, \mathcal{I}_2\}$ of $\mathcal{G}$. Then, from (6.2) and (6.4), we can write

$$\phi_\mathcal{G}(\mathcal{B}) = a_1(N_1 |\epsilon_1| + N_2 |\epsilon_2|) - a_2 b |\epsilon_1 - \epsilon_2|, \tag{6.6}$$

where $N_1 = |\mathcal{I}_1|$, $N_2 = |\mathcal{I}_2|$, b is the number of edges connecting vertices in $\mathcal{I}_1$ with vertices in $\mathcal{I}_2$ (see Figure 6.2), and ϵ_1, ϵ_2 are (different non-zero) constants depending on the generic vector $\hat{\mathbf{e}} \in \mathcal{S}$ whose clusterization corresponds to $\mathcal{B}$ according to (6.4).

Even though N_1, N_2, and b depend on the specific $\mathcal{B}$ being considered, we omit this dependence to simplify the notation. Since $\sum_{i=1}^{N} \hat{e}_i = 0$, then $N_1 \epsilon_1 + N_2 \epsilon_2 = 0$, that is $\epsilon_2 = -\frac{N_1}{N_2} \epsilon_1$. Therefore, we may rewrite

$$\phi_{\mathcal{G}}(\mathcal{B}) = 2a_1 N_1 |\epsilon_1| - a_2 b \frac{N_1 + N_2}{N_2} |\epsilon_1|.$$

Hence, $\phi_{\mathcal{G}}(\mathcal{B}) \leq 0$ if and only if

$$a_2 \geq \frac{2a_1 N_1 N_2}{(N_1 + N_2)b}, \tag{6.7}$$

independently from the value of the constants ϵ_1 and ϵ_2 associated to the specific vector whose clusterization is being considered.

(ii) Let us now consider a generic tripartition $\mathcal{T} = \{\mathcal{I}_1, \mathcal{I}_2, \mathcal{I}_3\}$. Using similar arguments to those presented for bipartitions, from (6.2) and (6.5), we obtain

$$\phi_{\mathcal{G}}(\mathcal{T}) = a_1(N_1 |\epsilon_1| + N_2 |\epsilon_2| + N_3 |0|) \\ - a_2(b |\epsilon_1 - \epsilon_2| + l_1 |\epsilon_1 - 0| + l_2 |\epsilon_2 - 0|), \tag{6.8}$$

where $N_1 = |\mathcal{I}_1|$, $N_2 = |\mathcal{I}_2|$, $N_3 = |\mathcal{I}_3|$, and b, l_1, l_2 are the numbers of edges connecting vertices in $\mathcal{I}_1$ with vertices in $\mathcal{I}_2$, vertices in $\mathcal{I}_1$ with vertices in $\mathcal{I}_3$, and vertices in $\mathcal{I}_2$ with vertices in $\mathcal{I}_3$, respectively (see Figure 6.3). N_1, N_2, N_3, b, l_1, and l_2 all depend on $\mathcal{T}$. Since $\sum_{i=1}^{N} \hat{e}_i = 0$, then $N_1 \epsilon_1 + N_2 \epsilon_2 + N_3 \cdot 0 = 0$, that is again $\epsilon_2 = -\frac{N_1}{N_2} \epsilon_1$. In view of this, and multiplying both sides of (6.8) by N_2, we obtain

$$N_2 \phi_{\mathcal{G}}(\mathcal{T}) = 2a_1 N_1 N_2 |\epsilon_1| \\ - a_2(b(N_1 + N_2) |\epsilon_1| + l_1 N_2 |\epsilon_1| + l_2 N_1 |\epsilon_2|).$$

As $N_2 > 0$, this yields that $\phi_{\mathcal{G}}(\mathcal{T}) \leq 0$ if and only if

$$a_2 \geq \frac{2a_1 N_1 N_2}{b(N_1 + N_2) + N_2 l_1 + N_1 l_2}. \tag{6.9}$$

(iii) We now show that

$$\forall \mathcal{T} \in \hat{\mathcal{T}} \; \exists \mathcal{B}' \in \hat{\mathcal{B}} \text{ such that} \quad \phi_{\mathcal{G}}(\mathcal{B}') \leq 0 \Rightarrow \phi_{\mathcal{G}}(\mathcal{T}) \leq 0. \tag{6.10}$$

Let us consider again the generic tripartition $\mathcal{T} = \{\mathcal{I}_1, \mathcal{I}_2, \mathcal{I}_3\}$ introduced in point (ii); see Figure 6.3 for a graphical representation. With an appropriate labelling of the clusters, without loss of generality we can assume that $l_2 \geq l_1$. To any $\mathcal{T}$, we can always associate a specific bipartition $\mathcal{B}' = \{\mathcal{I}_1', \mathcal{I}_2'\}$, where $\mathcal{I}_1' = \mathcal{I}_1$ and $\mathcal{I}_2' = \mathcal{I}_2 \cup \mathcal{I}_3$, characterised by $N_1' = |\mathcal{I}_1'|$, $N_2' = |\mathcal{I}_2'|$, and b' being the number of edges between $\mathcal{I}_1'$ and $\mathcal{I}_2'$. Thus, it follows that $N_1' = N_1$, $N_2' = N_2 + N_3$, and $b' = b + l_1$. According to (6.7), $\phi_{\mathcal{G}}(\mathcal{B}') \leq 0$ if and only if

$$a_2 \geq \frac{2a_1 N_1' N_2'}{(N_1' + N_2')b'} = \frac{2a_1 N_1 (N_2 + N_3)}{(N_1 + N_2 + N_3)(b + l_1)}. \tag{6.11}$$

Next, we prove that (6.11) implies (6.9), independently of $\mathcal{T}$. To that aim, we need to show that

$$\frac{2N_1(N_2 + N_3)}{(N_1 + N_2 + N_3)(b + l_1)} \geq \frac{2N_1 N_2}{b(N_1 + N_2) + N_2 l_1 + N_1 l_2},$$

which is trivially verified by recalling that $l_2 \geq l_1$. The thesis directly follows. $\qquad\square$

We are now ready to give the final result that summarises previous findings and will be used in the proof of the main theorems.

Lemma 6.13. *If $\phi_{\mathcal{G}} \leq 0$ on all the bipartitions of $\mathcal{G}$, then $\phi_{\mathcal{G}} \leq 0$ for all $\mathbf{e} \in \mathcal{S}$.*

Proof. According to Lemma 6.12, since $\phi_{\mathcal{G}}(\mathcal{B}) \leq 0$ for all $\mathcal{B} \in \hat{\mathcal{B}}$, then

$$\phi_{\mathcal{G}}(\mathcal{P}) \leq 0, \forall\, \mathcal{P} \in \hat{\mathcal{P}}. \tag{6.12}$$

Exploiting Lemma 6.11, the clusterization $\mathrm{clus}(\hat{\mathbf{e}})$ of each generator $\hat{\mathbf{e}} \in \hat{\mathcal{H}}$ is a partition $\mathcal{P} \in \hat{\mathcal{P}}$. Therefore, (6.12) implies that

$$\phi_{\mathcal{G}}(\hat{\mathbf{e}}) \leq 0, \forall\, \hat{\mathbf{e}} \in \hat{\mathcal{H}}. \tag{6.13}$$

Since $\phi_{\mathcal{G}}$ is a star function (Lemma 6.10), (6.13) implies the thesis through Lemma 6.9. $\qquad\square$

6.4   Proof of Theorem 5.5

The dynamics of the average state $\tilde{\mathbf{x}}$ of the network under the multilayer control action in (5.3) are given by

$$\dot{\tilde{\mathbf{x}}} = \frac{1}{N} \sum_{i=1}^{N} \mathbf{f}(\mathbf{x}_i; t) + \sum_{i=1}^{N} \sum_{j=1}^{N} L_{ij} \mathbf{\Gamma}(\mathbf{x}_j - \mathbf{x}_i) + \sum_{i=1}^{N} \sum_{j=1}^{N} L_{ij}^{\mathrm{d}} \mathbf{\Gamma}_{\mathrm{d}} \mathrm{sign}(\mathbf{x}_j - \mathbf{x}_i). \tag{6.14}$$

As $\mathbf{L}$ and $\mathbf{L}_{\mathrm{d}}$ are symmetric, the last two terms of the right-hand side of (6.14) are zero, and therefore we have $\dot{\tilde{\mathbf{x}}} = \frac{1}{N} \sum_{i=1}^{N} \mathbf{f}(\mathbf{x}_i; t)$. Therefore, the dynamics of the synchronization error $\mathbf{e}_i$ are given by

$$\dot{\mathbf{e}}_i = \dot{\mathbf{x}}_i - \dot{\tilde{\mathbf{x}}} = \mathbf{f}(\mathbf{x}_i; t) - \frac{1}{N} \sum_{i=1}^{N} \mathbf{f}(\mathbf{x}_i; t) - c \sum_{j=1}^{N} L_{ij} \mathbf{\Gamma} \mathbf{e}_j - c_{\mathrm{d}} \sum_{j=1}^{N} L_{ij}^{\mathrm{d}} \mathbf{\Gamma}_{\mathrm{d}} \mathrm{sign}(\mathbf{e}_j - \mathbf{e}_i),$$

where we used the fact that $\sum_{j=1}^{N} L_{ij}(\mathbf{x}_j - \mathbf{x}_i) = \sum_{j=1}^{N} L_{ij} \mathbf{x}_j = \sum_{j=1}^{N} L_{ij} \mathbf{e}_j$ and that $\mathrm{sign}(\mathbf{x}_j - \mathbf{x}_i) = \mathrm{sign}(\mathbf{e}_j - \mathbf{e}_i)$. Now, consider the candidate common Lyapunov function $V \triangleq \frac{1}{2} \sum_{i=1}^{N} \mathbf{e}_i^{\mathsf{T}} \mathbf{P} \mathbf{e}_i$. Its time derivative is $\dot{V} = \sum_{i=1}^{N} \mathbf{e}_i^{\mathsf{T}} \mathbf{P} \dot{\mathbf{e}}_i$, that is,

$$\begin{aligned}
\dot{V} = {}& \sum_{i=1}^{N} \mathbf{e}_i^{\mathsf{T}} \mathbf{P} \left(\mathbf{f}(\mathbf{x}_i; t) - \frac{1}{N} \sum_{i=1}^{N} \mathbf{f}(\mathbf{x}_i; t) \right) \\
& - c \sum_{i=1}^{N} \sum_{j=1}^{N} L_{ij} \mathbf{e}_i^{\mathsf{T}} \mathbf{P} \mathbf{\Gamma} \mathbf{e}_j - c_{\mathrm{d}} \sum_{i=1}^{N} \sum_{j=1}^{N} L_{ij}^{\mathrm{d}} \mathbf{e}_i^{\mathsf{T}} \mathbf{P} \mathbf{\Gamma}_{\mathrm{d}} \mathrm{sign}(\mathbf{e}_j - \mathbf{e}_i).
\end{aligned} \tag{6.15}$$

As $\sum_{i=1}^{N} \mathbf{e}_i = 0$, we have $\sum_{i=1}^{N} \mathbf{e}_i^\mathsf{T} \mathbf{P} \mathbf{f}(\tilde{\mathbf{x}}; t) = 0$ and $\sum_{i=1}^{N} \mathbf{e}_i^\mathsf{T} \mathbf{P} \left(\sum_{i=1}^{N} \mathbf{f}(\mathbf{x}_i; t)/N \right) = 0$. Thus, we can rewrite (6.15) as

$$\dot{V} = \sum_{i=1}^{N} \mathbf{e}_i^\mathsf{T} \mathbf{P} \left[\mathbf{f}(\mathbf{x}_i; t) - \mathbf{f}(\tilde{\mathbf{x}}; t) \right] - c \sum_{i=1}^{N} \sum_{j=1}^{N} L_{ij} \mathbf{e}_i^\mathsf{T} \mathbf{P} \mathbf{\Gamma} \mathbf{e}_j - c_\mathrm{d} \sum_{i=1}^{N} \sum_{j=1}^{N} L_{ij}^\mathrm{d} \mathbf{e}_i^\mathsf{T} \mathbf{P} \mathbf{\Gamma}_\mathrm{d} \mathrm{sign}(\mathbf{e}_j - \mathbf{e}_i).$$

In addition, the communication graphs are undirected; therefore, $L_{ij}^\mathrm{d} = L_{ji}^\mathrm{d}$, and for each term $\mathbf{e}_i^\mathsf{T} \mathbf{P} \mathbf{\Gamma}_\mathrm{d} \mathrm{sign}(\mathbf{e}_j - \mathbf{e}_i)$, there exists another term $\mathbf{e}_j^\mathsf{T} \mathbf{P} \mathbf{\Gamma}_\mathrm{d} \mathrm{sign}(\mathbf{e}_i - \mathbf{e}_j)$. Hence, we may recast $\dot{V}$ as

$$\dot{V} = \sum_{i=1}^{N} \mathbf{e}_i^\mathsf{T} \mathbf{P} \left[\mathbf{f}(\mathbf{x}_i; t) - \mathbf{f}(\tilde{\mathbf{x}}; t) \right] - c \sum_{i=1}^{N} \sum_{j=1}^{N} L_{ij} \mathbf{e}_i^\mathsf{T} \mathbf{P} \mathbf{\Gamma} \mathbf{e}_j - c_\mathrm{d} \sum_{(i,j) \in \mathcal{E}_\mathrm{d}} (\mathbf{e}_i - \mathbf{e}_j)^\mathsf{T} \mathbf{P} \mathbf{\Gamma}_\mathrm{d} \mathrm{sign}(\mathbf{e}_i - \mathbf{e}_j),$$

recalling that $\mathcal{E}_\mathrm{d}$ is the set of edges in the graph $\mathcal{G}_\mathrm{d}$. Then, we use the hypothesis that $\mathbf{f}$ is σ-QUAD and get

$$\dot{V} \le \sum_{i=1}^{N} \left(\mathbf{e}_i^\mathsf{T} \mathbf{Q} \mathbf{e}_i + \mathbf{e}_i^\mathsf{T} \mathbf{M} \mathrm{sign}(\mathbf{e}_i) \right)$$
$$- c \sum_{i=1}^{N} \sum_{j=1}^{N} L_{ij} \mathbf{e}_i^\mathsf{T} \mathbf{P} \mathbf{\Gamma} \mathbf{e}_j - c_\mathrm{d} \sum_{(i,j) \in \mathcal{E}_\mathrm{d}} (\mathbf{e}_i - \mathbf{e}_j)^\mathsf{T} \mathbf{P} \mathbf{\Gamma}_\mathrm{d} \mathrm{sign}(\mathbf{e}_i - \mathbf{e}_j). \tag{6.16}$$

Now, if we define $\bar{\mathbf{y}} \triangleq \left(\mathbf{B}_\mathrm{d}^\mathsf{T} \otimes \mathbf{I}_n \right) \bar{\mathbf{e}}$, where $\mathbf{B}_\mathrm{d}$ is the incidence matrix of $\mathcal{G}_\mathrm{d}$, then we can rewrite (6.16) as $\dot{V} \le W_1 + W_2$, where

$$W_1 \triangleq \bar{\mathbf{e}}^\mathsf{T} \left(\mathbf{I}_N \otimes \mathbf{Q} - c \mathbf{L} \otimes \mathbf{P} \mathbf{\Gamma} \right) \bar{\mathbf{e}}, \tag{6.17}$$

$$W_2 \triangleq \bar{\mathbf{e}}^\mathsf{T} \left(\mathbf{I}_N \otimes \mathbf{M} \right) \mathrm{sign}(\bar{\mathbf{e}}) - c_\mathrm{d} \bar{\mathbf{y}}^\mathsf{T} \left(\mathbf{I}_{N_{\mathcal{E}_\mathrm{d}}} \otimes \mathbf{P} \mathbf{\Gamma}_\mathrm{d} \right) \mathrm{sign}(\bar{\mathbf{y}}). \tag{6.18}$$

We can then study W_1 and W_2 separately, so as to find conditions that guarantee the former is negative definite and the latter is semi-negative definite.

6.4.1 Negativity of W_1

To find a condition such that $W_1 < 0$, we observe that

$$W_1 \le \|\bar{\mathbf{e}}\|_2^2 \|\mathbf{Q}\|_2 - \bar{\mathbf{e}}^\mathsf{T} \left(c \mathbf{L} \otimes \mathbf{P} \mathbf{\Gamma} \right) \bar{\mathbf{e}}.$$

Since $\sum_{i=1}^{N} \mathbf{e}_i = \mathbf{0}_n \Leftrightarrow \sum_{i=0}^{N-1} \bar{e}_{i \cdot n + h} = 0 \ \forall h = 1, \dots, n$, we can apply Corollary 13.4.2 in [68] and get

$$W_1 \le \|\bar{\mathbf{e}}\|_2^2 \left[\|\mathbf{Q}\|_2 - c \lambda_2(\mathbf{L}) \lambda_{\min}(\mathrm{sym}(\mathbf{P} \mathbf{\Gamma})) \right].$$

Therefore, $W_1 < 0$ if $c > c^*$, with c^* defined as in (5.11). Note that the fact that $\mathcal{G}$ is connected ensures that $\lambda_2(\mathbf{L}) > 0$.

6.4.2 Semi-negativity of W_2

Next, we seek an expression of the threshold value c_d^* such that $W_2 \leq 0$ if $c_d \geq c_d^*$. Firstly, consider that, from (6.18), using Lemmas 6.2 and 6.3, we have

$$W_2 \leq \|\bar{\mathbf{e}}\|_1 \|\mathbf{M}\|_\infty - c_d \|\bar{\mathbf{y}}\|_1 \mu_\infty^-(\mathbf{P\Gamma}_d). \tag{6.19}$$

Using the definition of the vector 1-norm, we have $\|\bar{\mathbf{e}}\|_1 = \sum_{i=1}^{nN} |\bar{e}_i| = \sum_{h=1}^n \|\mathbf{e}^h\|_1 = \sum_{h=1}^n \sum_{i=1}^N |\mathbf{i}_i^\mathsf{T} \mathbf{e}^h|$, where $\mathbf{i}_i$ and $\mathbf{e}^h$ are defined in Sections 1.5 and 2.1. Note that $\mathbf{e}^h \in \mathcal{S}$, with $\mathcal{S}$ being defined in (6.1). Similarly, it is straightforward to compute that $\|\bar{\mathbf{y}}\|_1 = \sum_{h=1}^n \sum_{i=1}^{N_{\mathcal{E}_d}} |\mathbf{b}_i^\mathsf{T} \mathbf{e}^h|$, where $\mathbf{b}_i$ are the columns of the incidence matrix $\mathbf{B}_d$ of $\mathcal{G}_d$. For the sake of compactness we define $M \triangleq \|\mathbf{M}\|_\infty$ and $\mu \triangleq \mu_\infty^-(\mathbf{P\Gamma}_d)$. Thus, we can recast (6.19) as $W_2 \leq \sum_{h=1}^n W_2^h$, where

$$W_2^h(\mathbf{e}^h) \triangleq M \sum_{i=1}^N |\mathbf{i}_i^\mathsf{T} \mathbf{e}^h| - c_d \mu \sum_{i=1}^{N_{\mathcal{E}_d}} |\mathbf{b}_i^\mathsf{T} \mathbf{e}^h|. \tag{6.20}$$

The analytical framework and results presented in Sections 6.2 and 6.3 can be used to more easily assess the semi-negativity of W_2^h. In fact, W_2^h is in the form (6.2), and thus is a star function associated to the graph $\mathcal{G}_d$; see Definition 6.8 and Lemma 6.10. Exploiting Lemma 6.13, it is immediate to state that $W_2^h(\mathbf{e}^h) \leq 0$ for all $\mathbf{e}^h \in \mathcal{S}$, i.e., globally, if $W_2^h(\mathcal{B}) \leq 0$ for all $\mathcal{B} \in \hat{\mathcal{B}}$; $\hat{\mathcal{B}}$ being the set of all bipartitions of $\mathcal{G}_d$.

Consider a generic bipartition $\mathcal{B} = \{\mathcal{I}_1, \mathcal{I}_2\}$ of $\mathcal{G}_d$, where $\mathcal{I}_1$ and $\mathcal{I}_2$ are the indices of the vertices in the two connected clusters. Moreover, let $N_1 = |\mathcal{I}_1|$, $N_2 = |\mathcal{I}_2|$, and b be the number of edges connecting a vertex in $\mathcal{I}_1$ with a vertex in $\mathcal{I}_2$ (see Figure 6.2); note that N_1, N_2, and b depend on $\mathcal{B}$. According to (6.6) and (6.7), $W_2^h(\mathcal{B}) \leq 0$ if and only if

$$c_d \geq \frac{2M}{N\mu} \left(\frac{N_1 N_2}{b} \right), \tag{6.21}$$

where we used the fact that $N_1 + N_2 = N$. We highlight that this last step is independent from h; therefore, if (6.21) holds, then $W_2^h(\mathcal{B}) \leq 0 \;\forall h = 1, \ldots, n$. From the hypotheses we know that

$$c_d \geq c_d^* \triangleq \frac{1}{\delta_{\mathcal{G}_d}} \frac{M}{\mu} = \frac{2M}{N\mu} \frac{1}{\min_{C \in \hat{C}_{\mathcal{G}_d}} \left(\frac{b}{N_1 N_2} \right)}. \tag{6.22}$$

where $\delta_{\mathcal{G}_d}$ is the minimum density of $\mathcal{G}_d$ (Definition 4.9) and $\hat{C}_{\mathcal{G}_d}$ is the set of all possible cuts on $\mathcal{G}_d$. (6.22) can be reformulated as

$$c_d \geq \frac{2M}{N\mu} \frac{1}{\min_{\mathcal{B} \in \hat{\mathcal{B}}} \left(\frac{b}{N_1 N_2} \right)} = \frac{2M}{N\mu} \max_{\mathcal{B} \in \hat{\mathcal{B}}} \left(\frac{N_1 N_2}{b} \right).$$

Therefore, (6.21) holds for all $\mathcal{B} \in \hat{\mathcal{B}}$. This ensures that $W_2^h(\mathcal{B}) \leq 0$ for all $\mathcal{B} \in \hat{\mathcal{B}}$, which through Lemma 6.13 gives $W_2^h \leq 0$ globally. As mentioned previously, if $W_2^h \leq 0$ for some h, then $W_2^h \leq 0$ for all h, and hence $W_2 \leq 0$. This completes the proof, as $\dot{V} = W_1 + W_2 < 0$ globally.

6.5   Proof of Theorem 5.6

Starting from (6.16) in the proof of Theorem 5.5, exploiting the fact that $\mathbf{M} = \mathrm{diag}([m_1 \quad \cdots \quad m_n])$ and $\mathbf{P\Gamma}_{\mathrm{d}} = \mathrm{diag}([\gamma_1 \quad \cdots \quad \gamma_n])$, we have

$$\dot{V} \leq \sum_{i=1}^{N} \mathbf{e}_i^{\mathsf{T}} \mathbf{Q} \mathbf{e}_i - c \sum_{i=1}^{N} \sum_{j=1}^{N} L_{ij} \mathbf{e}_i^{\mathsf{T}} \mathbf{P\Gamma} \mathbf{e}_j + \sum_{i=1}^{N} \sum_{h=1}^{n} m_h \left| e_{i,h} \right| - c_{\mathrm{d}} \sum_{(i,j) \in \mathcal{E}_{\mathrm{d}}} \sum_{h=1}^{n} \gamma_h \left| e_{i,h} - e_{j,h} \right|$$

$$\triangleq W_1 + \widehat{W}_2,$$

where W_1 is defined as in (6.17) and $\widehat{W}_2 = \sum_{h=1}^{n} \widehat{W}_2^h$, with

$$\widehat{W}_2^h \triangleq m_h \sum_{i=1}^{N} \left| \mathbf{i}_i^{\mathsf{T}} \mathbf{e}^h \right| - c_{\mathrm{d}} \gamma_h \sum_{i=1}^{N_{\mathcal{E}_{\mathrm{d}}}} \left| \mathbf{b}_i^{\mathsf{T}} \mathbf{e}^h \right|. \tag{6.23}$$

In Theorem 5.3, we have proved that $W_1 < 0$ if the hypotheses of the present theorem hold.[2] Note that $\widehat{W}_2^h$ has the exact same structure as W_2^h in (6.20), with the difference being the multiplicative constants M and μ in W_2^h, and m_h and γ_h in $\widehat{W}_2^h$. In (6.23), if $m_h \leq 0$, then $\widehat{W}_2^h \leq 0$ even if $\gamma_h = 0$ (recall that in general $\gamma_h \geq 0$). Differently, if $m_h > 0$, following steps analogous to that in the proof of Theorem 5.5, it is possible to show that $\widehat{W}_2^h \leq 0$ if

$$c_{\mathrm{d}} \geq \frac{1}{\delta_{\mathcal{G}_{\mathrm{d}}}} \frac{m_h}{\gamma_h}.$$

Finally, in order to have $\widehat{W}_2^h \leq 0$ for all $h = 1, \ldots, n$, we require that $c_{\mathrm{d}} \geq c_{\mathrm{d}}^*$, with c_{d}^* being defined in (5.13). Therefore, we get $\widehat{W}_2 = \sum_{h=1}^{n} \widehat{W}_2^h \leq 0$ and $\dot{V} = W_1 + \widehat{W}_2 < 0$, globally.

---

[2]In Theorem 5.3, a matrix named $\mathbf{G}$ is present in place of $\mathbf{P\Gamma}$.

7 Discussion

We addressed the challenging problem of proving global asymptotic convergence to synchronization in a network of piecewise-smooth dynamical systems.

Initially, we have discussed spontaneous synchronizability. Specifically, we started by providing sufficient conditions for ensembles of QUAD PWS systems, applicable to problems with a large variety of coupling laws, including linear diffusive coupling with indefinite inner coupling matrix. Then, we showed that, for more general σ-QUAD agents, adding a discontinuous coupling layer to the commonly used diffusive coupling protocol is sufficient to ensure convergence. All this without employing, as done in previous attempts in the literature, costly centralised control actions on all the nodes. In all cases we provided critical values of the coupling gains required for convergence, even when the inner coupling matrices are not positive definite. The conditions depend explicitly on structural properties of the underlying network graphs that can be computed algorithmically. In particular, we introduced the concept of *minimum density* of a graph that can be used to compute the critical coupling gain of the discontinuous control layer.

An open problem left for further study is to investigate if there exist some best structures of the diffusive and discontinuous coupling layers in terms of performance, robustness and stability. For example, numerical simulations reported in Section 5.5.4 show that different layers' structures can enhance the regions in the control parameter space where synchronization is attained.

Part II

Control and estimation of piecewise-smooth systems

8   Adaptive and quasi-sliding control of shimmy in landing gears

8.1   Introduction to shimmy in landing gears

When taking-off, landing or taxiing, any airplane might experience vibrations due to unstable oscillation of the nose landing gear (NLG). This phenomenon, also known as *shimmy*, is often unpredictable with consequences ranging from annoying vibrations to serious damage or even collapse of the airplane [11]. Shimmy is not an exclusive problem in aeronautics; in fact, motorcycles and cars also display a similar issue which is often termed as *wobble* [88].

The study of shimmy can be traced back to the early 20s when the first tires were manufactured [120]. Since then, many mathematical models have been proposed aiming at replicating these oscillations and uncovering the main causes for their emergence (see [11, 132, 120] and references therein for a detailed list of shimmy models). One of the main causes of shimmy is the interaction of the tire with the road. As a matter of fact, the presence of a lateral force on the tire produces a side slip angle, and thus rotations of the NLG. This in turn produces further lateral forces on the tire, thus creating a repetitive (positive-feedback) loop that causes oscillations. Recently, it has also been shown that shimmy can be caused by other nonlinear effects such as friction [154], free-play, and gyroscopic forces [72]. Therefore, designing and implementing control approaches for suppressing shimmy despite model uncertainties is of great importance for reliability and safety of airplanes on the ground. It is worth mentioning that shimmy control strategies should guarantee fast convergence and most importantly a small overshoot of approximately one degree at most. The classic solutions to reduce shimmy are based on the adoption of passive strategies, where the aim is to increase the NLG stiffness and damping constant by using different construction materials or additional passive dampers, respectively [118]. However, airplanes are subject to a plethora of unexpected and dynamic disturbances like changing loads and nonuniform tire-road interfaces; in addition, aircrafts require frequent maintenance, making passive approaches less effective and costly [133].

Moreover, recent developments in the aircraft industry are aimed at implementing fly-by-wire strategy, replacing mechanical and pneumatic actuators by electromechanical devices [12]. In fact, novel steering architectures consider electromechanical actuators where the gear rotation is controlled by a brush-less motor located on the top of the turning tube [89]. Within this context, the use of active control solutions for suppressing shimmy can be easily implemented [13]. Indeed, in the last decade, different active control strategies for shimmy have been proposed. For instance, in [69], a feedback linearization approach based on full state measurements has been shown to be effective in suppressing the oscillations; however, nonlinearities in the model are assumed to be perfectly known. This approach was later extended in [118] to the case where the nonlinear functions are unknown and they are estimated using adaptive strategies and fuzzy logic theory. More recently, in [70], a robust model predictive control was designed for a linearized model of an NLG. Differently, in [133], a nonlinear optimal control was presented based on the use of state-dependent Riccati equations; furthermore, a switching action in the controller was added to better stabilize the closed-loop system. Finally, a simpler PID controller is utilized in [107], where the control gains are designed using a decline population swarm optimization technique.

Previous control approaches either consider linearized models and assume full state measurements to be available or adopt very complex and sophisticated control solutions [118, 70, 133, 107]. In contrast, in this work we only use partial state measurements and we also test the controllers in the case that the nonlinear terms in the model are uncertain. In particular, we propose the use of either a model reference adaptive control (MRAC) with minimal control synthesis (MCS) [129], or a zero-average dynamics (ZAD) control [62]. To reconstruct the inaccessible states, and hence close the loop, we make use of a classic Luenberger observer which is designed under the assumption that the vector field is QUAD [39] rather than Lipschitz continuous (as is usually done in this type of problem). We show that the QUAD condition provides less conservative results, so that lower values of the control gains can be chosen, thus avoiding large overshoots in the closed-loop system.

8.2   Problem Statement

8.2.1   Nose landing gear model

We consider a simplified model of a single wheeled aircraft's nose landing gear (NLG) with an electromechanical actuator (see Figure 8.1), which is described by the third order nonlinear differential equation given by [127]

$$\begin{cases} I_z \ddot{\psi}(t) = M_N(\psi(t), \dot{\psi}(t)) + M_T(\alpha(t), \dot{\psi}(t)) + \tau(t), \\ \sigma \dot{\alpha}(t) = V(\psi(t) - \alpha(t)) + (e - a)\dot{\psi}(t), \end{cases}$$

where $\psi(t)$ [rad] and $\alpha(t)$ [rad] are the state variables denoting the yaw and slip angles respectively, I_z is the moment of inertia about the z-axis, V is the wheel forward velocity, e is the wheel caster length, a is the half contact length of the tire on the ground, and σ is
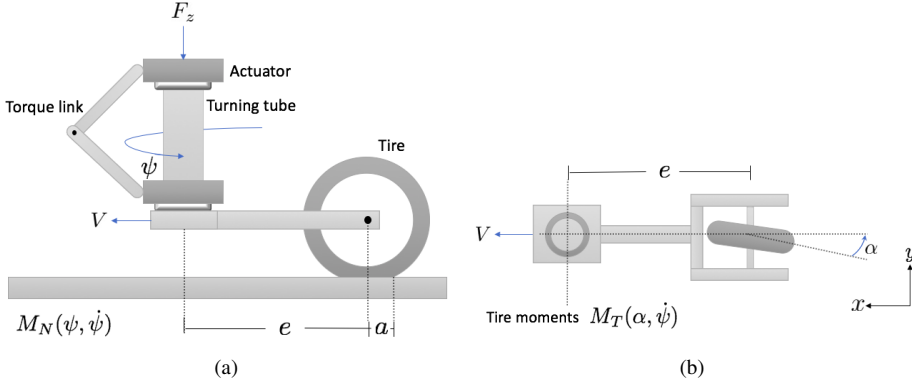
Figure 8.1: Simplified model of an NLG: (a) side and (b) top views.

the relaxation length of tire deflection. The torque $M_N(\psi(t), \dot\psi(t)) \triangleq c\psi(t) + k\dot\psi(t)$ is the sum of a linear elastic torque provided by the turning tube, with constant torsional rate c, and a linear damping term, with coefficient k, that models viscous frictions coming from the shock absorber on the bearing of the oil-pneumatic and the shimmy damper. An external torque, $\tau(t) \triangleq u(t) + \zeta(t)$, models the action $u(t)$ exerted by the control input and some disturbance $\zeta(t)$. For what concerns the values of the parameters, we use those reported in Table 8.1, as in [127]. Moreover, $M_T(\alpha(t), \dot\psi(t)) \triangleq M_D(\dot\psi) + M_G(\alpha)$ represents the tire moments originated from tire damping and deformations. Specifically, $M_D(\dot\psi) \triangleq (\kappa/V)\psi(t)$ is the damping term with coefficient κ, whereas $M_G(\alpha)$ describes the interaction between the tire and the ground. This interaction is highly nonlinear and is due to lateral tire deformations caused by side slip; it is given by

$$M_G(\alpha) = M_z(\alpha) - eF_y(\alpha),$$

where $M_z(\alpha)$ and $F_y(\alpha)$ are nonlinear functions representing the aligning torque about the tire's center and the tire side force, respectively. In particular, we consider two different pairs of functions approximating $M_z(\alpha)$ and $F_y(\alpha)$. The first one is a *piecewise-smooth approximation*:

$$M_{z,1}(\alpha) = \begin{cases} F_z c_{M,\alpha} \dfrac{\alpha_g}{\pi} \sin\left(\dfrac{\pi\alpha}{\alpha_g}\right), & \text{if } |\alpha| \leq \alpha_g, \\ 0, & \text{otherwise,} \end{cases} \tag{8.1}$$

$$F_{y,1}(\alpha) = \frac{c_{F,\alpha} F_z}{2} \left(|\alpha + \delta| - |\alpha - \delta|\right), \tag{8.2}$$

where $\alpha_g = 10\pi/180$ and $\delta = 5\pi/180$. The second one is a *smooth approximation*:

$$M_{z,2}(\alpha) = c_{M,\alpha} F_z \gamma_M \frac{2\alpha\alpha_M}{\alpha^2 + \alpha_M^2}, \tag{8.3}$$

Table 8.1: NLG parameters

Parameter	Symbol	Value	Unit
velocity	V	$[0, 80]$	m/s
half contact length	a	0.1	m
caster length	e	0.1	m
moment of inertia	I_z	1	kg·m^2
vertical force	F_z	9000	N
torsional spring rate	c	-100000	N·m/rad
side force derivative	$c_{F,\alpha}$	20	1/rad
moment derivative	$c_{M,\alpha}$	-2	m/rad
torsional damping constant	k	-10	N·m·s/rad
tread width moment constant	κ	-270	N·m^2/rad
relaxation length	$\sigma = 3a$	0.3	m

$$F_{y,2}(\alpha) = c_{F,\alpha} F_z \gamma_F \frac{2\alpha\alpha_F}{\alpha^2 + \alpha_F^2}, \qquad (8.4)$$

where $\alpha_M = 3\pi/180$, $\gamma_M = 0.1\alpha_g/\pi$, $\alpha_F = 3\alpha_g$, and $\gamma_F = 0.085$. The functions $M_{z,1}(\alpha)$, $M_{z,2}(\alpha)$, $F_{y,1}(\alpha)$, and $F_{y,2}(\alpha)$ are shown in Figure 8.2.

The NLG dynamics can be written in compact form as

$$\begin{cases} \dot{\mathbf{x}}(t) = \mathbf{A}\mathbf{x}(t) + \mathbf{f}(\mathbf{x}) + \mathbf{B}u(t) + \mathbf{B}\zeta(t), \\ \mathbf{y}(t) = \mathbf{C}\mathbf{x}(t), \end{cases} \qquad \mathbf{C} = \begin{bmatrix} 1 & 0 & 0 \\ 0 & 1 & 0 \end{bmatrix}, \ \mathbf{x}(0) = \mathbf{x}_0, \qquad (8.5)$$

where $\mathbf{y}$ is the output, and

$$\mathbf{x} \triangleq \begin{bmatrix} \psi \\ \dot{\psi} \\ \alpha \end{bmatrix}, \quad \mathbf{f}(\mathbf{x}) \triangleq \begin{bmatrix} 0 \\ M_G(\alpha)/I_z \\ 0 \end{bmatrix}, \quad \mathbf{B} \triangleq \begin{bmatrix} 0 \\ 1/I_z \\ 0 \end{bmatrix},$$

and

$$\mathbf{A} \triangleq \begin{bmatrix} 0 & 1 & 0 \\ c/I_z & (k/I_z) + (\kappa/(I_z V)) & 0 \\ V/\sigma & (e-a)/\sigma & -V/\sigma \end{bmatrix}.$$

Note that we only consider the yaw angle ψ and its velocity $\dot{\psi}$ as the available outputs. In fact, ψ can be measured using a RVDT (Rotary Variable Differential Transformer) sensor on the NLG, while the velocity $\dot{\psi}$ can be easily obtained from ψ or using a dedicated sensor [118]. Moreover, the state variable α is related to the lateral displacement of the tire, and, as a consequence, it is much more cumbersome to design appropriate sensors to accurately measure this variable [118]. Therefore, the challenge is to design an appropriate observer for reconstructing this missing state, together with robust controllers that suppress undesired oscillations, while guaranteeing fast convergence and overshoots lower than 1°.
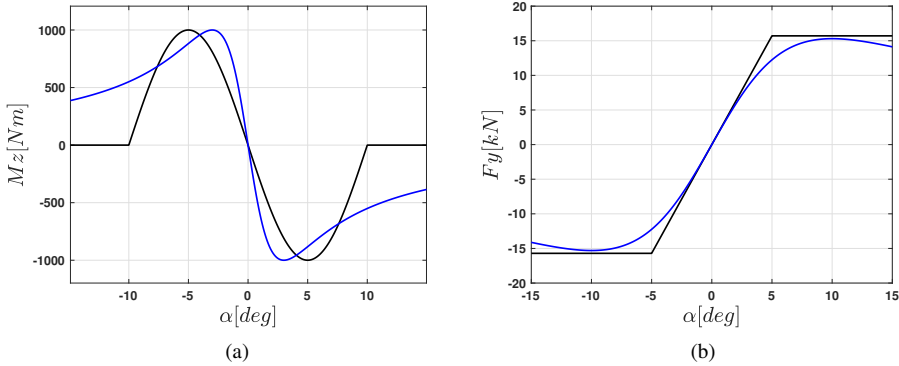
Figure 8.2: Approximating functions for $M_z(\alpha)$ (a) and $F_y(\alpha)$ (b). Black and blue lines represent the piecewise-smooth and smooth approximations, respectively.

8.2.2   Open-loop dynamics: bifurcation diagrams

To illustrate the control problem, we start by showing the NLG dynamics in the absence of control ($u(t) = 0$). More specifically, we describe how using either of the two different approximations for the nonlinear forces M_z and M_y affects the system dynamics. To that aim, we compute bifurcation diagrams of system (8.5) for both approximations. Indeed, bifurcation diagrams are an important tool for analysis of nonlinear systems and have been recently used for studying shimmy behavior [72]. We select the forward velocity V as bifurcation parameter, as increasing or decreasing it corresponds to the common scenarios of taking off, landing or taxiing. We choose to vary the velocity in the interval $[0, 80]$ m/s—common in small planes—using unitary steps. For each value of the forward velocity, we plot the minimum and maximum amplitudes $\tilde{\psi}$ and $\tilde{\alpha}$ of the steady state response for the states ψ and α, respectively (see Figure 8.3). Note that, for both the piecewise-smooth and the smooth approximation, we observe the system undergo a Hopf bifurcation at $V = 20$ and $V = 16.5$, respectively. This suggests that different approximations of the nonlinear moment M_D shift the bifurcation point. Hence, designing robust control strategies that can cope with uncertainty on the nonlinear forces M_z and M_y is crucial, given that in real world scenarios these moments are not known exactly or their parameters might change over time. Moreover, the peak oscillation amplitude $\tilde{\psi}$ is found to be 26.4 for both approximations, and is reached when $V = 30$ and $V = 46.5$, respectively. As for the frequency of the oscillations, in both cases it is approximately 50 Hz.
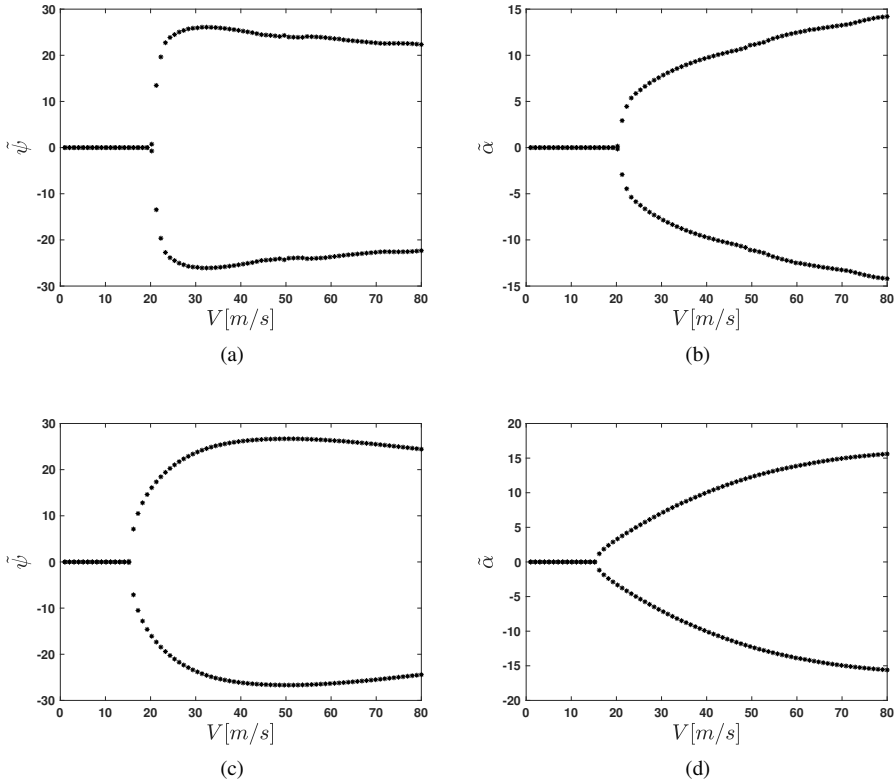
Figure 8.3: Bifurcation diagrams varying the velocity V with the nonlinear function $\mathbf{f}(\mathbf{x})$ being: (a, b) non-smooth, (c, d) smooth. $\tilde{\psi}$ (a, c) and $\tilde{\alpha}$ (b, d) represent the minimum and maximum amplitude of the steady state trajectory for ψ and α, respectively.

8.3 Controlling Shimmy

We employ two different control strategies for attenuating shimmy vibrations: namely, a Zero Average Dynamics (ZAD) control [62] and a model reference control based on Minimal Control Synthesis (MCS) [129]. These control strategies require full knowledge of the state variables; however, we only have access to the output $\mathbf{y}(t)$. Hence, first we need to design an observer for reconstructing the missing states.

8.3.1 Observer design

Consider the classic Luenberger observer given by

$$\dot{\mathbf{x}}(t) = \mathbf{A}\hat{\mathbf{x}}(t) + \mathbf{B}u(t) + \mathbf{f}(\hat{\mathbf{x}}(t)) - \mathbf{L}(\mathbf{C}\hat{\mathbf{x}}(t) - \mathbf{y}(t)). \qquad (8.6)$$

The pressing challenge is to design appropriately the matrix $\mathbf{L}$ that guarantees $\hat{\mathbf{x}}(t) \to \mathbf{x}(t)$ as $t \to \infty$. To that aim we define the observation error $\mathbf{e}(t) \triangleq \hat{\mathbf{x}}(t) - \mathbf{x}(t)$ and present the following result.

Proposition 8.1. *Observer* (8.6) *asymptotically reconstructs the states of system* (8.5), *that is,* $\lim_{t \to +\infty} \|\mathbf{e}(t)\| = 0$, *if the following conditions are fulfilled:*

(i) *there exist a nonzero constant ρ and a symmetric positive definite matrix $\mathbf{P}$ such that* $(\mathbf{v}_1 - \mathbf{v}_2)^\mathsf{T}\mathbf{P}(\mathbf{f}(\mathbf{v}_1) - \mathbf{f}(\mathbf{v}_2)) \leq \rho(\mathbf{v}_1 - \mathbf{v}_2)^\mathsf{T}(\mathbf{v}_1 - \mathbf{v}_2), \forall\, \mathbf{v}_1, \mathbf{v}_2 \in \Omega \subseteq \mathbb{R}^3$,
(ii) *there exist a generic matrix $\mathbf{L}$ and a symmetric positive definite matrix $\mathbf{Q}$ such that* $\mathbf{P}(\mathbf{A} - \mathbf{LC}) + (\mathbf{A} - \mathbf{LC})^\mathsf{T}\mathbf{P} = -\mathbf{Q}$,
(iii) $\lambda_{\min}(\mathbf{Q}) > \rho$.

Proof. The proof follows from choosing $V = \mathbf{e}^\mathsf{T}\mathbf{Pe}$ as candidate Lyapunov function [119], yielding $\dot{V} \leq -\mathbf{e}^\mathsf{T}\mathbf{Qe} + \mathbf{e}^\mathsf{T}\mathbf{P}(\mathbf{f}(\hat{\mathbf{x}}) - \mathbf{f}(\mathbf{x}))$. Then, $\dot{V} < 0$ if the three conditions are fulfilled, which completes the proof. □

We wish to highlight two facts. Firstly, condition (i) is the *QUAD* condition (given in Definition 2.3), widely used for proving convergence in complex networks [39] (the special case when $\mathbf{P} = \mathbf{I}_n$ is also known as *one-sided Lipschitz continuity* [34, 151], given in Definition A.2). In fact, several nonlinear possibly chaotic systems satisfy this condition [39]. Moreover, condition (ii) is standard within the context of observer design [119, 151], and can be easily solved by using standard optimization software. Secondly, one of the main issues when designing Luenberger observers for nonlinear systems are the restrictive synthesis conditions based on Lipschitz continuity of the vector-fields [119]. In fact, for some systems, this condition might not be fulfilled or the Lipschitz constant might be excessively large, yielding to overly conservative results [149]. Indeed, as we show below, the high value of the Lipschitz constant for the NLG model considered here yields a matrix $\mathbf{L}$ with large entries. Although convergence is guaranteed, performance is not, since high gains (entries of $\mathbf{L}$) would cause overshoots larger than $1°$. On the other hand, the QUAD condition is more general than the Lipschitz condition [39] (i.e. a wider class of nonlinear systems satisfy it), and most importantly it provides less conservative results. As a matter of fact, any contracting vector field or system with bounded Jacobian is QUAD [39].

Next, we use Proposition 8.1 to find the matrix $\mathbf{L}$. Thus, we first start by noticing that the nonlinear function $\mathbf{f}(\mathbf{x})$ given by either (8.1)-(8.2) or (8.3)-(8.4) has bounded Jacobian. For the sake of simplicity, we only consider the piecewise-linear function (8.1)-(8.2),

whose Jacobian matrix $\mathbf{Df}$ is given by

$$\mathbf{Df} = \begin{bmatrix} 0 & 0 & 0 \\ 0 & 0 & Df_{23} \\ 0 & 0 & 0 \end{bmatrix},$$

where

$$Df_{23} = \begin{cases} m_1 \cos(\alpha\pi/\alpha_g) - m_2, & \text{if } |\alpha| \leq \delta \\ m_1 \cos(\alpha\pi/\alpha_g), & \text{if } |\alpha| > \delta \text{ and } |\alpha| \leq \alpha_g, \\ 0, & \text{otherwise} \end{cases}$$

with $m_1 \triangleq F_z c_{M,\alpha}$ and $m_2 = ec_{F,\alpha}F_z$. Next, we define $\mathbf{g}(\theta) \triangleq \mathbf{f}(\mathbf{v}_2 + \theta(\mathbf{v}_1 - \mathbf{v}_2))$, for $\theta \in [0,1]$. From the fundamental theorem of calculus, one has

$$\mathbf{f}(\mathbf{v}_1) - \mathbf{f}(\mathbf{v}_2) = \mathbf{g}(1) - \mathbf{g}(0) = \int_0^1 \frac{d\mathbf{g}(\theta)}{d\theta} d\theta = \left[\int_0^1 \mathbf{Df}(\mathbf{v}_2 + \theta(\mathbf{v}_1 - \mathbf{v}_2))d\theta \right] (\mathbf{v}_1 - \mathbf{v}_2).$$

Thus, we have that

$$\|\mathbf{f}(\mathbf{v}_1) - \mathbf{f}(\mathbf{v}_2)\| \leq \sup_{\theta \in [0,1]} \|\mathbf{Df}(\mathbf{v}_2 + \theta(\mathbf{v}_1 - \mathbf{v}_2))\| \, \|\mathbf{v}_1 - \mathbf{v}_2\|,$$

and from the fact that

$$\sup_{\theta \in [0,1]} \|\mathbf{Df}(\mathbf{v}_2 + \theta(\mathbf{v}_1 - \mathbf{v}_2))\| \leq |Df_{23}| = |m_1 \cos(\alpha\pi/\alpha_g) - m_2|,$$

we have

$$\|\mathbf{f}(\mathbf{v}_1) - \mathbf{f}(\mathbf{v}_2)\| \leq L_f \|\mathbf{v}_1 - \mathbf{v}_2\|,$$

with $L_f = 36000$ being the Lipschitz constant. This quantity is excessively large, and using the classic approach would lead to very conservative results [149]. Therefore, we consider the less restrictive QUAD condition instead. Indeed, the function $\mathbf{f}$ satisfies the QUAD condition by setting $\rho = L_f$ and $\mathbf{P} = \mathbf{I}_N$ [39]. However, to find the lowest value of ρ, we need to find the optimal matrices $\mathbf{P}$ and $\mathbf{L}$ such that condition (i) and (ii) are fulfilled. To do so, we rewrite these two conditions as a constrained nonlinear multivariate optimization problem, that is, $\min_{\mathbf{v}_1, \mathbf{v}_2, \mathbf{P}, \mathbf{L}} \{\rho\}$ such that (i) and (ii) hold. We solve it using the Matlab's Optimization Toolbox, and we find that $\rho = 27.86$,

$$\mathbf{P} = \begin{bmatrix} 0.6995 & 0 & -0.004 \\ 0 & 0.001 & 0 \\ -0.004 & 0 & 3 \end{bmatrix}, \quad \mathbf{L} = \begin{bmatrix} 21 & -141 \\ 0.12 & 14705 \\ 267 & -0.18 \end{bmatrix},$$

and $\mathbf{Q} = \text{diag}\{29.437, 29.437, 1624.266\}$. Note that both $\mathbf{P}$ and $\mathbf{Q}$ are symmetric and positive definite. Moreover, $\lambda_{\min}(\mathbf{Q}) = 29.437$; hence, the third condition (iii) $\lambda_{\min}(\mathbf{Q}) > 27.8644$ of Proposition 8.1 is fulfilled and the synthesis of the observer is complete.

8.3.2 Zero Average Dynamics (ZAD)

The ZAD controller is a quasi-sliding technique, where the goal is forcing the switching function to be zero on average over a finite period of time. This strategy was originally developed for controlling DC-DC power converters in [62]; however, it has been also recently used for controlling gene expression in synthetic biology [59]. This strategy has been shown to provide low regulation error and most importantly fixed switching frequency. In fact, when compared with traditional sliding control, where there is typically an infinite number of commutations (thus inducing chattering), ZAD control guarantees a finite number of switches over a finite period of time. Specifically, we consider the control input $u(t)$ to be given by a centered PWM of the form

$$
u(t) = \begin{cases} \mu, & \text{if } kT \leq t \leq kT + d_k/2 \\ -\mu, & \text{if } kT + d_k/2 < t < (k+1)T - d_k/2 \ , \\ \mu, & \text{if } (k+1)T - d_k/2 \leq t < (k+1)T \end{cases}
$$

where T is the switching period, $k \in \{0, 1, 2, \ldots, m\}$, with m being the number of samples, $\mu > 0$, and d_k is the *duty cycle* (i.e. the time that the switch remains ON). We choose the sliding surface to be a combination of a proportional and a derivative term, i.e. $S(\psi(t), \dot{\psi}(t)) \triangleq \psi(t) - k_{\mathrm{s}}\dot{\psi}(t)$, with $k_{\mathrm{s}} > 0$ [4]. Then, the main design problem is to find the duty cycle d_k such that

$$
\int_{kT}^{(k+1)T} S(\psi, \dot{\psi}) \, \mathrm{d}t = 0, \quad \forall k \in \{1, 2, \ldots, m\}.
$$

As pointed out in [4], solving this transcendental equation for each time interval demands high computation cost. Therefore, using a linear approximation of the sliding surface and solving for the variable d_k yields a simple expression for the duty cycle and its normalization $d_{\mathrm{c}} \triangleq d_k/T$ (for further details about this approximation, see [4] and references therein):

$$
d_k = \frac{2S(kT) + T\dot{S}_2(kT)}{\dot{S}_2(kT) - \dot{S}_1(kT)},
$$

where $\dot{S}_1(kT)$ and $\dot{S}_2(kT)$ are given by

$$
\dot{S}_1(kT) = \dot{S}(kT)|_{u=\mu} = (\dot{\psi}(kT) + k_{\mathrm{s}}\ddot{\psi}(kT))|_{u=\mu},
$$
$$
\dot{S}_2(kT) = \dot{S}(kT)|_{u=-\mu} = (\dot{\psi}(kT) + k_{\mathrm{s}}\ddot{\psi}(kT))|_{u=-\mu}.
$$

Note that, in order to find $\dot{S}_1(kT)$ and $\dot{S}_2(kT)$, we need the knowledge of $\alpha(kT)$; instead, we will use the estimation $\hat{\alpha}(kT)$ provided by the observer.

8.3.3   Minimal Control Synthesis (MCS)

Minimal Control Synthesis (MCS) is a strategy used to determine the control gains of a classical Model-Reference Adaptive Controller (MRAC) [129]. The aim is that of making the plant, typically assumed to be in controllable canonical form, track asymptotically the output, $\mathbf{y}_m$, of some linear reference model described by the matrices $\mathbf{A}_m$, $\mathbf{B}_m$, $\mathbf{C}_m$, so as to make the error $\mathbf{e}_m \triangleq \mathbf{y}_m - \mathbf{y}$ asymptotically null. To this aim, the control input is selected as $u(t) = -\mathbf{K}(t)\mathbf{x}(t)$, where

$$\mathbf{K}(t) = k_P \left(w(t)\mathbf{x}^\mathsf{T}(t) \right) + k_I \left(\int_0^t w(\tau)\mathbf{x}^\mathsf{T}(\tau)\mathrm{d}\tau \right),$$

with k_P and k_I being constants, $w(t) \triangleq \mathbf{B}_m^\mathsf{T}\mathbf{P}\mathbf{e}_m(t)$ and $\mathbf{P}$ being a symmetric positive definite matrix that verifies the Lyapunov equation $\mathbf{P}\mathbf{A}_m + \mathbf{A}_m^\mathsf{T}\mathbf{P} = -\mathbf{Q}$, with $\mathbf{Q} > 0$. Here, we present an empirical implementation of the MCS on the NLG model in equations (8.5) by selecting $\mathbf{A}_m = \mathbf{A}$, $\mathbf{B}_m = \mathbf{B}$, $\mathbf{C}_m = \mathbf{C}$, $k_P = 10^3$, $k_I = 10^4$, and $\mathbf{P} = \mathbf{I}_3$. Note that all nonlinear terms in model (8.5) are assumed as nonlinear disturbances acting on the linear terms of the plant. As in the case of the ZAD controller, again here the observer is needed to estimate the whole state vector required to compute the control action $u(t)$.

8.4   Numerical Results

In this section, we test the two control strategies described in the previous one. In particular, we consider two different tests that have been widely used in the literature for evaluating the performance of shimmy control techniques [118].

- *Test 1: Tire damage.* In this case, we assume a constant speed $V = 80$ with zero initial conditions. Then, for $0.2 \le t \le 0.3$, an impulse function acting as a disturbance torque in (8.5) is present, that is, $\zeta(t) = 1000$ nM, as shown in Figure 8.4a.
- *Test 2: Taxiing on non-uniform road.* In this scenario, the aircraft is taxiing with increasing velocity, that is the velocity varies according to the ramp depicted in Figure 8.4d, while the disturbance $\zeta(t)$ is given by the function shown in Figure 8.4b, which simulates potholes on the road. Note that the velocity range adopted here is similar to that explored in the bifurcation diagrams of Figure 8.1, where it has been shown that shimmy occurs for velocities grater than 20 m/s.

To further test the robustness of the control strategies, we add uncertainty to the nonlinear function $\mathbf{f}(\mathbf{x})$ by using the piecewise-smooth approximation (8.1)-(8.2) for the NLG model, while the smooth approximation (8.3)-(8.4) is used for the observer and the controllers. For the sake of comparison, we first present the open-loop responses of the NLG in Tests 1 and 2, in Figures 8.4e and 8.4f, respectively. Note that in both cases oscillations with large amplitude are present.

8.4.1   Test 1: Tire damage

We first test the ZAD controller in the case of constant speed and impulsive disturbance. In particular, we set the sampling period $T = 10^{-3}$, the constant $k_s = 0.5$, the control gain $\mu = 1000$ and zero initial conditions. The time response of the closed-loop systems is shown in Figure 8.5a, where it is evident that the yaw angle ψ is driven to zero and the maximum overshoot is less than one degree. Furthermore, the normalized duty cycle d_c converges to a constant value and hence the control action exhibits fixed switching frequency.

Next, we perform Test 1 for the NLG controlled by MCS. The time trajectories are shown in Figure 8.5b, which shows that the controller is able to suppress the undesired oscillations despite the presence of uncertain nonlinear terms, while guaranteeing boundedness of the adaptive control action.

8.4.2   Test 2: Taxiing on non-uniform road

The time response of the NLG controlled by ZAD and MCS is shown in Figures 8.6a and 8.6b, respectively. Note that even in this case, where there are multiple perturbations (due to the potholes), the controllers are able to effectively suppress shimmy.

8.5   Discussion

We have proposed the use of ZAD and MCS control approaches for suppressing shimmy in a NLG with uncertain non-linearities and partial state measurements. In so doing, we adopted less conservative conditions for designing observers with nonlinear terms, so that large overshoots can be avoided. Using numerical simulations, we showed the effectiveness of the proposed control strategies under two representative scenarios. Future work is needed to develop stability analysis of the closed-loop systems, together with an accurate performance assessment of both control techniques. In addition, the control approaches can be also tested using more realistic NLG models as those considered in [72].
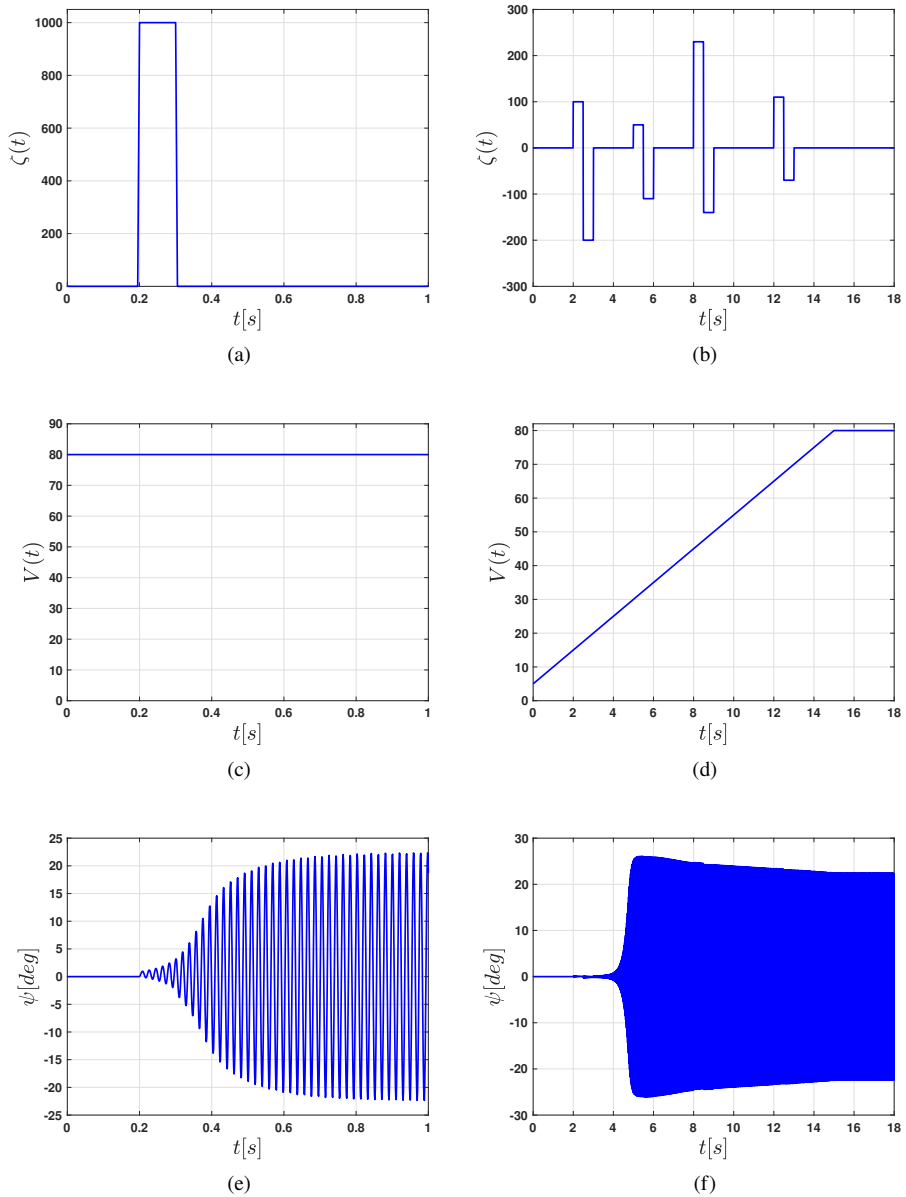
Figure 8.4: Time trajectories of disturbance ζ (a, b), velocity V (c, d) and wheel angle ψ (e, f) in the cases of Test 1 (a, c, e) and Test 2 (b, d, f).
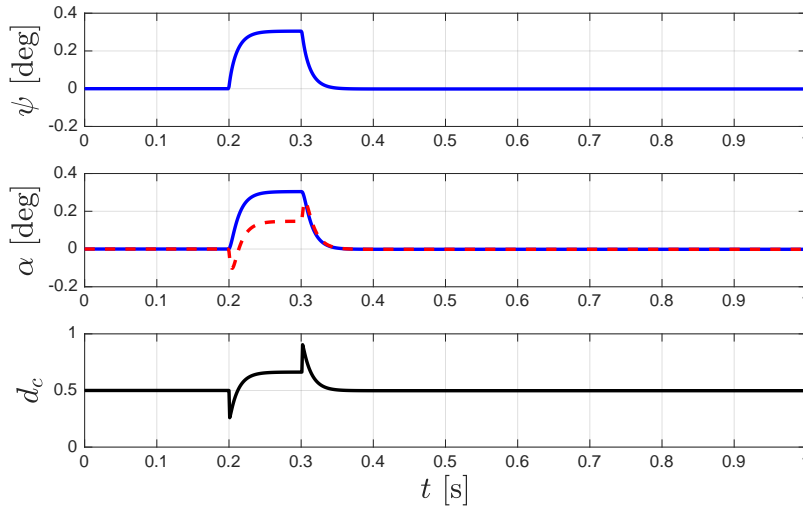
(a)
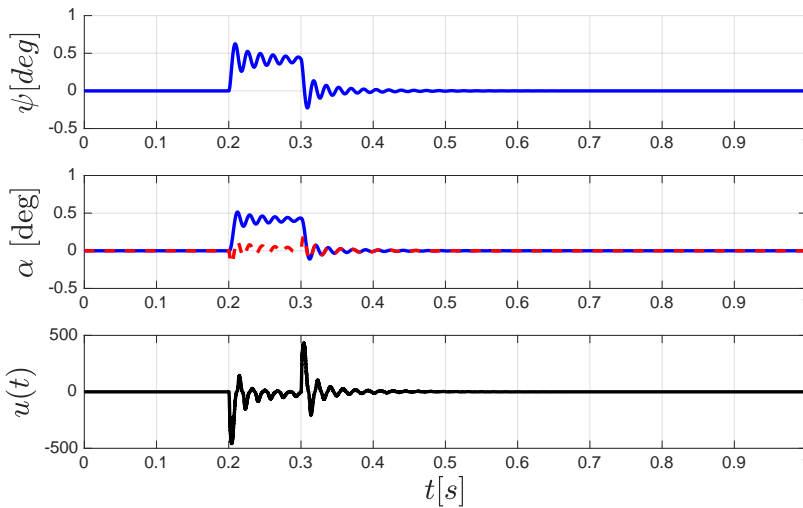
(b)

Figure 8.5: Time response of the NLG under impulsive disturbance, controlled by (a) ZAD strategy and (b) MCS. In the top, middle and bottom panels, $\psi(t)$, $\alpha(t)$, and $d_c(t)$ (or $u(t)$) are shown respectively. The red dashed line represents the estimation $\hat{\alpha}(t)$ made by the observer, whereas the solid line line is $\alpha(t)$.
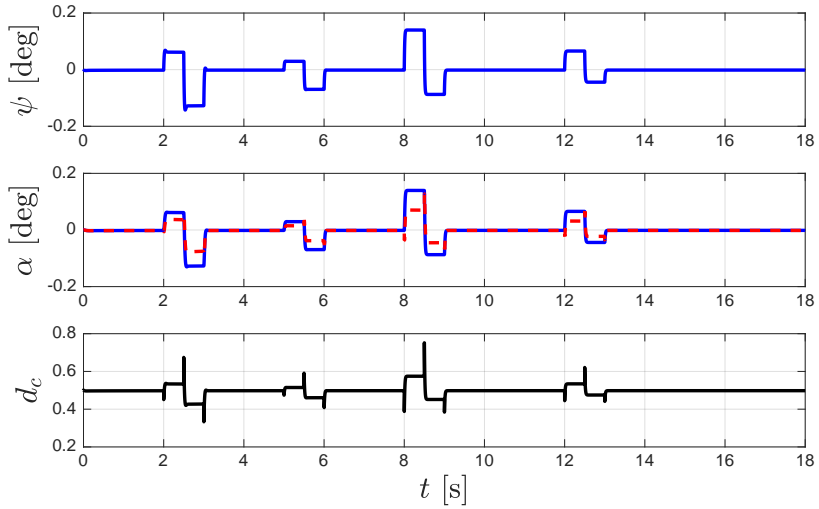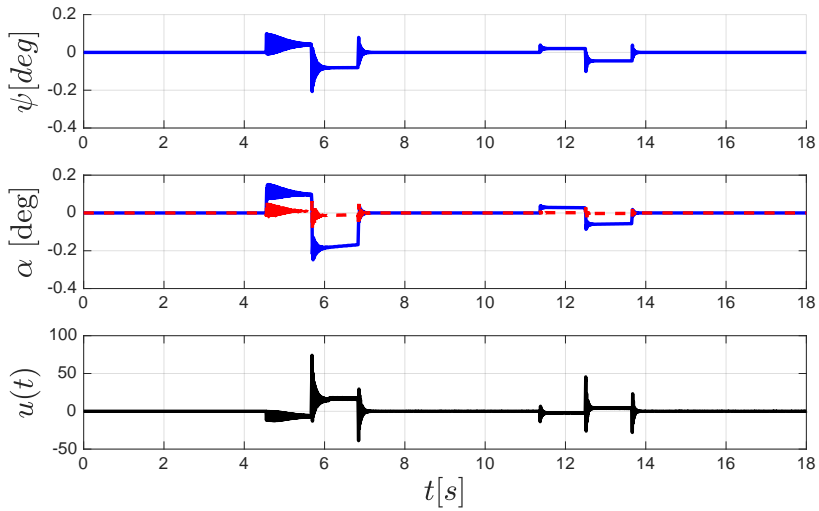
Figure 8.6: Time response of the NLG for time-varying velocity and non-uniform road, controlled by (a) ZAD strategy and (b) MCS. In the top, middle and bottom panels, $\psi(t)$, $\alpha(t)$, and $d_{\mathrm{c}}(t)$ (or $u(t)$) are shown respectively.

9 Control of Painlevé Paradox in a Robotic System

9.1 Introduction to the Painlevé Paradox and application to robotic arms

Most people have experienced at least once the annoying high-pitched sound that chalk may produce when pressed against a blackboard. As it is now well known [24], the sound is the result of fast vibrations of the piece of chalk that quickly and repeatedly detaches from the blackboard and comes back into contact with it. This phenomenon is paradoxical as the more one presses the chalk against the surface, the more likely bouncing motion becomes. This type of oscillatory behaviour is not only annoying but can be costly and troublesome when it manifests in practical applications. For example, the repeated lift of an automated tool performing a cut leads to imprecise processing, resulting in unusable goods or ones with reduced value [73]. Moreover, in an assembly line, a robotic arm used grasping objects from a moving belt may abruptly be pushed away from the belt, resulting in decreases in speed and accuracy [25].

The phenomenon described above was named after Paul Painlevé, who, in 1905, published the first studies related to the paradox, providing a mathematical model. In particular, in [108], he analysed the dynamics of a rigid stick sliding on a surface, showing that, assuming a Coulomb friction law, when the friction coefficient was higher than a certain threshold value, a non-trivial phenomenon occurs. Namely, the solution to the differential equations describing the motion of the stick may become indeterminate or inconsistent, in the sense that the model would predict the stick to penetrate the rigid surface, which clearly is not realistic. In the following years, many mathematicians and scientists have been interested in the study of this paradoxical phenomenon, but, as pointed out by Champneys in [24], to this date, all the ways in which the stick can enter the inconsistent or indeterminate solution modes have not been determined analytically. For this reason, most of the research follows a numerical or experimental approach in the investigation of the problem.

For example, in [97], Lötstedt created a digital simulation of the dynamics of rigid mechanical systems under unilateral constraints, in order to study the Painlevé phenomenon. In [147] and [21], numerical simulations are used to investigate how the paradox affects

the motion of an inverted pendulum sliding on an inclined plane and that of a double pendulum, respectively. Furthermore, in [83], Leine et al. studied through numerical simulations the paradox in a specific two-masses system, called *frictional impact oscillator*. They showed that the critical friction value was strictly linked to the masses ratio, and the Painlevé paradox was the cause of a Hopf bifurcation, in which a sliding equilibrium loses its stability and a periodic bouncing motion appears. Similar results can be found in [81].

Another system whose motion is influenced by the paradox, is the prismatic revolute robotic set-up analysed in [51] via numerical simulations. It is also important to highlight that the phenomenon studied by Painlevé can influence the motion of walking robots. As a matter of fact, most of the passive walking models such as the *compass biped* or the *rimless wheel* [28], assume that there is a frictional sticking contact between the foot and the surface, whereas in reality there is always a slipping of the foot. For instance, the numerical results obtained in [106] showed that regular periodic gait can be subject to an instability, related to the Painlevé phenomenon. Moreover, in recent work by Zhao et al. [153], the occurrence of the Painlevé paradox was demonstrated experimentally in a two link robotic arm whose end effector is in contact with a sliding belt. It was shown that for certain parameter values, the arm can lift off from the moving belt, showing, for the first time in the literature, a physical demonstration of the paradox in a realistic robotic set-up.

To the best of our knowledge, the only instance of a control strategy employed to avoid the onset of the paradox is described in [86], where a PID regulator is used to control the sliding of a two-links robot on a vertical wall.

The contribution of our work is twofold. Firstly, we extend the analysis of the system originally presented in [153] unfolding the bifurcation mechanisms behind the occurrence of the Painlevé paradox. Secondly, we exploit this new information to synthesise appropriate control strategies to prevent the paradox from taking place; being this one of the very few attempts at using active controllers to address the problem, along with [86]. In particular, in order to better understand the conditions that trigger the onset of the phenomenon, we present a characterisation of the steady state dynamics for different values of the velocity of the belt. Specifically, we find that the paradox manifests itself only when the speed of the belt is in a certain critical interval. However, we show that, even when the velocity of the belt is within that critical interval, some control strategies may be employed to avoid the undesired lift-off and bouncing motion stemming from it. In particular, we show how a PID regulator and a hybrid force/motion control scheme can be exploited to reach some positioning control goals while keeping the robot in a region of the phase space such that the paradox is not triggered. According to our simulations, the hybrid control shows the most promising results, representing an innovation with respect to [86], where only a PID control strategy was used. Our results nicely combine bifurcation analysis with control system design, offering a novel approach for the active suppression of the Painlevé paradox in realistic mechanical systems.
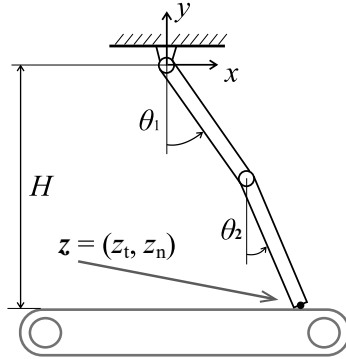
Figure 9.1: A double-revolute robotic arm on a moving belt.

9.2 Bifurcation analysis

9.2.1 Model description

We consider a two-links mechanical set-up as that represented in Figure 9.1. Rotational dashpots with damping coefficient σ are present in both the joints, and a rotational spring with elastic constant k is mounted in the lower joint; moreover, the belt is moving at a speed v_{belt}. We define the generalised coordinates $\mathbf{q} \triangleq [\theta_1 \; \theta_2]^{\mathsf{T}}$, the coordinates of the end effector $\mathbf{z} \triangleq [z_{\text{t}} \; z_{\text{n}}]^{\mathsf{T}}$, and, for later use, the state vector $\mathbf{x} \triangleq [\theta_1 \; \dot{\theta}_1 \; \theta_2 \; \dot{\theta}_2]^{\mathsf{T}}$. Then, a mathematical model of the system can be given as

$$\ddot{\mathbf{q}} = \mathbf{M}^{-1}(-\mathbf{w} - \mathbf{c} + \mathbf{J}^{\mathsf{T}}\mathbf{f} + \mathbf{u}), \tag{9.1}$$

where:

- **M** is the mass matrix;
- **w** contains the torques determined by the elastic force, viscous friction, and gravity;
- **c** are the torques determined by the centrifugal and Coriolis forces;
- **J** is the Jacobian, defined by the relation $\dot{\mathbf{z}} = \mathbf{J}\dot{\mathbf{q}}$;
- $\mathbf{u} = [u_1 - u_2 \; u_2]^{\mathsf{T}}$ contains the control torques, with u_1 and u_2 being the torques applied to the first and the second joint, respectively;
- $\mathbf{f} = [f_{\text{t}} \; f_{\text{n}}]^{\mathsf{T}}$ are the contact forces acting on the end effector, with f_{n} being the normal reaction and f_{t} being the Coulomb friction. In particular, $f_{\text{t}} = -\mu \operatorname{sign}(\dot{z}_{\text{r}}) f_{\text{n}}$, where $\dot{z}_{\text{r}} \triangleq \dot{z}_{\text{t}} - v_{\text{belt}}$ is the velocity of the contact point with respect to the belt and μ is the friction coefficient.

The expressions of the above quantities are

$$\mathbf{M} = \begin{bmatrix} \frac{4}{3}ml^2 & \frac{ml^2}{2}\cos(\theta_2 - \theta_1) \\ \frac{ml^2}{2}\cos(\theta_2 - \theta_1) & \frac{ml^2}{3} \end{bmatrix},$$

Table 9.1: Robot parameters

Parameter	Symbol	Value	Unit
belt speed	v_{belt}	$[-1, -0.1]$	m/s
friction coefficient	μ	$[0.1, 1]$	-
links mass	m	0.12	kg
links length	l	0.21	m
damping coefficient	σ	0.005	N·s/m
elastic constant	k	1.3	N/m
robot height	H	0.3775	m
spring rest position	α_0	13.72	degrees

$$\mathbf{w} = \begin{bmatrix} \frac{3mgl}{2}\sin\theta_1 - k(\theta_2 - \theta_1 + \alpha_0) - \sigma(\dot{\theta}_2 - 2\dot{\theta}_1) \\ \frac{mgl}{2}\sin\theta_2 + k(\theta_2 - \theta_1 + \alpha_0) + \sigma(\dot{\theta}_2 - \dot{\theta}_1) \end{bmatrix},$$

$$\mathbf{c} = \begin{bmatrix} \frac{ml^2}{2}\dot{\theta}_2^2\sin(\theta_1 - \theta_2) \\ \frac{ml^2}{2}\dot{\theta}_1^2\sin(\theta_2 - \theta_1) \end{bmatrix},$$

$$\mathbf{J} = \begin{bmatrix} \mathbf{j}_1^{\mathsf{T}} \\ \mathbf{j}_2^{\mathsf{T}} \end{bmatrix} = \begin{bmatrix} l\cos\theta_1 & l\cos\theta_2 \\ l\sin\theta_1 & l\sin\theta_2 \end{bmatrix}.$$

The values of the parameters are set using the experimentally derived ones reported in [153] and are given in Table 9.1.

Model (9.1) can be recast in terms of the position $\mathbf{z}$ of the end effector as

$$\ddot{\mathbf{z}} = -\mathbf{J}\mathbf{M}^{-1}(\mathbf{w} + \mathbf{c} - \mathbf{u}) + \mathbf{Q}\mathbf{f} + \mathbf{s}, \tag{9.2}$$

where $\mathbf{Q} \triangleq \mathbf{J}\mathbf{M}^{-1}\mathbf{J}^{\mathsf{T}} = (Q_{i,j})$, $i, j = 1, 2$, and $\mathbf{s}$ is the centripetal acceleration, given by

$$\mathbf{s} = \begin{bmatrix} s_1 \\ s_2 \end{bmatrix} = \begin{bmatrix} -l(\dot{\theta}_1^2\sin\theta_1 + \dot{\theta}_2^2\sin\theta_2) \\ l(\dot{\theta}_1^2\cos\theta_1 + \dot{\theta}_2^2\cos\theta_2) \end{bmatrix}.$$

Model (9.2) can be expressed componentwise as

$$\ddot{z}_{\text{t}} = -\mathbf{j}_1^{\mathsf{T}}\mathbf{M}^{-1}(\mathbf{w} + \mathbf{c} - \mathbf{u}) + f_{\text{n}}(-\mu\,\text{sign}(\dot{z}_r)Q_{1,1} + Q_{1,2}) + s_1, \tag{9.3}$$

$$\ddot{z}_{\text{n}} = -\mathbf{j}_2^{\mathsf{T}}\mathbf{M}^{-1}(\mathbf{w} + \mathbf{c} - \mathbf{u}) + f_{\text{n}}(-\mu\,\text{sign}(\dot{z}_r)Q_{2,1} + Q_{2,2}) + s_2. \tag{9.4}$$

For a fixed value of μ, when $\dot{z}_r > 0$, we will show that there exists a region in the state space, say $\mathcal{R}^+ \subseteq \mathbb{R}^4$, such that when the state vector $\mathbf{x} \in \mathcal{R}^+$ the paradox is triggered. Differently, when $\dot{z}_r < 0$, the paradox manifests itself if $\mathbf{x} \in \mathcal{R}^- \subseteq \mathbb{R}^4$. However, the sets of positions and velocities represented by $\mathcal{R}^+$ are symmetrical with respect to the y-axis to those contained in $\mathcal{R}^-$. Therefore, for the sake of simplicity, we can limit our analysis

to the case that $\dot{z}_r$ is positive; the results might then easily be extended to the case that $\dot{z}_r$ is negative by simply taking into account the symmetry between $\mathcal{R}^+$ and $\mathcal{R}^-$. Defining the functions $p : \mathbb{R}^3 \to \mathbb{R}$ and $b : \mathbb{R}^6 \to \mathbb{R}$, given by

$$b \triangleq -\mathbf{j}_2^T\mathbf{M}^{-1}(\mathbf{w} + \mathbf{c} - \mathbf{u}) + s_2,$$
$$p \triangleq -\mu Q_{2,1} + Q_{2,2},$$

we can rewrite (9.4) as

$$\ddot{z}_n = b(\mathbf{q}, \dot{\mathbf{q}}, \mathbf{u}) + p(\mathbf{q}, \mu) f_n. \tag{9.5}$$

In (9.5), the physical meaning of the newly introduced functions b and p is more evident. b is the *free normal acceleration*, i.e. the normal acceleration in the absence of contact forces, whereas p determines how the normal reaction f_n influences the normal acceleration $\ddot{z}_n$ of the end effector.

When $z_n = -H$, the end effector is in contact with the moving belt, reproducing a situation analogous to that originally investigated by Painlevé. As explained in [108] for a more general case, if μ is greater than a critical value μ_c, system (9.2) can display four different types of solution, depending on the signs of b and p, which in turn depend on $\mathbf{q}$, $\dot{\mathbf{q}}$, $\mathbf{u}$, and μ. The first two modes, *sliding* and *flight*, are associated to solutions to the motion equation (9.5), both characterized by $p > 0$; while, when $p < 0$, the solution to (9.5) is *indeterminate* or *inconsistent*. Next, we describe each solution mode in greater detail.

(i) *Sliding, $p > 0$, $b < 0$.* — The end effector is in contact with the belt, i.e. $z_n = -H$, $f_n = -\frac{b}{p}$, and possibly $\dot{z}_t \neq 0$.

(ii) *Flight, $p > 0$, $b > 0$.* — Either $z_n > 0$, or $z_n = -H$ and $\ddot{z}_n > 0$.

(iii) *Indeterminate, $p < 0$, $b > 0$.* — The solution is not unique; nonetheless, according to [51], when simulating the system, it is possible to resolve the indeterminate mode into a flight mode.

(iv) *Inconsistent, $p < 0$, $b < 0$.* — Given the signs of p and b, we would have $\ddot{z}_n < 0$, which, recalling that $z_n = -H$, is not physically feasible, because both the robot and the belt are assumed to be rigid. This troublesome scenario can be resolved, as explained in [153], as an *impact without collision* [67], in which $\dot{z}_n$ turns from zero to positive, determining the lift-off of the end effector, followed by a succession of bounces on the belt.

In Figure 9.2, we provide an example of the regions associated to each of the four solution modes.
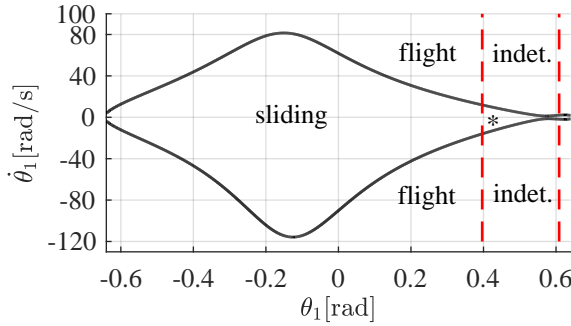
Figure 9.2: Different modes of solution for different values of θ_1 and $\dot{\theta}_1$. Here $\mu = 0.6$, $\mathbf{u} = \mathbf{0}$, and θ_2 and $\dot{\theta}_2$ are chosen in order to have the tip of the robot in contact with the belt. "indet." stands for indeterminate and "$*$" stands for inconsistent. The black solid line is the place where $b = 0$, while the dashed red lines are the places where $p = 0$.

9.2.2 Bifurcation diagrams

To better understand the occurrence of the paradox causing the lift-off of the end effector, we traced a two-dimensional numerical bifurcation diagram in the parameter space consisting of the friction coefficient μ and the speed of the belt v_{belt}.

The system was simulated using event-detection routines available in Matlab to detect transitions between each of the solution modes described in Section 9.2.1. The bifurcation diagram was constructed via a brute-force method [74] by simulating the system from a set of random initial conditions for parameters selected in a grid defined by the ranges $0.1 \leq \mu \leq 1$ and $-1 \leq v_{\text{belt}} \leq -0.1$, with steps of 0.1, and 0.005, respectively. In each run, the state values are recorded, after a transient time of 250 s, over a time interval of 50 s. Then, if in a certain run $\max \dot{\theta}_1 > 0$, it means that the parameter values used in that simulation are such that persistent bouncing motion manifests, which is undesired.

We observed that the bounces appear only for $\mu \geq \mu_c = 0.4$, that is $\max \dot{\theta}_1 = 0$ if $\mu < \mu_c$, for all values of v_{belt}. Moreover, we verified that, when $\mu \geq \mu_c$, features of the bouncing motion such as duration and (a)periodicity depend only on v_{belt}. Given that the bifurcation diagram is flat for $\mu < \mu_c$, and independent of μ provided that $\mu \geq \mu_c$, we only present a two-dimensional section of the diagram, in Figure 9.3, where $\mu = 0.6$ was considered. We note that (i) not all initial conditions trigger the bounces (see the red dashed line), and that (ii) bounces are present only when $-0.575 \leq v_{\text{belt}} \leq -0.3$.

In order to gain greater knowledge on the specific behaviour of the system when $-0.575 \leq v_{\text{belt}} \leq -0.3$ (still with $\mu = 0.6$), we traced a second more detailed bifurcation diagram in Figure 9.4, in which we plot the value of θ_1 when $\dot{\theta}_1$ turns from negative to positive, as a function of the parameter value. The diagram shows the presence of both periodic and chaotic solutions, providing evidence for the onset of complex seemingly aperiodic behaviour in the parameter regions depicted in red in Figure 9.4c.
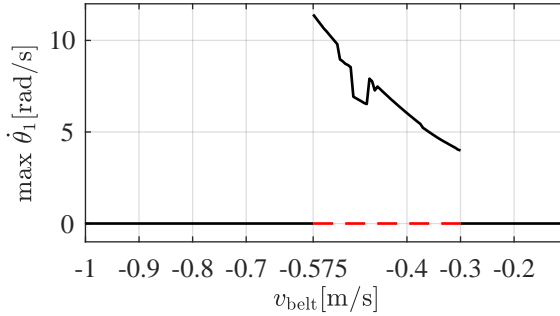
Figure 9.3: Bifurcation diagram with $\mu = 0.6$. The black solid line corresponds to initial conditions $\mathbf{x}_{0,a} = [32 \ 0 \ 18.27 \ 0]^\mathsf{T}$, whereas the dashed red line corresponds to $\mathbf{x}_{0,d} = [-11.4 \ 0 \ -35.1 \ 0]^\mathsf{T}$.

Table 9.2: Admissible configurations for $\mu = 0.6$

Elbow position	Admissible configurations [m]
elbow up $(\theta_2 - \theta_1 > 0)$	$-0.184 \leq z_t < 0.183$
elbow down $(\theta_2 - \theta_1 < 0)$	$-0.184 \leq z_t < 0.168$

9.3 Control synthesis

Next, we wish to design a controller able to avoid the onset of the bouncing motion due to the paradox and keep the robot moving in contact with the belt. This in turn requires using a feedback control to guarantee that $p > 0$ and $b > 0$ at all times in (9.5). Without loss of generality, we set $v_{\text{belt}} = -0.4$, that is a value that allows the occurrence of the paradox. Firstly, setting $\mu = 0.6$, in Table 9.2 we determine analytically the values of z_t such that $p > 0$; we call these *admissible configurations*, given that indeterminate and inconsistent solutions will not appear for such values of z_t. Secondly, one should determine, among the admissible configurations, those corresponding to $b < 0$; nevertheless, this task is not easy to achieve analytically, because, differently from p, b is also a function of $\dot{\mathbf{q}}$ and $\mathbf{u}$. However, $b < 0$ can be attained using a control scheme that aims at keeping $f_n > 0$, as it is easy to verify from (9.4), when $\ddot{z}_n = 0$. We start by using a simpler PID controller, showing that such strategy can keep the end effector in contact with the belt only in a narrow range of the admissible configurations. Next, we move to a hybrid force/motion control [125] (that allows the regulation of f_n) and demonstrate that this latter approach guarantees avoidance of the lift-off of the end effector in a wider range of the admissible configurations.

9.3.1 PID strategy

For the sake of simplicity, we started by considering a simpler PID control approach to test its feasibility to solve the control goal. Let $\mathbf{z}^*$ be the reference value for the end effector coordinates, $e \triangleq z_t^* - z_t$ a reference error, and $\mathbf{q}' \triangleq [\theta_1 \ \ \theta_2 - \theta_1]^\mathsf{T}$. Say $\mathbf{q}'^*$ the reference value for $\mathbf{q}'$, computed from $\mathbf{z}^*$ using inverse kynematics as explained in [125]. Hence, the control terms u_i, $i = 1, 2$, obtained using a PID control scheme are given by

$$ u_i = K_{P,i}(q_i'^* - q_i') + K_{I,i} \int_0^\tau (q_i'^* - q_i')\mathrm{d}t + K_{D,i}(\dot{q}_i'^* - \dot{q}_i'), $$

where $K_{P,i}$, $K_{I,i}$, $K_{D,i}$, $i = 1, 2$, are constants. The PID gains were selected heuristically by running a series of numerical simulations from two sets of initial conditions. These are $\mathbf{x}_{0,d} = [-11.4 \ \ 0 \ \ -35.1 \ \ 0]^\mathsf{T}$ and $\mathbf{x}_{0,u} = [-35.1 \ \ 0 \ \ -11.4 \ \ 0]^\mathsf{T}$, both corresponding to $\mathbf{z} = [-0.1624 \ \ 0]^\mathsf{T}$, with the only difference that $\mathbf{x}_{0,d}$ is an "elbow down" posture ($\theta_2 - \theta_1 < 0$) and $\mathbf{x}_{0,u}$ is an "elbow up" posture ($\theta_2 - \theta_1 > 0$). The gains were adjusted in a trial-and-error process with the aim of obtaining a large value of $Z_{t,\text{sliding}}$, that is the largest value of z_t such that no lift-off occurs. We observed different results, depending on the initial condition. For $\mathbf{x}(t = 0) = \mathbf{x}_{0,d}$, $Z_{t,\text{sliding}} = 0.0375$, and acceptable values of the gains were found to be $K_{P,1} = 200, K_{I,1} = 25, K_{D,1} = 2$, and $K_{P,2} = K_{I,2} = K_{D,2} = 0$. The corresponding simulation graphs, are shown in Figure 9.5. Differently, for $\mathbf{x}(t = 0) = \mathbf{x}_{0,u}$, the simulations results showed that the PID control is not able to effectively avoid the onset of the paradox. As a matter of fact, we could not find values of the control gains such that lift-off was avoided. An example is visible in Figure 9.6, where the time evolution of the normal reaction f_n is depicted; notice that it eventually becomes zero, meaning that the end effector detaches from the belt.

9.3.2 Hybrid force/motion control

Next, we show that better performance can be achieved with a force/motion control scheme [125], since it allows to regulate the value of the normal reaction f_n in addition to the end effector's tangential position z_t. In particular, defining the unit vectors $\mathbf{i}_1 \triangleq [1 \ \ 0]^\mathsf{T}$ and $\mathbf{i}_2 \triangleq [0 \ \ 1]^\mathsf{T}$, associated to the x and y Cartesian axes, the control action is given by

$$ \mathbf{u} = \mathbf{w} + \mathbf{c} + \mathbf{M}\mathbf{J}^{-1}\left(-\dot{\mathbf{J}}\dot{\mathbf{q}} + \mathbf{i}_1\alpha_v\right) + \mathbf{J}^\mathsf{T}\left(-\mathbf{i}_1 f_t - \mathbf{i}_2\alpha_f\right). \tag{9.6} $$

Note that, in (9.6), on the right-hand side, the first, second, and fifth terms compensate corresponding terms in (9.2). Differently, the fourth and and sixth terms are used to assign dynamics for z_t and f_n, respectively. Specifically, letting f_n^* be a reference value for the normal reaction, we choose

$$ \alpha_v = \ddot{z}_t^* + K_P'(z_t^* - z_t) + K_D'(\dot{z}_t^* - \dot{z}_t), $$

$$ \alpha_f = f_n^* + K_I' \int_0^\tau (f_n^* - f_n)\mathrm{d}t, $$

where K_P', K_D', and K_I' are control gains. A block diagram of the hybrid force/motion control scheme is illustrated in Figure 9.7.

To test the performance of the control system, we ran a series of simulations from the same initial conditions used to validate the PID control strategy; the control gains being selected heuristically as $K'_P = K'_D = 900, K'_I = 650$ for $\mathbf{x}(t = 0) = \mathbf{x}_{0,d}$ and $K'_P = K'_D = 900, K'_I = 0$ for $\mathbf{x}(t = 0) = \mathbf{x}_{0,u}$. The numerical results showed that, for $\mathbf{x}_{0,d}$, $Z_{t,sliding} = 0.148$, whereas, for $\mathbf{x}_{0,u}$, $Z_{t,sliding} = 0.163$, which are both higher than the values obtained with the PID, meaning that the force/motion control scheme allows the robot to operate in a wider range of configurations. Examples of simulations are shown in Figures 9.8 and 9.9, representing the results of the simulations starting from $\mathbf{x}_{0,d}$ and $\mathbf{x}_{0,u}$, respectively. Moreover, we verified that when using the present control strategy, the persistent bouncing motion is suppressed for all $v_{belt} \in [-1, -0.1]$. This is shown in the closed-loop bifurcation diagram in Figure 9.10, which can be compared with that in Figure 9.3, representing the bifurcation diagram for the open loop system. As expected, the closed-loop system remains in contact with the belt over the entire parameter region of interest without any bifurcation to persistent bouncing motion.

9.4   Discussion

We dealt with the analysis and control of the Painlevé paradox in a two-links robot in contact with a moving belt. The paradox determines occasional lift-off of the tip of the robot, which is undesired for a number of applications, like cutting or objects moving. We started by conducting a bifurcation study varying the belt speed, finding that some values determine a chaotic motion of the end effector, while for others the motion is a periodic bouncing. Then, we used the results of the bifurcation analysis to inform the control design and proposed two control schemes, a PID controller and a hybrid force/motion control strategy, which we compared through numerical simulations. We showed that the latter strategy is effective in preventing the paradox from occurring and hence guaranteeing that end effector of the robot stays in contact with the belt over a wider parameter range with respect to the PID.

(a)

(b)

(c)
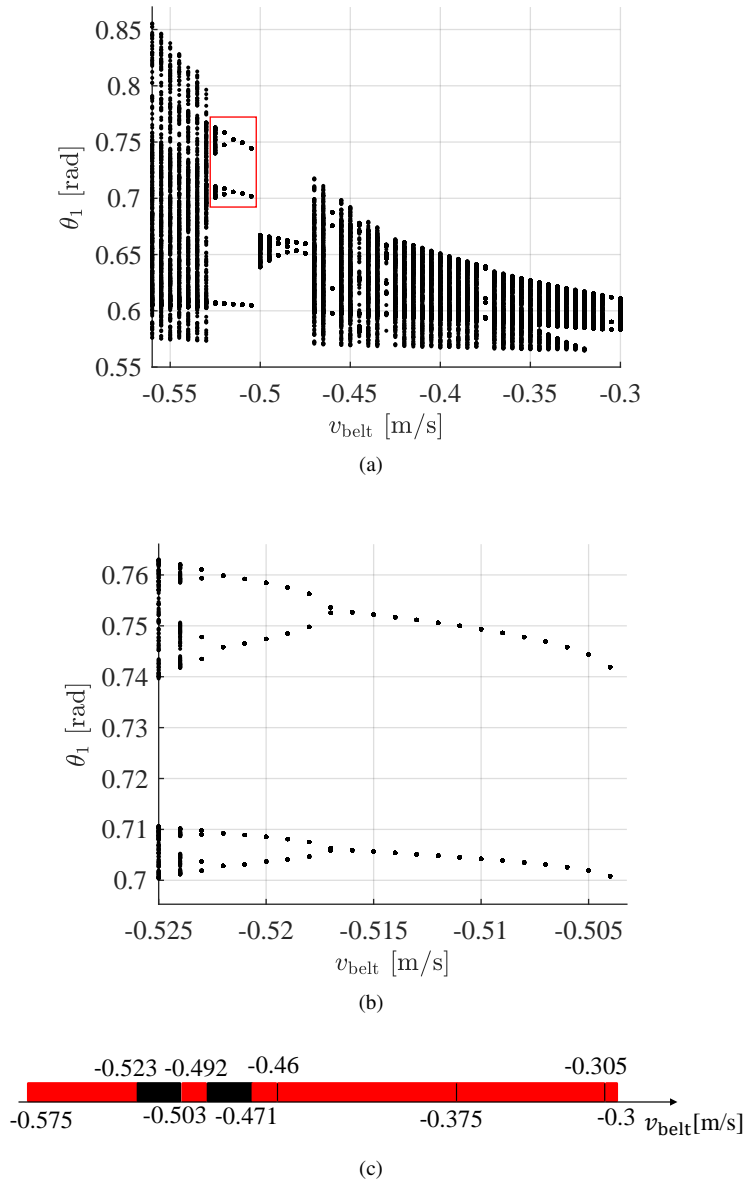
Figure 9.4: Bifurcation diagram with $\mu = 0.6$ and initial conditions $\mathbf{x}_{0,a} = [32\ 0\ 18.27\ 0]^{\mathsf{T}}$. (a) is the full picture, while (b) is an enlargement of the portion in the red box traced in (a); (c) depicts the type of the asymptotic behaviour: red represents a chaotic dynamics, whereas black stands for periodic motion.
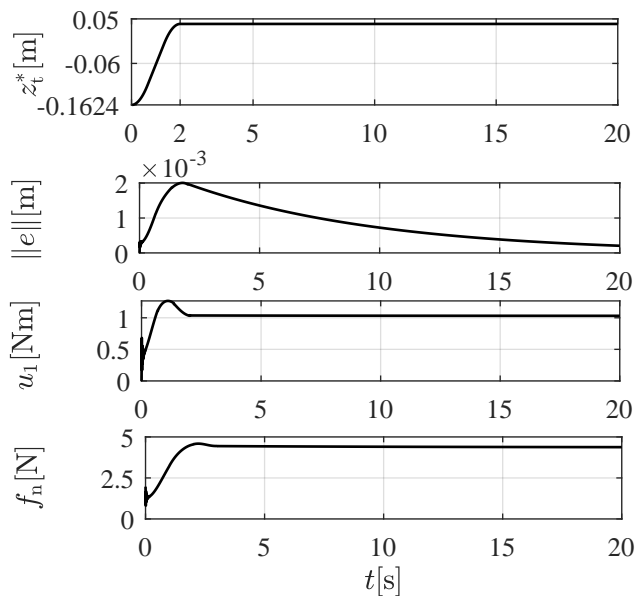
Figure 9.5: Simulation with PID control and $\mathbf{x}(t = 0) = \mathbf{x}_{0,\mathrm{d}}$.
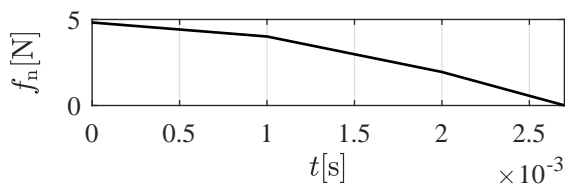
Figure 9.6: Simulation with PID control, $\mathbf{x}(t = 0) = \mathbf{x}_{0,\mathrm{u}}$ and z_{t}^* as in Figure 9.5.
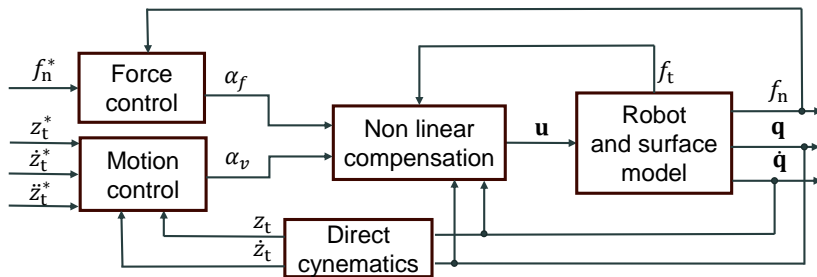
Figure 9.7: Hybrid force/motion control scheme.
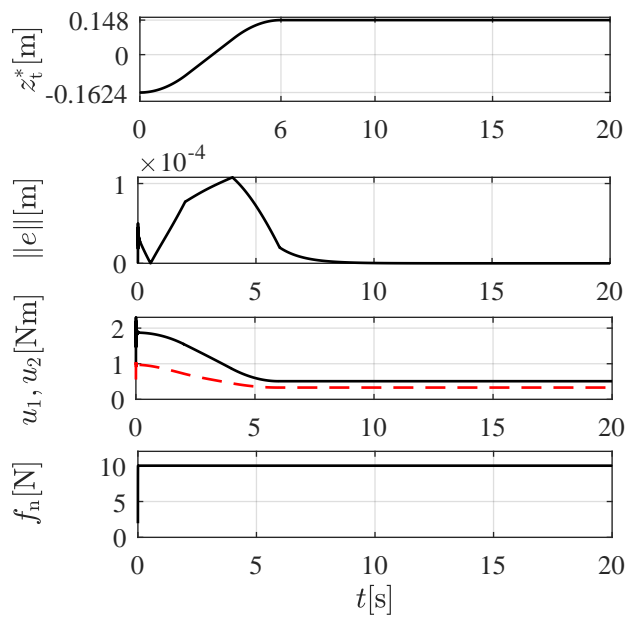
Figure 9.8: Simulation with force/motion control, $\mathbf{x}(t = 0) = \mathbf{x}_{0,\mathrm{d}}$ and $f_{\mathrm{n}}^* = 10$ N. In the third panel from the top, the black solid line is u_1, whereas the red dashed line is u_2.
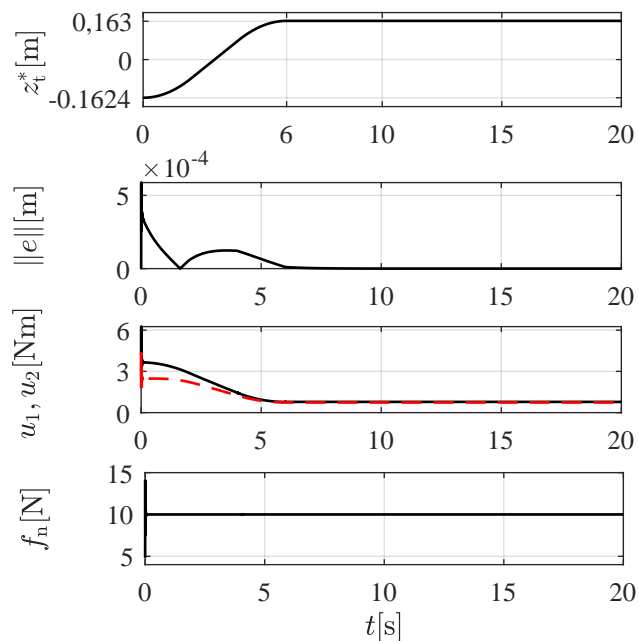
Figure 9.9: Simulation with force/motion control, $\mathbf{x}(t = 0) = \mathbf{x}_{0,\mathrm{u}}$ and $f_{\mathrm{n}}^* = 10$ N. In the third panel from the top, the black solid line is u_1, whereas the red dashed line is u_2.
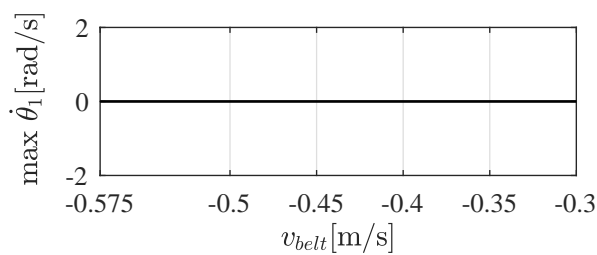
Figure 9.10: Closed loop bifurcation diagram obtained with $\mathbf{x}(t = 0) = \mathbf{x}_{0,\mathrm{d}}$, the same references as that in Figure 9.8, and in the presence of the force/motion control.

10 Observer design for piecewise-smooth systems via contraction theory

10.1 Introduction to observer design for piecewise-smooth systems

The problem of designing state observers for nondifferentiable systems is the subject of current research. For example, the design of observers for Lipschitz continuous nonlinear systems was investigated in [119, 150], while in [5, 15] design approaches based on passivity theory were proposed for Lur'e-type systems. Also, in [76, 50] sufficient conditions were presented to ensure stability of the estimation error for state observers of bimodal piecewise-linear (PWL) systems (both continuous and discontinuous on the switching surface). The analysis was conducted analyzing the quadri-modal estimation error dynamics based on quadratic Lyapunov functions and LMIs. Related results were presented in [138] for the case of piecewise-affine (PWA) systems. Therein, using theoretical results developed in [110], sufficient conditions guaranteeing exponential stability of the estimation error were given in terms of a set of appropriate LMIs. More recently, the state estimation problem was investigated in [71] for linear complementarity systems and in [61] for hybrid systems with impacts.

Contraction theory [94, 122, 75, 60, 2] is a powerful analysis tool providing sufficient conditions for incremental stability [3] of a dynamical system. Namely, if the system vector field is contracting in a set of interest, any two of its trajectories will converge towards each other in that set, a property that can be effectively exploited to design state observers and solve tracking control problems as discussed, for instance, in [94, 138, 14, 48, 101, 100, 45]. More specifically, incremental exponential stability over a given forward invariant set is guaranteed if some matrix measure, say μ, of the system Jacobian matrix is uniformly negative in that set for all time.

The original results on contraction analysis were presented for continuously differentiable vector fields limiting their application to observer design for this class of dynamical systems. Recently, extensions have been presented in the literature for applying contraction

and convergence analysis to different classes of nondifferentiable and discontinuous vector fields [95, 110, 47, 99, 46, 44, 58].

In this work, we propose a methodology to design state observers for nondifferentiable bimodal vector fields, which stems from the results presented in [58] on extending contraction analysis to Filippov systems. Specifically, we derive conditions on the observer dynamics for the estimation error to converge exponentially to zero. These conditions, when particularized to the case of PWA systems, generalize those presented in [138] to the case of non-Euclidean norms.

In what follows, after reviewing some key results on contraction analysis of switched systems, we present our procedure for state observer design complementing the theoretical derivations with some illustrative examples.

10.2 Contraction analysis of switched systems

10.2.1 Incremental stability and contraction theory

Let $U \subseteq \mathbb{R}^n$ be an open set. Consider the system of ordinary differential equations

$$\dot{\mathbf{x}} = \mathbf{f}(\mathbf{x}; t), \qquad (10.1)$$

where $\mathbf{f}$ is a continuously differentiable vector field defined $\mathbf{x} \in U$ and for $t \in [0, \infty)$, that is $\mathbf{f} \in C^1(U \times \mathbb{R}_{\geq 0}, \mathbb{R}^n)$.

We denote by $\boldsymbol{\psi}(t, t_0, \mathbf{x}_0)$ the value of the solution $\mathbf{x}(t)$ at time t of the differential equation (10.1) with initial value $\mathbf{x}(t_0) = \mathbf{x}_0$. We say that a set $C \subseteq \mathbb{R}^n$ is *forward invariant* for system (10.1) if $\mathbf{x}_0 \in C$ implies $\boldsymbol{\psi}(t, t_0, \mathbf{x}_0) \in C$ for all $t \geq t_0$.

A nonlinear dynamical system (10.1) is *contracting* if it forgets initial conditions or temporary state perturbations exponentially fast, implying convergence of system trajectories towards each other and consequently towards a steady-state solution which is determined only by the input (*entrainment* property). Theorem 10.3 summarises the basic results of contraction theory [122, 94].

Definition 10.1 (Contractivity [39]). *Let $C \subseteq U$ be a forward invariant[a] K-reachable[b] set. The continuously differentiable vector field (10.1) is* contractive *on C if there exist a norm with associated matrix measure[c] μ and a constant $c > 0$, called the* contraction rate, *such that, for all $\mathbf{x} \in C$, $t \in \mathbb{R}_{\geq 0}$, it holds that*

$$\mu\left(\frac{\partial \mathbf{f}(\mathbf{x}; t)}{\partial \mathbf{x}}\right) \leq -c. \qquad (10.2)$$

If μ is induced by the p-norm, we say that $\mathbf{f}$ is contractive in norm p.

---

[a]A set C is *forward invariant* for a system if $\mathbf{x}_0 \in C$ implies $\boldsymbol{\psi}(t, t_0, \mathbf{x}_0) \in C$ for all t.
[b]A set $C \subseteq \mathbb{R}^n$ is *K-reachable* if, for any two points $\mathbf{x}_1, \mathbf{x}_2 \in C$, there exists a continuously

differentiable curve $\gamma : [0, 1] \to C$, with $\gamma(0) = \mathbf{x}_1$ and $\gamma(1) = \mathbf{x}_2$ such that, for all $r \in [0, 1]$, it holds that $|d\gamma(r)/dr| \leq K |\mathbf{x}_1 - \mathbf{x}_2|$. It is immediate to show that convex sets are 1-reachable and vice-versa.

[c]For more detail on matrix measures, see Section 4.1.

Definition 10.2 (Incremental exponential stability). *If for every two solutions of system* (10.1)*, say* $\mathbf{x}_1(t) = \boldsymbol{\psi}(t, t_0, \mathbf{x}_0)$ *and* $\mathbf{y}(t) = \boldsymbol{\psi}(t, t_0, \mathbf{y}_0)$ *with initial conditions* $\mathbf{x}_0, \mathbf{y}_0 \in C$, *there exists* $c > 0$, *called the* convergence rate, *it holds that*

$$\|\mathbf{x}(t) - \mathbf{y}(t)\| \leq K \, \mathrm{e}^{-c(t-t_0)} \, \|\mathbf{x}_0 - \mathbf{y}_0\|, \quad \forall t \geq t_0, \tag{10.3}$$

then the system is incrementally exponentially stable *(IES) in C.*

Theorem 10.3. *If the vector field in system* (10.1) *is contractive in C with contraction rate c, then, the system is incrementally exponentially stable in C with convergence rate c.*

In this work, we analyze contraction properties of dynamical systems based on norms and matrix measures [94, 122]. Other more general definitions exist in the literature, for example results based on Riemannian metrics [94] and Finsler-Lyapunov functions [60]. The relationships between these three definitions and the definition of convergence [111] were investigated in [60].

10.2.2 Switched systems

Switched (or bimodal) Filippov systems are dynamical systems $\dot{\mathbf{x}} = \mathbf{f}(\mathbf{x})$ where $\mathbf{f}(\mathbf{x})$ is a piecewise-continuous vector field having a codimension-one submanifold Σ as its discontinuity set [56, 137]. The submanifold Σ is called the *switching manifold* and is defined as the zero set of a smooth function $h : U \subseteq \mathbb{R}^n \to \mathbb{R}$, that is $\Sigma \triangleq \{\mathbf{x} \in U \mid h(\mathbf{x}) = 0\}$, where $0 \in \mathbb{R}$ is a regular value of h, i.e., $\nabla h(\mathbf{x}) \neq \mathbf{0}, \forall \mathbf{x} \in \Sigma$. Σ divides U in two disjoint regions, $\mathcal{S}^+ \triangleq \{\mathbf{x} \in U \mid h(\mathbf{x}) > 0\}$ and $\mathcal{S}^- \triangleq \{\mathbf{x} \in U \mid h(\mathbf{x}) < 0\}$ (see Figure 10.1).

Hence, a bimodal Filippov system can be defined as

$$\dot{\mathbf{x}} = \begin{cases} \mathbf{f}^+(\mathbf{x}), & \text{if } \mathbf{x} \in \mathcal{S}^+ \\ \mathbf{f}^-(\mathbf{x}), & \text{if } \mathbf{x} \in \mathcal{S}^- \end{cases}, \tag{10.4}$$

where $\mathbf{f}^+, \mathbf{f}^- \in C^1(U, \mathbb{R}^n)$. We assume that solutions of system (10.4) are defined in the sense of Filippov (and therefore admitting *sliding* motions on Σ) and they have the property of *right-uniqueness* in U [56, pag. 106]. Condition (10.2) was previously presented as a sufficient condition for a dynamical system to be incrementally exponentially stable, but it cannot be directly applied to system (10.4) because its vector field is not continuously differentiable. In recent work reported in [58], sufficient conditions were derived for convergence of any two trajectories of a Filippov system towards each other. Instead
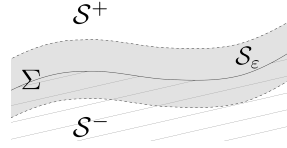
Figure 10.1: Regions of state space: switching manifold Σ, $\mathcal{S}^+$, $\mathcal{S}^-$ (hatched zone) and $\mathcal{S}_\varepsilon$ (grey zone).

of directly analyzing the Filippov vector field on Σ, the analysis is conducted on its regularization, say $\mathbf{f}_\varepsilon(\mathbf{x})$, defined as

$$\mathbf{f}_\varepsilon(\mathbf{x}) = \frac{1 + \varphi_\varepsilon\,(h(\mathbf{x}))}{2}\,\mathbf{f}^+(\mathbf{x}) + \frac{1 - \varphi_\varepsilon\,(h(\mathbf{x}))}{2}\,\mathbf{f}^-(\mathbf{x}),$$

where $\varphi_\varepsilon \in C^1(\mathbb{R}, \mathbb{R})$ is the so-called transition function. In this new system the switching manifold Σ is replaced by a boundary layer $\mathcal{S}_\varepsilon$ (Figure 10.1) of width 2ε, defined as $\mathcal{S}_\varepsilon \triangleq \{\mathbf{x} \in U \mid -\varepsilon < h(\mathbf{x}) < \varepsilon\}$, and, more importantly, $\mathbf{f}_\varepsilon$ is continuously differentiable in U, so that condition (10.2) can be applied to it. Finally, contraction properties of Filippov systems (10.4) are recovered taking the limit for $\varepsilon \to 0$ and considering the following Lemma.

Lemma 10.4. *Denoting by $\mathbf{x}_\varepsilon(t)$ a solution to the regularized system and by $\mathbf{x}(t)$ a solution to the switched system with the same initial conditions $\mathbf{x}_0$, then $\|\mathbf{x}_\varepsilon(t) - \mathbf{x}(t)\| = O(\varepsilon)$, uniformly for all $t \geq t_0$ and for all $\mathbf{x}_0 \in U$.*

For further details see [128, 137, 58]. The resulting sufficient conditions for a bimodal Filippov system to be incrementally exponentially stable in a certain set are stated in the following theorem (see [58] for a complete proof and further details).

Theorem 10.5. *The bimodal switched system* (10.4) *is incrementally exponentially stable in a K-reachable set $C \subseteq U$ with convergence rate $c \triangleq \min\{c_1, c_2\}$ if there exists some norm in C, with associated matrix measure μ, such that, for some positive constants c_1, c_2,*

$$\mu\left(\frac{\partial \mathbf{f}^+}{\partial \mathbf{x}}(\mathbf{x})\right) \leq -c_1, \quad \forall \mathbf{x} \in \bar{\mathcal{S}}^+,$$

$$\mu\left(\frac{\partial \mathbf{f}^-}{\partial \mathbf{x}}(\mathbf{x})\right) \leq -c_2, \quad \forall \mathbf{x} \in \bar{\mathcal{S}}^-,$$

$$\mu\left(\left[\mathbf{f}^+(\mathbf{x}) - \mathbf{f}^-(\mathbf{x})\right]\nabla h(\mathbf{x})\right) = 0, \quad \forall \mathbf{x} \in \Sigma.$$

In the above relations $\bar{\mathcal{S}}^+$ and $\bar{\mathcal{S}}^-$ represent the closures of the sets $\mathcal{S}^+$ and $\mathcal{S}^-$, respectively.

10.3   State observer design

10.3.1   Problem formulation

Consider the bimodal switched system

$$\dot{\mathbf{x}} = \begin{cases} \mathbf{f}^+(\mathbf{x}) + \mathbf{u}(t), & h(\mathbf{x}) > 0 \\ \mathbf{f}^-(\mathbf{x}) + \mathbf{u}(t), & h(\mathbf{x}) < 0 \end{cases}, \tag{10.5}$$

$$\mathbf{y} = \mathbf{g}(\mathbf{x}), \tag{10.6}$$

where $\mathbf{x} \in \mathbb{R}^n, \mathbf{y} \in \mathbb{R}^p, \mathbf{u} \in \mathbb{R}^n$ are the state, output and the input of the system, respectively, and $\mathbf{f}^+, \mathbf{f}^-, \mathbf{g}$ are continuously differentiable vector fields.

As an observer for the system (10.5)-(10.6), we propose a bimodal Luenberger-like switched observer of the form

$$\dot{\hat{\mathbf{x}}} = \begin{cases} \mathbf{f}^+(\hat{\mathbf{x}}) + \mathbf{L}^+(\mathbf{y} - \hat{\mathbf{y}}) + \mathbf{u}(t), & h(\hat{\mathbf{x}}) > 0 \\ \mathbf{f}^-(\hat{\mathbf{x}}) + \mathbf{L}^-(\mathbf{y} - \hat{\mathbf{y}}) + \mathbf{u}(t), & h(\hat{\mathbf{x}}) < 0 \end{cases}, \tag{10.7}$$

$$\hat{\mathbf{y}} = \mathbf{g}(\hat{\mathbf{x}}), \tag{10.8}$$

where $\hat{\mathbf{x}}(t) \in \mathbb{R}^n$ is the estimated state and $\mathbf{L}^+, \mathbf{L}^- \in \mathbb{R}^{n \times p}$ are observer gain matrices to be selected appropriately.

We are interested in deriving conditions on the observer gain matrices $\mathbf{L}^+$ and $\mathbf{L}^-$ that guarantee exponential convergence to 0 of the estimation error $\mathbf{e}(t) \triangleq \mathbf{x}(t) - \hat{\mathbf{x}}(t)$ for all $\mathbf{x}(t) : \mathbb{R}^+ \to \mathbb{R}^n$ satisfying (10.5)-(10.6) for any given continuous function $\mathbf{u}(t) : \mathbb{R}^+ \to \mathbb{R}^n$. Note that in what follows we will not require system (10.5)-(10.6) to be contracting, i.e. Theorem 10.5 must not necessarily hold for this system. Instead, contraction theory will be exploited to analyze convergence of the system describing the dynamics of the estimation error.

10.3.2   Main results

Theorem 10.6. *The state estimation error* $\mathbf{e}(t)$ *converges exponentially to zero, that is, for some* $c > 0$,

$$\|\mathbf{e}(t)\| \leq K \, e^{-c(t-t_0)} \|\mathbf{x}(t_0)\|, \quad \forall t \geq t_0, \tag{10.9}$$

if there exists some matrix measure μ, *such that, for some positive constants* c_1, c_2,

$$\mu\left(\frac{\partial \mathbf{f}^+}{\partial \mathbf{x}}(\hat{\mathbf{x}}) - \mathbf{L}^+ \frac{\partial \mathbf{g}}{\partial \mathbf{x}}(\hat{\mathbf{x}}) \right) \leq -c_1, \forall \hat{\mathbf{x}} : h(\hat{\mathbf{x}}) > 0, \tag{10.10}$$

$$\mu\left(\frac{\partial \mathbf{f}^-}{\partial \mathbf{x}}(\hat{\mathbf{x}}) - \mathbf{L}^- \frac{\partial \mathbf{g}}{\partial \mathbf{x}}(\hat{\mathbf{x}}) \right) \leq -c_2, \forall \hat{\mathbf{x}} : h(\hat{\mathbf{x}}) < 0, \tag{10.11}$$

$$\mu\left(\left[\Delta\mathbf{f}(\hat{\mathbf{x}}) + \Delta\mathbf{L}(y - \hat{y})\right]\nabla h(\hat{\mathbf{x}})\right) = 0, \forall\hat{\mathbf{x}} : h(\hat{\mathbf{x}}) = 0, \qquad (10.12)$$

where $\Delta\mathbf{f}(\hat{\mathbf{x}}) = \mathbf{f}^+(\hat{\mathbf{x}}) - \mathbf{f}^-(\hat{\mathbf{x}})$ and $\Delta\mathbf{L} = \mathbf{L}^+ - \mathbf{L}^-$. Moreover, the convergence rate c can be estimated as $\min\{c_1, c_2\}$.

Proof. Conditions (10.10)-(10.12) come from the application of Theorem 10.5 to the dynamics of the state observer (10.7)-(10.8) by rewriting them as

$$\dot{\hat{\mathbf{x}}} = \begin{cases} \bar{\mathbf{f}}^+(\hat{\mathbf{x}}) + \boldsymbol{\eta}^+(t), & h(\hat{\mathbf{x}}) > 0 \\ \bar{\mathbf{f}}^-(\hat{\mathbf{x}}) + \boldsymbol{\eta}^-(t), & h(\hat{\mathbf{x}}) < 0 \end{cases},$$

where $\bar{\mathbf{f}}^\pm(\hat{\mathbf{x}}) = \mathbf{f}^\pm(\hat{\mathbf{x}}) - L^\pm\mathbf{g}(\hat{\mathbf{x}})$ depends only on $\hat{\mathbf{x}}$, and $\boldsymbol{\eta}^\pm(t) = \mathbf{L}^\pm\mathbf{g}(\mathbf{x}(t)) + \mathbf{u}(t)$ is a function of t.

Hence, if such conditions are satisfied, then the state observer is contracting; this in turn implies that, for two generic solutions $\hat{\mathbf{x}}_1(t)$ and $\hat{\mathbf{x}}_2(t)$, (10.3) holds, i.e.

$$\|\hat{\mathbf{x}}_1(t) - \hat{\mathbf{x}}_2(t)\| \leq K\,\mathrm{e}^{-c(t-t_0)}\,\|\hat{\mathbf{x}}_1(t_0) - \hat{\mathbf{x}}_2(t_0)\|, \ \forall t \geq t_0.$$

Now, notice that a solution $\mathbf{x}(t)$ of system (10.5) is a particular solution of the observer (10.7) — because (10.5) and (10.7) have the same structure, except for the correction term $\mathbf{g}(\mathbf{x}) - \mathbf{g}(\hat{\mathbf{x}})$, which is null when considering $\mathbf{x}(t)$ as a solution of the observer. Then, we can replace $\hat{\mathbf{x}}_2(t)$ with $\mathbf{x}(t)$, rename $\hat{\mathbf{x}}_1(t)$ as the general solution $\hat{\mathbf{x}}(t)$, and write

$$\|\mathbf{e}(t)\| = \|\mathbf{x}(t) - \hat{\mathbf{x}}(t)\| \leq K\,\mathrm{e}^{-c(t-t_0)}\,\|\mathbf{x}(t_0)\|,$$

for all $t \geq t_0$, where $\hat{\mathbf{x}}(t_0) = 0$ as usual in observer design. Hence, the exponential convergence to zero of the estimation error is proved. $\qquad\square$

Remark 10.7. *Alternatively, the theorem can be proved considering the regularized dynamics of both system (10.5) and observer (10.7). Denoting by $\mathbf{x}_\varepsilon(t)$ a solution to the regularized switched system (10.5), and by $\hat{\mathbf{x}}_\varepsilon(t)$ a solution to the regularized observer (10.7), we have*

$$\|\mathbf{e}(t)\| = \|\mathbf{x}(t) - \hat{\mathbf{x}}(t)\|$$
$$\leq \|\mathbf{x}(t) - \mathbf{x}_\varepsilon(t)\| + \|\mathbf{x}_\varepsilon(t) - \hat{\mathbf{x}}_\varepsilon(t)\| + \|\hat{\mathbf{x}}_\varepsilon(t) - \hat{\mathbf{x}}(t)\|.$$

The first and the third terms are the error between a solution to the discontinuous system and a solution to its regularized counterpart; hence, from Lemma 10.4 we know that $\|\mathbf{x}(t) - \mathbf{x}_\varepsilon(t)\| = O(\varepsilon)$, and $\|\hat{\mathbf{x}}(t) - \hat{\mathbf{x}}_\varepsilon(t)\| = O(\varepsilon)$.

Furthermore, similarly to what done in [58], it can be shown that conditions (10.10)-(10.12) imply incremental stability of the trajectories of the regularized observer, thus

$$\left\|\hat{\mathbf{x}}_{\varepsilon,1}(t) - \hat{\mathbf{x}}_{\varepsilon,2}(t)\right\| \leq K\,\mathrm{e}^{-c(t-t_0)}\left\|\hat{\mathbf{x}}_{\varepsilon,1}(t_0) - \hat{\mathbf{x}}_{\varepsilon,2}(t_0)\right\|, \forall t \geq t_0.$$

The theorem is finally proved by taking the limit for $\varepsilon \to 0^+$ and taking the same last

step as that in the proof of Theorem 10.6.

Remark 10.8. *If one of the two modes, $\mathbf{f}^+$ or $\mathbf{f}^-$, of the observed system (10.5) is already contracting, the corresponding observer gain matrix, $\mathbf{L}^+$ or $\mathbf{L}^-$, in (10.7) can be set to zero to simplify the design problem. The drawback is that the convergence rate of the estimation error will depend on that of the contracting mode that cannot be altered if this choice is made.*

Remark 10.9. *In the presence of bounded disturbances or uncertainties on the models, contraction properties of the vector fields guarantee boundedness of the estimation error (a more detailed analysis is not the aim of the current paper; the interested reader can refer to [94]).*

10.4   Examples

Here we present some examples to illustrate the use of Theorem 10.6 for the design of observers for switched systems. All simulations presented in this section have been computed using the numerical solver in [114].

10.4.1   Example 1: A nonlinear piecewise-smooth system

Consider a nonlinear bimodal switched system as in (10.5)-(10.6) with

$$\mathbf{f}^+(\mathbf{x}) = \begin{bmatrix} -9x_1 - 3x_1^2 - 18 \\ -4x_2 \end{bmatrix}, \ \mathbf{f}^-(\mathbf{x}) = \begin{bmatrix} -9x_1 + 3x_1^2 + 18 \\ -4x_2 \end{bmatrix},$$

and $h(x) = x_1$, $y = g(x) = x_1^2$.

According to Theorem 10.6, a state observer as in (10.7)-(10.8) with $\mathbf{L}^+ = [\ell_1^+ \ \ell_2^+]^T$ and $\mathbf{L}^- = [\ell_1^- \ \ell_2^-]^T$ for this system has the property that its estimation error converges exponentially to zero if there exist choices of the gain matrices $\mathbf{L}^+$ and $\mathbf{L}^-$ so that all three conditions (10.10)-(10.12) are satisfied.

To find $\mathbf{L}^+$ and $\mathbf{L}^-$, it is first necessary to select a specific matrix measure; here we use the measure μ_1, associated to the so-called ℓ^1-norm (see Section 4.1). Therefore, conditions (10.10) and (10.11) translate respectively to

$$\mu_1 \left(\begin{bmatrix} -9 - 6\hat{x}_1 - 2\ell_1^+ \hat{x}_1 & 0 \\ -2\ell_2^+ \hat{x}_1 & -4 \end{bmatrix} \right) < 0, \quad \text{with } \hat{x}_1 > 0,$$

$$\mu_1 \left(\begin{bmatrix} -9 + 6\hat{x}_1 - 2\ell_1^- \hat{x}_1 & 0 \\ -2\ell_2^- \hat{x}_1 & -4 \end{bmatrix} \right) < 0, \quad \text{with } \hat{x}_1 < 0.$$

Selecting for simplicity $\ell_2^+ = \ell_2^- = 0$, the above inequalities are satisfied if

$$\max\{-9 - 6\hat{x}_1 - 2\ell_1^+ \hat{x}_1, \ -4\} < 0, \quad \text{with } \hat{x}_1 > 0,$$
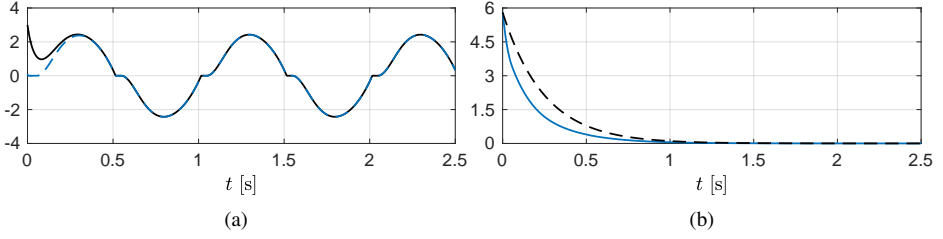
Figure 10.2: Panel a: Time evolution of the states $x_1(t)$ (solid line) and $\hat{x}_1(t)$ (dashed line) of Example 1, with initial conditions $\mathbf{x}_0 = [3 \; 3]^T$, $\hat{\mathbf{x}}_0 = [0 \; 0]^T$. Panel b: Norm of the estimation error $\|\mathbf{e}(t)\|_1$. The dashed line represents the analytical estimate (10.9) with $c = 4$ and $K = 1$. Parameters: $\mathbf{L}^+ = [-2 \; 0]^T$ and $\mathbf{L}^- = [2 \; 0]^T$.

$$\max\{-9 + 6\hat{x}_1 - 2\ell_1^- \hat{x}_1, \; -4\} < 0, \quad \text{with } \hat{x}_1 < 0.$$

This is true if $\ell_1^+ > -3$ and $\ell_1^- < 3$.
Next, from the the third condition (10.12), we have

$$\mu_1\left(\begin{bmatrix} -6\hat{x}_1^2 - 36 + (\ell_1^+ - \ell_1^-)(x_1^2 - \hat{x}_1^2) \\ 0 \end{bmatrix} \begin{bmatrix} 1 & 0 \end{bmatrix}\right) = 0,$$

with $\hat{x}_1 = 0$, which is verified if $\max\{-36+(\ell_1^+-\ell_1^-)x_1^2, \; 0\} = 0$, i.e. if $-36+(\ell_1^+-\ell_1^-)x_1^2 < 0$, which holds for all x_1 if $\ell_1^+ < \ell_1^-$. Therefore, to satisfy all three conditions of Theorem 10.6, it is possible for example to select $\mathbf{L}^+ = [-2 \; 0]^T$ and $\mathbf{L}^- = [2 \; 0]^T$. The resulting state observer is contracting and its estimation error satisfies (10.9) with convergence rate $c = 4$. In Figure 10.2(a) we show numerical simulations of the evolution of the states x_1 and $\hat{x}_1$ when an input $\mathbf{u}(t) = [1 \; 1]^T \sin(2\pi t)$ of period $T = 1$ is applied to the system. In Figure 10.2(b) the evolution of the ℓ^1-norm of the state estimation error $e(t)$ is reported, confirming the analytical estimate (10.9).

10.4.2 Example 2: A piecewise-affine system

Consider a piecewise-affine (PWA) system of the form

$$\dot{\mathbf{x}} = \begin{cases} \mathbf{A}_1\mathbf{x} + \mathbf{b}_1 + \mathbf{B}u, & \text{if } \mathbf{h}^T\mathbf{x} > 0 \\ \mathbf{A}_2\mathbf{x} + \mathbf{b}_2 + \mathbf{B}u, & \text{if } \mathbf{h}^T\mathbf{x} < 0 \end{cases}, \tag{10.13}$$

$$y = \mathbf{c}^T\mathbf{x}, \tag{10.14}$$

where

$$\mathbf{A}_1 = \begin{bmatrix} -1 & 0 \\ 2 & -2 \end{bmatrix}, \; \mathbf{b}_1 = \begin{bmatrix} -1 \\ -3 \end{bmatrix}, \; \mathbf{A}_2 = \begin{bmatrix} -1 & 0 \\ 2 & -3 \end{bmatrix}, \; \mathbf{b}_2 = \begin{bmatrix} 2 \\ 4 \end{bmatrix},$$

and $\mathbf{B} = [0 \ 1]^\mathsf{T}$, $\mathbf{h} = [0 \ 1]^\mathsf{T}$, $\mathbf{c} = [1 \ 1]^\mathsf{T}$.

A state observer as in (10.7)-(10.8) for this system has the structure

$$\dot{\hat{\mathbf{x}}} = \begin{cases} \mathbf{A}_1\hat{\mathbf{x}} + \mathbf{b}_1 + \mathbf{L}^+(y - \hat{y}) + \mathbf{B}u, & \text{if } \mathbf{h}^\mathsf{T}\hat{\mathbf{x}} > 0 \\ \mathbf{A}_2\hat{\mathbf{x}} + \mathbf{b}_2 + \mathbf{L}^-(y - \hat{y}) + \mathbf{B}u, & \text{if } \mathbf{h}^\mathsf{T}\hat{\mathbf{x}} < 0 \end{cases}, \tag{10.15}$$

$$\hat{y} = \mathbf{c}^\mathsf{T}\hat{\mathbf{x}}, \tag{10.16}$$

where, for the sake of simplicity, we choose $\mathbf{L}^+ = \mathbf{L}^- = \mathbf{L}$. Again we decide to proceed using the matrix measure induced by the ℓ^1-norm. In this case, conditions (10.10) and (10.11) yield respectively $\mu_1\left(\mathbf{A}_1 - \mathbf{Lc}^\mathsf{T}\right) = \max\{-1 - \ell_1 + |2 - \ell_2|, -2 - \ell_2 + |\ell_1|\}$, and $\mu_1\left(\mathbf{A}_2 - \mathbf{Lc}^\mathsf{T}\right) = \max\{-1 - \ell_1 + |2 - \ell_2|, -3 - \ell_2 + |\ell_1|\}$. It is easy to verify that choosing $\ell_1 = \ell_2 = 1$ both measures are equal to -1. Condition (10.12) is verified independently of $\mathbf{L}$.

Hence, the designed observer (10.15) is contracting and the estimation error converges exponentially to zero with rate $c = 1$. In Figure 10.3(a) we show numerical simulations of the evolution of the states x_2 and $\hat{x}_2$ when an input $u(t) = 4 \sin(2\pi t)$ of period $T = 1$ is applied to the system. In Figure 10.3(b) the evolution is reported of the ℓ^1-norm of the state estimation error $e(t)$.

Note that faster convergence can be obtained by choosing higher values of ℓ_1 and ℓ_2 fulfilling conditions (25)-(26). For example choosing $\mathbf{L} = [1.5 \ \ 2]^\mathsf{T}$ we obtain a convergence rate $c = 2.5$, as shown in Figure 10.3(c).

10.4.3 Example 3: An actuated dry friction oscillator

Consider now a harmonic oscillator affected by Coulomb friction, described by the equations

$$\begin{cases} \dot{x}_1 = x_2, \\ \dot{x}_2 = -\omega_\mathrm{n}^2 x_1 - \dfrac{\omega_\mathrm{n}}{Q}x_2 - \dfrac{F_\mathrm{f}}{m}\mathrm{sgn}(x_2) + \dfrac{F_\mathrm{d}}{m}\sin(\omega_\mathrm{d}t), \end{cases} \tag{10.17}$$

$$y = x_1, \tag{10.18}$$

where $x_1 \in \mathbb{R}$ is the position of the oscillator, $x_2 \in \mathbb{R}$ is its velocity, ω_n is its natural frequency, Q is said Q *factor* and is inversely proportional to the damping, m is the mass of the oscillator, F_d is the amplitude of the driving force, ω_d is the driving frequency and F_f is the amplitude of the dry friction force which is modeled through the sign function as in [35]. The proposed observer for system (10.17)-(10.18) has the form

$$\begin{cases} \dot{\hat{x}}_1 = \hat{x}_2 + \ell_1(x_1 - \hat{x}_1), \\ \dot{\hat{x}}_2 = -\omega_\mathrm{n}\hat{x}_1 - \dfrac{\omega_\mathrm{n}}{Q}\hat{x}_2 - \dfrac{F_\mathrm{f}}{m}\mathrm{sgn}(\hat{x}_2) + \ell_2(x_1 - \hat{x}_1) + \dfrac{F_\mathrm{d}}{m}\sin(\omega_\mathrm{d}t), \end{cases}$$

$$\hat{y} = \hat{x}_1.$$

Note that system (10.17) may be viewed as a PWA system (10.13) where

$$\mathbf{A}_1 = \mathbf{A}_2 = \begin{bmatrix} 0 & 1 \\ -\omega_\mathrm{d} & -\omega_\mathrm{d}/Q \end{bmatrix},$$
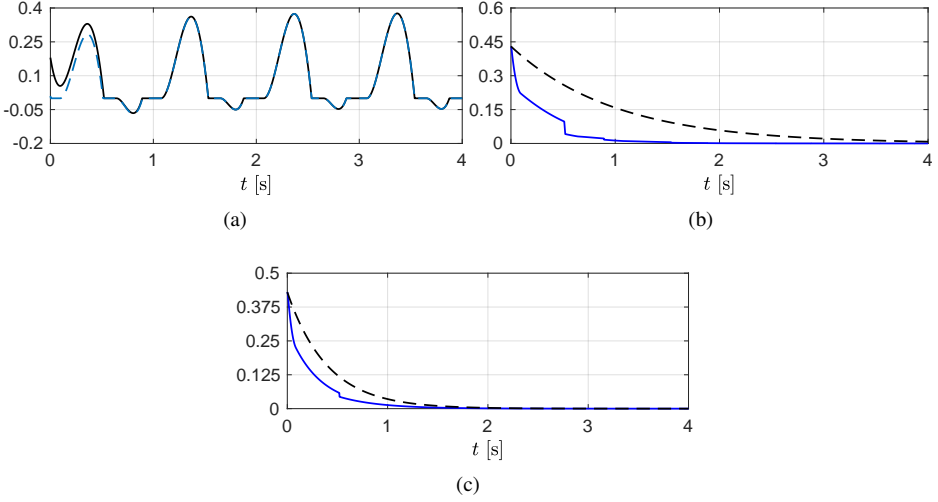
Figure 10.3: Panel a: Time evolution of the states $x_2(t)$ (solid line) and $\hat{x}_2(t)$ (dashed line) of Example 2, with initial conditions $\mathbf{x}_0 = [0.3\ \ 0.3]^\mathsf{T}$, $\hat{\mathbf{x}}_0 = [0\ \ 0]^\mathsf{T}$. Panel b: Norm of the estimation error $\|\mathbf{e}(t)\|_1$. The dashed line represents the analytical estimate (10.9) with $c = 1$ and $K = 1$. Parameters: $\mathbf{L}^+ = \mathbf{L}^- = [1\ \ 1]^\mathsf{T}$. Panel c: Norm of the estimation error using observer gain $\mathbf{L} = [1.5\ \ 2]^\mathsf{T}$.

$\mathbf{B} = [0\ \ 1/m]^\mathsf{T}$, $\mathbf{b}_1 = [0\ \ -F_{\mathrm{f}}/m]^\mathsf{T}$, $\mathbf{b}_2 = [0\ \ F_{\mathrm{f}}/m]^\mathsf{T}$, $\mathbf{h} = [0\ \ 1]^\mathsf{T}$, and excited by an input $u(t) = F_{\mathrm{d}}\sin(\omega_{\mathrm{d}}t)$.

Using the measure μ_∞ induced by the uniform norm (see Section 4.1), conditions (10.10) and (10.11) of Theorem 10.6, combined, yield

$$\mu_\infty\left(\begin{bmatrix} -\ell_1 & 1 \\ -\omega_{\mathrm{n}} - \ell_2 & -\omega_{\mathrm{n}}/Q \end{bmatrix}\right) < 0, \quad \text{with } \hat{x}_2 \neq 0,$$

which in turn is equivalent to

$$\max\{-\ell_1 + 1, -frac\omega_{\mathrm{n}}Q + |-\omega_{\mathrm{n}} - \ell_2|\} < 0, \quad \text{with } \hat{x}_2 \neq 0.$$

Therefore ℓ_1 and ℓ_2 must be chosen so that $\ell_1 > 1$, and $-\omega_{\mathrm{n}}(1 + 1/Q) < \ell_2 < -\omega_{\mathrm{n}}(1 - 1/Q)$.

Furthermore, condition (10.12) is verified if $\max\{0, -F_{\mathrm{f}}/m\} = 0$, which always holds because $F_{\mathrm{f}}, m > 0$.

Numerical simulations reported in Figure 10.4 confirm the theoretical predictions, showing that the estimation error converges to zero. In practice, the exact value of the parameter F_f is not known. This implies bounded convergence of the estimation error, as stated in Remark 10.9.

(a)   (b)
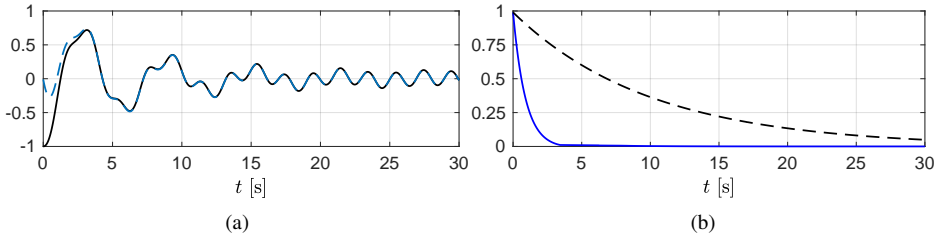
Figure 10.4:   Panel a: time evolution of the states $x_1(t)$ (solid line) and $\hat{x}_1(t)$ (dashed line) of Example 3, with initial conditions $\mathbf{x}_0 = [-1 \ \ 0]^\mathsf{T}$, $\hat{\mathbf{x}}_0 = [0 \ \ 0]^\mathsf{T}$. Panel b: Norm of the estimation error $\|\mathbf{e}(t)\|_\infty$. The dashed line represents the analytical estimate (10.9) with $c = 0.1$ and $K = 1$. Parameters: $\omega_\mathrm{n} = 1$ rad/s, $Q = 10$, $m = 1$ kg, $F_\mathrm{d} = 1$ N, $\omega_\mathrm{d} = \pi$ rad/s, $F_\mathrm{f} = 0.1$ N, $\ell_1 = 1.1$, $\ell_2 = -1$.

10.5   Discussion

We presented an approach based on contraction for the design of state observers for a large class of nonlinear switched systems including those exhibiting sliding motion, such as the friction oscillator. The design methodology is based on the analysis of incremental exponential stability based on the extension of contraction theory to switched bimodal Filippov systems derived in [58]. The conditions were formulated in terms of matrix measures of the Jacobians of the observer dynamics and of an additional condition on the vector fields on the discontinuity set. The theoretical results were illustrated through simple but representative examples demonstrating the effectiveness of the proposed methodology. Future work will be aimed at extending the approach to a wider class of switched systems, investigating constructive methods to design both metrics and observer gains, and reformulating the design procedure as a convex optimization problem to compute them numerically.

11 Conclusion

In Part I, we addressed the challenging problem of proving global asymptotic convergence to synchronization in a network of piecewise-smooth dynamical systems, without employing, as done in previous attempts in the literature, costly centralised control actions on all the nodes. We showed that, under some assumptions on the agents' vector field, adding a discontinuous coupling layer to the commonly used diffusive linear coupling protocol is sufficient to ensure convergence. We derived sufficient conditions that allow computation of the critical values of the coupling gains required for convergence, even when the inner coupling matrices are not positive definite. The conditions depend explicitly on structural properties of the underlying network graphs that can be computed algorithmically. In particular, we introduced the concept of *minimum density* of a graph that can be used to compute the critical coupling gain of the discontinuous control layer.

An open problem left for further study is to investigate if there exist some best structures of the diffusive and discontinuous coupling layers in terms of performance, robustness and stability. For example, numerical simulations reported in §5.5.4 show that different layers' structures can enhance the regions in the control parameter space where synchronization is attained. On the other hand, as illustrated in §5.5.2, some edges are more important than others in order to determine small thresholds on the coupling gains. Finally, in the future we will thoroughly investigate and discuss the application of the discontinuous coupling action to achieve asymptotic synchronization in networks of non-identical systems. As a matter of fact, In Appendix C, we demonstrated the feasibility of this approach.

In Part II, we focused on three problems related to the control of piecewise-smooth systems. In particular, (i, ii) we compared the performances of known control-schemes in the suppression of undesired oscillation in two different mechanical systems—an aircraft landing gear and a two-link planar robot, respectively—and (iii) expanded the mathematical design tools to synthesise observers of PWS systems. In nonlinear PWS systems, there are multiple different factors that can give birth to instabilities such as oscillations. Hence, the control schemes that best suit each case depend on the application. In the case of landing gear, we found that a zero average dynamics sliding control and a model reference adaptive controller with minimal control synthesis are both able to stabilise the system, even though the former gave slightly better performance. As far as the planar robot is concerned, we found out that hybrid force/motion control performs significantly better than a simpler PID control in the task of stabilisation. In both scenarios,

we have employed bifurcation analysis to guide the control synthesis process. Lastly, concerning observer design, our contribution owes much to recent advances in contraction theory for bimodal PWS systems. One of the main reasons this theory proves advantageous is that it allows to perform the design using any norm, when satisfying certain conditions, rather than only the euclidean norm, which is what was previously possible.

In these last lines, we would like to highlight what are the pieces that are still missing in the puzzle that piecewise-smooth systems are. First, concerning networks, we only studied state synchronization, where the states of all the agents converge towards the same trajectory. However, there exist a plethora of different collective behaviours that still deserve further investigation; these feature cluster synchronization, formation control, and partial state synchronization, among others. Moreover, one huge issue that hinders progress in network science as a hole, also for smooth systems, is the limitation that non-positive-definite inner coupling matrices pose (we are referring to the matrices Γ and Γ_d in (5.3)). Evidence suggests that in many cases it is not required that these matrices are positive definite to achieve synchronization (e.g., smooth mechanical oscillators coupled diffusively on position). Nonetheless, to the best of our knowledge, there are no fairly generic techniques to prove this globally, at the current state. Regarding the control theory on PWS systems, depicting a holistic framework of which research directions are the most pressing in this immensely vast topic would be beyond the scope of this thesis. Although, one current gap that emerged from our study of the literature is the observation of *multimodal* (i.e., not bimodal) PWS systems. If one thought that multimodal systems are rare, consider that one emerges as soon as a bimodal system is controlled with another one that does not share perfectly the switching hyper-plane. Besides, given the known relations between observability and controllability, advancements in the former field could easily contribute to research into the latter.

A Regularity conditions on vector fields

For the sake of comparison with the QUAD and σ-QUAD conditions (Definitions 2.3 and 2.4) presented in Section 2.2, we list here other regularity conditions for vector fields used in the literature on synchronization. The relations between the various conditions are reviewed in Figure A.1. Note that, as stated in Section 4.2, if a function $\mathbf{f}$ is discontinuous, when stating that a certain condition holds on $\mathbf{f}$, we imply that the condition must hold for all $\boldsymbol{\phi} \in \mathcal{F}[\mathbf{f}]$.

Definition A.1 (Lipschitz continuity [126]). *A function* $\mathbf{f} : \mathbb{R}^n \times \mathbb{R}_{\geq 0} \to \mathbb{R}^n$ *is* Lipschitz continuous *if there exists* $Q \in \mathbb{R}_{\geq 0}$ *such that, for all* $\boldsymbol{\xi}_1, \boldsymbol{\xi}_2 \in \mathbb{R}^n$, $t \in \mathbb{R}_{\geq 0}$, *it holds that*

$$\|\mathbf{f}(\boldsymbol{\xi}_1; t) - \mathbf{f}(\boldsymbol{\xi}_2; t)\| \leq Q \|\boldsymbol{\xi}_1 - \boldsymbol{\xi}_2\|.$$

Note that all Lipschitz continuous functions are continuous, but the converse is not true.

Definition A.2 (One-sided Lipschitz continuity [49]). *A function* $\mathbf{f} : \mathbb{R}^n \times \mathbb{R}_{\geq 0} \to \mathbb{R}^n$ *is* one-sided Lipschitz continuous *if there exists* $Q \in \mathbb{R}_{\geq 0}$ *such that, for all* $\boldsymbol{\xi}_1, \boldsymbol{\xi}_2 \in \mathbb{R}^n$, $t \in \mathbb{R}_{\geq 0}$, *it holds that*

$$(\boldsymbol{\xi}_1 - \boldsymbol{\xi}_2)^\mathsf{T} (\mathbf{f}(\boldsymbol{\xi}_1; t) - \mathbf{f}(\boldsymbol{\xi}_2; t)) \leq Q \|\boldsymbol{\xi}_1 - \boldsymbol{\xi}_2\|^2.$$

As examples, $f(x) = -x^3$ and $f(x) = -\text{sign}(x)$ are one-sided Lipschitz, but are not Lipschitz; $f(x) = +\text{sign}(x)$ is not one-sided Lipschitz, but is σ-QUAD. As a further note, it is immediate to show that if a function is QUAD($\mathbf{I}, \mathbf{Q}$), then it is one-sided Lipschitz with constant $Q = \lambda_{\min}(\text{sym}(\mathbf{Q}))$.

In the following proposition, we describe the relationship between QUADness (Definition 2.3) and contractivity (Definition 10.1).

Proposition A.3 (Relation between QUADness and contractivity [39]). *Consider a function* $\mathbf{f} : \mathbb{R}^n \times \mathbb{R}_{\geq 0} \to \mathbb{R}^n$.

- *If* $\mathbf{f}$ *is differentiable and QUAD($\mathbf{I}, \mathbf{Q}$) with* $\mathbf{Q}$ *being diagonal and* $\mathbf{Q} \geq -k\mathbf{I}$,
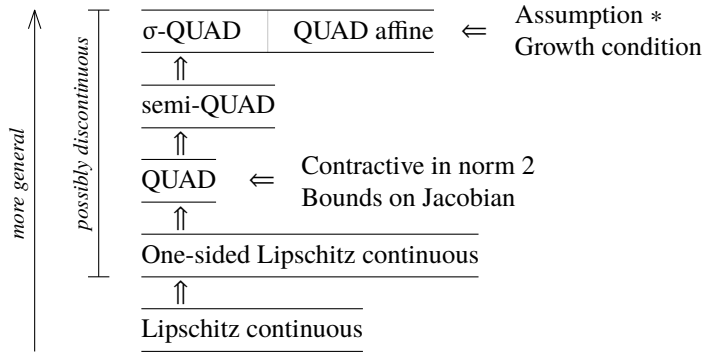
Figure A.1: Relations between regularity properties of vector fields. "Assumption ∗" refers to Assumption A.7. The horizontal implication in the top line refers to both σ-QUAD and QUAD affine.

with $k > 0$, then $\mathbf{f}$ is contractive in norm 2 with contraction rate $c \leq k$.
- If $\mathbf{f}$ is contractive in norm 2 with convergence rate $c > 0$, then $\mathbf{f}$ is QUAD($\mathbf{I}$, $\mathbf{Q}$) with $\mathbf{Q}$ being diagonal and $\mathbf{Q} \geq -c\mathbf{I}_n$.

It is also possible to show that if certain simple bounds hold on the Jacobian of a vector field $\mathbf{f}$, then it is QUAD.

Proposition A.4 (Bounds on Jacobian to infer QUADness). *If a function* $\mathbf{f} : \mathbb{R}^n \rightarrow \mathbb{R}^n$ *has an upper bounded Jacobian in* $\Omega \subseteq \mathbb{R}^n$, *in the sense that, for all* $\boldsymbol{\xi} \in \Omega$, *it holds that*

$$\frac{\partial f_i}{\partial x_i}(\boldsymbol{\xi}) \leq S_{ii},$$

$$\left| \frac{\partial f_i}{\partial x_j}(\boldsymbol{\xi}) \right| \leq S_{ij}, \quad i \neq j,$$

for $S_{ij} \in \mathbb{R}_{\geq 0}$, $i, j = 1, \ldots, n$, *then* $\mathbf{f}$ *is QUAD($\mathbf{I}$, $\mathbf{Q}$) in* Ω, *with* $\mathbf{Q}$ *being diagonal and* $Q_{ii} = S_{ii} + \sum_{j=1, j \neq i}^{n} \frac{S_{ij} + S_{ji}}{2}$.

Proof. Let us define $\boldsymbol{\xi}, \boldsymbol{\delta} \in \mathbb{R}^n$, so that $\boldsymbol{\xi}, \boldsymbol{\xi} + \boldsymbol{\delta} \in \Omega$. According to the mean value theorem for vector-valued functions, there exists $\lambda_i \in [0, 1]$ such that

$$f_i(\boldsymbol{\xi} + \boldsymbol{\delta}) - f_i(\boldsymbol{\xi}) = \nabla f_i(\boldsymbol{\xi} + \lambda_i \boldsymbol{\delta}) \, \boldsymbol{\delta}.$$

We can rewrite

$$f_i(\boldsymbol{\xi} + \boldsymbol{\delta}) - f_i(\boldsymbol{\xi}) = \sum_{j=1}^{n} \frac{\partial f_i(\boldsymbol{\xi} + \lambda_i \boldsymbol{\delta})}{\partial x_j} \delta_j.$$

We denote $\frac{\partial f_i(\boldsymbol{\xi})}{\partial x_j}$ by $J_{ij}(\boldsymbol{\xi})$ and multiply both sides by δ_i to get

$$\delta_i(f_i(\boldsymbol{\xi} + \boldsymbol{\delta}) - f_i(\boldsymbol{\xi})) = \sum_{j=1}^{n} J_{ij}(\boldsymbol{\xi} + \lambda_i \boldsymbol{\delta}) \, \delta_i \delta_j. \tag{A.1}$$

To streamline notation, we denote $J_{ij}(\boldsymbol{\xi} + \lambda_i \boldsymbol{\delta})$ simply by $\hat{J}_{ij}$. Adding (A.1) for all $i = 1, \ldots, n$, we have

$$\boldsymbol{\delta}^{\mathsf{T}}(\mathbf{f}(\boldsymbol{\xi} + \boldsymbol{\delta}) - \mathbf{f}(\boldsymbol{\xi})) = \sum_{i=1}^{n} \sum_{j=1}^{n} \hat{J}_{ij} \delta_i \delta_j = \sum_{i=1}^{n} \hat{J}_{ii} \delta_i^2 + \sum_{i=1}^{n} \sum_{j=1, j \neq i}^{n} \hat{J}_{ij} \delta_i \delta_j.$$

Notice that, recalling the expression of the square of a binomial and the bounds on the Jacobian, it holds that

$$\hat{J}_{ij} \delta_i \delta_j \leq \left| \hat{J}_{ij} \delta_i \delta_j \right| \leq \frac{\left| \hat{J}_{ij} \right|}{2} \left(\delta_i^2 + \delta_j^2 \right) \leq \frac{S_{ij}}{2} \left(\delta_i^2 + \delta_j^2 \right).$$

Then,

$$\boldsymbol{\delta}^{\mathsf{T}}(\mathbf{f}(\boldsymbol{\xi} + \boldsymbol{\delta}) - \mathbf{f}(\boldsymbol{\xi})) \leq \sum_{i=1}^{n} \hat{J}_{ii} \delta_i^2 + \sum_{i=1}^{n} \sum_{j=1, j \neq i}^{n} \frac{S_{ij}}{2} \left(\delta_i^2 + \delta_j^2 \right)$$

$$\leq \sum_{i=1}^{n} S_{ii} \delta_i^2 + \sum_{i=1}^{n} \sum_{j=1, j \neq i}^{n} \frac{S_{ij}}{2} \left(\delta_i^2 + \delta_j^2 \right)$$

$$\leq \sum_{i=1}^{n} \left(S_{ii} + \sum_{j=1, j \neq i}^{n} \frac{S_{ij} + S_{ji}}{2} \right) \delta_i^2.$$

Let $Q_{ii} = S_{ii} + \sum_{j=1, j \neq i}^{n} \frac{S_{ij} + S_{ji}}{2}$, $Q_{ij} = 0$ for $i \neq j$. Define $\boldsymbol{\xi}_1 \triangleq \boldsymbol{\xi} + \boldsymbol{\delta}$, and rename $\boldsymbol{\xi}$ as $\boldsymbol{\xi}_1$; the thesis is evident as we can rewrite

$$(\boldsymbol{\xi}_1 - \boldsymbol{\xi}_2)^{\mathsf{T}}(\mathbf{f}(\boldsymbol{\xi}_1) - \mathbf{f}(\boldsymbol{\xi}_2)) \leq (\boldsymbol{\xi}_1 - \boldsymbol{\xi}_2)^{\mathsf{T}} \mathbf{Q}(\boldsymbol{\xi}_1 - \boldsymbol{\xi}_2).$$

$\square$

Definition A.5 (semi-QUADness [90]). *A function* $\mathbf{f} : \mathbb{R}^n \times \mathbb{R}_{\geq 0} \to \mathbb{R}^n$ *is* semi-QUAD *if there exists* $\mathbf{g} : \mathbb{R}^n \times \mathbb{R}_{\geq 0} \to \mathbb{R}^n$ *such that*

   (i) *"condition λ" in [90] holds,[a]*
   (ii) $\mathbf{g}$ *is QUAD*$(\mathbf{P}, \mathbf{Q})$ *with* $\mathbf{Q}$ *being a diagonal matrix,*
   (iii) $\lim_{t \to +\infty} \mathbf{f}(\boldsymbol{\xi}; t) - \mathbf{g}(\boldsymbol{\xi}; t) = \mathbf{0}$, *for all* $\boldsymbol{\xi} \in \mathbb{R}^n$,
   (iv) $\int_0^{+\infty} \sup_{\boldsymbol{\xi}} |\mathbf{f}(\boldsymbol{\xi}; \tau) - \mathbf{g}(\boldsymbol{\xi}; \tau)| \, \mathrm{d}\tau < +\infty$, *for all* $\boldsymbol{\xi} \in \mathbb{R}^n$.

   ---
   [a]This a set of 6 more regularity conditions on $\mathcal{F}[\mathbf{f}]$.

Definition A.6 (QUAD affine condition [38]). *A function* $\mathbf{f} : \mathbb{R}^n \times \mathbb{R}_{\geq 0} \to \mathbb{R}^n$ *is* QUAD affine *if there exist* $\mathbf{g}, \mathbf{h} : \mathbb{R}^n \times \mathbb{R}_{\geq 0} \to \mathbb{R}^n$ *and* $M < +\infty$ *such that*

   (i) $\mathbf{f}(\boldsymbol{\xi}; t) = \mathbf{g}(\boldsymbol{\xi}; t) + \mathbf{h}(\boldsymbol{\xi}; t)$, *for all* $\boldsymbol{\xi} \in \mathbb{R}^n$, $t \in \mathbb{R}_{\geq 0}$,

  (ii) $\mathbf{g}$ *is QUAD,*

 (iii) $\|\mathbf{h}(\boldsymbol{\xi}; t)\|_2 < M$, *for all* $\boldsymbol{\xi} \in \mathbb{R}^n$, $t \in \mathbb{R}_{\geq 0}$.

Next, we report an assumption from [146] that was used to prove synchronization in piecewise-smooth networks.

Assumption A.7 ([146]). *Given* $\mathbf{f} : \mathbb{R}^n \times \mathbb{R}_{\geq 0} \to \mathbb{R}^n$, *there exist* $Q, M \in \mathbb{R}_{\geq 0}$ *such that, for all* $\boldsymbol{\xi}_1, \boldsymbol{\xi}_2 \in \mathbb{R}^n$, $t \in \mathbb{R}_{\geq 0}$, *it holds that*

$$(\boldsymbol{\xi}_1 - \boldsymbol{\xi}_2)^\top (\mathbf{f}(\boldsymbol{\xi}_1; t) - \mathbf{f}(\boldsymbol{\xi}_2; t)) \leq Q \|\boldsymbol{\xi}_1 - \boldsymbol{\xi}_2\|^2 + M \sum_{i=1}^{n} |\xi_{1,i} - \xi_{2,i}|.$$

Definition A.8 (Growth condition [93, 92]). *A function* $\mathbf{f} : \mathbb{R}^n \times \mathbb{R}_{\geq 0} \to \mathbb{R}^n$ *satisfies the* growth condition *if there exist* $Q, M \in \mathbb{R}_{\geq 0}$ *such that*

  (i) *it is continuously differentiable except on a finite set of isolated points, where the limit exist along all directions, and*

 (ii) $\|\mathbf{f}(\boldsymbol{\xi}; t)\|_p \leq Q \|\boldsymbol{\xi}\|_p + M$, *for all* $\boldsymbol{\xi} \in \mathbb{R}^n$, $t \in \mathbb{R}_{\geq 0}$, $p = 1, 2, \ldots, +\infty$.

B Minimum density
for selected topologies

With reference to the minimum density introduced in Definition 4.9 and in Section 4.3, we give a series of propositions that contain analytical expressions of this topological measure for complete, path, ring, star, and l-nearest neighbours graphs, which are represented in the examples in Figure 4.1.

Proposition B.1. *The minimum density of a complete graph $\mathcal{G}$ with N vertices is*

$$\delta_{\mathcal{G}} = N/2.$$

All cuts are a sparsest cut.

Proof. We apply a generic cut C that splits the graph in two subgraphs $\mathcal{G}_1 = (\mathcal{V}_1, \mathcal{E}_1)$ and $\mathcal{G}_2 = (\mathcal{V}_2, \mathcal{E}_2)$, with cardinalities N_1 and N_2, respectively. Since the graph $\mathcal{G}$ is a complete graph, each vertex in $\mathcal{V}_1$ is connected to each vertex in $\mathcal{V}_2$. Therefore, the number b of edges between the two subgraphs is $N_1 N_2$, independently of the cut. Then, exploiting (4.2), the thesis is proved. □

Proposition B.2. *The minimum density of a path graph $\mathcal{G}$ with N vertices is*

$$\delta_{\mathcal{G}} = \begin{cases} 2/N, & \text{if N is even,} \\ 2N/(N^2 - 1), & \text{if N is odd.} \end{cases}$$

A cut is a sparsest cut if and only if it minimises the difference in size between the two subgraphs.

Proof. We apply a generic cut C that splits the graph in two subgraphs $\mathcal{G}_1 = (\mathcal{V}_1, \mathcal{E}_1)$ and $\mathcal{G}_2 = (\mathcal{V}_2, \mathcal{E}_2)$, with cardinalities N_1 and N_2, respectively. Since the graph $\mathcal{G}$ is a path, the number b of edges between the two subgraphs is 1, independently of C. Then, in order to solve the minimisation problem in (4.2), we consider the problem $\max_{N_1, N_2} N_1 N_2$, which is solved when N_1 and N_2 are the closest (this also characterises the sparsest cut(s)).

Namely, when N is even, we take $N_1 = N_2 = N/2$; differently if N is odd, we select $N_1 = (N - 1)/2$ and $N_2 = (N + 1)/2$ or vice versa. These values of N_1 and N_2, when inserted in (4.2), prove the thesis. $\qquad\square$

Proposition B.3. *The minimum density of a ring graph $\mathcal{G}$ with $N \geq 3$ vertices is*

$$\delta_{\mathcal{G}} = \begin{cases} 4/N, & \text{if } N \text{ is even,} \\ 4N/(N^2 - 1), & \text{if } N \text{ is odd.} \end{cases}$$

A cut is a sparsest cut if and only if it minimises the difference in size between the two subgraphs.

Proof. The proof is almost identical to that of Proposition B.2, with the difference that here $b = 2$ (rather than $b = 1$). Note that if the hypothesis that $N \geq 3$ were not satisfied, the graph would be a path and not a ring. $\qquad\square$

Proposition B.4. *The minimum density of a star graph with N vertices is*

$$\delta_{\mathcal{G}} = N/2(N - 1).$$

A cut is a sparsest cut if and only if it generates a subgraph composed only of a single vertex that is not the centre of the star.

Proof. We apply a generic cut C that splits the graph in two subgraphs $\mathcal{G}_1 = (\mathcal{V}_1, \mathcal{E}_1)$ and $\mathcal{G}_2 = (\mathcal{V}_2, \mathcal{E}_2)$, with cardinalities N_1 and N_2, respectively. Without loss of generality, assume it is $\mathcal{G}_1$ that contains the centre vertex in the star. Then, the number b of edges between the two subgraphs is equal to N_2, as all vertices in $\mathcal{G}_2$ are connected only to the centre of the star in $\mathcal{G}_1$. Then, from (4.2),

$$\delta_{\mathcal{G}} = \frac{N}{2} \min_{C \in \hat{C}_{\mathcal{G}}} \frac{N_2}{N_1 N_2} = \frac{N}{2} \min_{C \in \hat{C}_{\mathcal{G}}} \frac{1}{N_1} = \frac{N}{2} \frac{1}{N - 1},$$

which corresponds to the thesis. For the minimisation, we took $N_1 = N - 1$, with $\mathcal{G}_1$ containing all vertices but one that is not the centre of the star. $\qquad\square$

Proposition B.5. *The minimum density of a l-nearest neighbours graph with N vertices and $l < (N - 1)/2$ is*

$$\delta_{\mathcal{G}} = \begin{cases} \dfrac{4 \sum_{k=0}^{l-1}(l - k)}{N}, & \text{if } N \text{ is even,} \\[3mm] \dfrac{4N \sum_{k=0}^{l-1}(l - k)}{N^2 - 1}, & \text{if } N \text{ is odd.} \end{cases}$$

A cut is a sparsest cut if and only if it minimises the difference in size between the two

subgraphs.

Proof. First, note that we require $l < (N-1)/2$ to ensure that $\mathcal{G}$ is not a complete graph. We apply a generic cut C that splits the graph in two subgraphs $\mathcal{G}_1 = (\mathcal{V}_1, \mathcal{E}_1)$ and $\mathcal{G}_2 = (\mathcal{V}_2, \mathcal{E}_2)$, with cardinalities N_1 and N_2, respectively. Assume, without loss of generality, that $N_1 \leq N_2$. It is straightforward to verify that the number b of edges between the two subgraphs is given as

$$b = 2 \sum_{k=0}^{K} (l-k), \quad K = \begin{cases} N_1 - 1, & \text{if } N_1 < l \\ l - 1, & \text{if } N_1 \geq l \end{cases} \tag{B.1}$$

First, we aim to show that

$$\left(\frac{b}{N_1 N_2} \right)_{1 \leq N_1 < l} \geq \left(\frac{b}{N_1 N_2} \right)_{N_1 = l},$$

which we will prove by demonstrating that

$$\left(\frac{b}{N_1 N_2} \right)_{N_1 = N_1^* - 1} \geq \left(\frac{b}{N_1 N_2} \right)_{N_1 = N_1^*}, \quad 2 \leq N_1^* \leq l. \tag{B.2}$$

In light of (B.1) and the fact that $N_2 = N - N_1$, (B.2), becomes

$$\frac{\sum_{k=0}^{N_1 - 2} (l-k)}{(N_1 - 1)(N - N_1 + 1)} \geq \frac{\sum_{k=0}^{N_1 - 1} (l-k)}{N_1 (N - N_1)}, \quad 2 \leq N_1 \leq l. \tag{B.3}$$

First, define

$$a \triangleq \sum_{k=0}^{N_1 - 1} (l - k) \tag{B.4}$$

and consider that

$$\sum_{k=0}^{N_1 - 2} (l - k) = a - (l - N_1 + 1). \tag{B.5}$$

At this point, using (B.4) and (B.5), (B.3) becomes

$$\frac{a - (l - N_1 + 1)}{(N_1 - 1)(N - N_1 + 1)} \geq \frac{a}{N_1 (N - N_1)}.$$

Through some manipulations, we get the following refinements:

$$[a - (l - N_1 + 1)][N_1(N - N_1)] - a[(N_1 - 1)(N - N_1 + 1)] \geq 0;$$

$$aN_1 N - aN_1^2 - lN_1 N + lN_1^2 + N_1^2 N - N_1^3 - N_1 N + N_1^2 - aN_1 N + aN_1^2 - aN_1 + aN - aN_1 + a \geq 0;$$

$$-lN_1 N + lN_1^2 + N_1^2 N - N_1^3 - N_1 N + N_1^2 - 2aN_1 + aN + a \geq 0. \tag{B.6}$$

Now, consider that

$$a = \sum_{k=0}^{N_1-1}(l - k) = N_1 l - \sum_{k=0}^{N_1-1} k = N_1 l - \frac{(N_1 - 1)N_1}{2},$$

which, inserted into (B.6), gives

$$-lN_1 N + lN_1^2 + N_1^2 N - N_1^3 - N_1 N + N_1^2 + \left(N_1 l - \frac{(N_1 - 1)N_1}{2}\right)(-2N_1 + N + 1) \geq 0;$$

$$-lN + lN_1 + N_1 N - N_1^2 - N + N_1 - 2lN_1 + lN + l + N_1^2 - N_1 - \frac{NN_1 - N}{2} - \frac{(N_1 - 1)}{2} \geq 0;$$

$$-2lN_1 + N_1 N - N + 2l - N_1 + 1 \geq 0;$$

$$(N - 2l - 1)(N_1 - 1) \geq 0.$$

The last inequality is satisfied because $N - 2l - 1 > 0$ and $N_1 - 1 \geq 0$, which proves that (B.2) actually holds. Through (B.2), we can establish that the optimal value of N_1 (generated by the sparsest cut) for (4.2) is at least equal to l. Next, we consider that in order to solve the minimisation in (4.2), we need to solve the problem

$$\min_{l \leq N_1 \leq N-1} \left(\frac{\sum_{k=0}^{l-1}(l - k)}{N_1(N - N_1)}\right),$$

that is equivalent to $\max_{N_1} N_1(N - N_1) = \max_{N_1} N_1 N_2$. This last problem is solved for N_1 being the closest to N_2 (this also characterises the sparsest cut(s)). That is, the optimal values of N_1 are $N/2$ if N is even, and $(N - 1)/2$ (or equivalently $(N + 1)/2$) if N is odd. This last consideration, together with (4.2) and (B.1), proves the value of the minimum density in the thesis. □

C An extension: Synchronization of heterogeneous systems

The theoretical results in Chapter 6 can be extended without great effort to prove synchronization in the case of networks of (smooth or non-smooth) heterogeneous agents. A thorough description of the state of the art on synchronization of heterogeneous systems is beyond the scope of this thesis. Nonetheless, we remark that it is known that a diffusive linear coupling action is not able to asymptotically synchronize heterogeneous networks [38, 109], but can only guarantee bounded convergence.

C.1 Theoretical results

In this framework each agent can have a different internal dynamics $\mathbf{f}_i(\mathbf{x}_i)$. Assume the presence of both a linear diffusive and a discontinuous coupling layers, the dynamics of the network is given by

$$\dot{\mathbf{x}}_i(t) = \mathbf{f}_i(\mathbf{x}_i; t) - c \sum_{j=1}^{N} L_{ij} \mathbf{\Gamma}(\mathbf{x}_j - \mathbf{x}_i) - c_{\mathrm{d}} \sum_{j=1}^{N} L_{ij}^{\mathrm{d}} \mathbf{\Gamma}_{\mathrm{d}} \mathrm{sign}(\mathbf{x}_j - \mathbf{x}_i), \quad i = 1, \ldots, N, \ \ (\text{C.1})$$

where the symbols have the same meaning as those in (5.3). Let us define the average vector field $\tilde{\mathbf{f}} : \mathbb{R}^{nN} \to \mathbb{R}^n$ as

$$\tilde{\mathbf{f}}(\bar{\mathbf{x}}) \triangleq \frac{1}{N} \sum_{i=1}^{N} \mathbf{f}_i(\mathbf{x}_i) = \dot{\bar{\mathbf{x}}}, \tag{C.2}$$

where the coupling terms in $\dot{\bar{\mathbf{x}}}$ cancel out thanks to the fact that $\mathbf{L}$ and $\mathbf{L}_{\mathrm{d}}$ are symmetric. We also let $\mathcal{A}_r^{\mathrm{c}}$ be a closed ball of the origin with radius $r \in \mathbb{R}_{>0}$, and introduce the following definition.

Definition C.1 (Uniform ultimate boundedness). *A dynamical system is* uniformly ultimately bounded *to $\mathcal{A}_r^c$, if there exists a function $T : \mathbb{R}^n \rightarrow [0, +\infty[$ such that*

$$\forall t \geq T(\mathbf{x}(0)), \quad \|\mathbf{x}(t)\| \leq r.$$

Theorem C.2. *Consider network* (C.1). *If*

   (a) *the network is uniformly ultimately bounded to some ball $\mathcal{A}_r^c$,*
   (b) *each agent dynamics $\mathbf{f}_i$ is QUAD($\mathbf{P}$, $\mathbf{Q}_i$) in $\mathcal{A}_r^c$, and* sym($\mathbf{P}\Gamma$) > 0 *and* $\mu_\infty^-(\mathbf{P}\Gamma_d) > 0$.
   (c) *$\mathcal{G}$ and $\mathcal{G}_d$ are connected graphs,*

then

   (a) *there exist some thresholds c^* and c_d^* such that, if both $c > c^*$ and $c_d \geq c_d^*$, then global asymptotic synchronization is achieved. Moreover, the asymptotic synchronous trajectory $\mathbf{s}(t)$ is a solution to $\dot{\mathbf{s}}(t) = \frac{1}{N} \sum_{i=1}^{N} \mathbf{f}_i(\mathbf{s}(t); t)$.*
   (b) *c^* and c_d^* are given by*

$$c^* \triangleq \frac{\max_i (\|\mathbf{Q}_i\|_2)}{\lambda_2(\mathbf{L})\lambda_{\min}(\text{sym } \mathbf{P}\Gamma)}, \quad c_d^* \triangleq \frac{\|(|\mathbf{P}|)\,\mathbf{m}\|_\infty}{\delta_{\mathcal{G}_d}\mu_\infty^-(\mathbf{P}\Gamma_d)}, \tag{C.3}$$

where $\mathbf{m}$ is a vector such that

$$\mathbf{m} \geq \left|\mathbf{f}_i(\tilde{\mathbf{x}}) - \tilde{\mathbf{f}}(\tilde{\mathbf{x}})\right|, \qquad \forall i \in [1, \ldots, N], \forall \tilde{\mathbf{x}} \in \mathcal{A}_r^c.$$

Proof. Recalling that $\mathbf{e}_i \triangleq \mathbf{x}_i - \tilde{\mathbf{x}}$, we can compute that

$$\dot{\mathbf{e}}_i = \dot{\mathbf{x}}_i - \dot{\tilde{\mathbf{x}}} = \mathbf{f}_i(\mathbf{x}_i) - c\sum_{j=1}^{N} L_{ij}\Gamma(\mathbf{x}_j - \mathbf{x}_i) - c_d\sum_{j=1}^{N} L_{ij}^d\Gamma_d\text{sign}(\mathbf{x}_j - \mathbf{x}_i) - \tilde{\mathbf{f}}(\tilde{\mathbf{x}}). \tag{C.4}$$

Consider the candidate common Lyapunov function $V \triangleq \frac{1}{2}\sum_{i=1}^{N} \mathbf{e}_i^{\mathsf{T}}\mathbf{P}\mathbf{e}_i$. Then, exploiting (C.4), and following steps analogous to the proof of Theorem 5.5 in Section 6.4, we have

$$\dot{V} = \sum_{i=1}^{N} \mathbf{e}_i^{\mathsf{T}}\mathbf{P}\left(\mathbf{f}_i(\mathbf{x}_i) - \tilde{\mathbf{f}}(\tilde{\mathbf{x}})\right) - c\sum_{i=1}^{N}\sum_{j=1}^{N} L_{ij}\mathbf{e}_i^{\mathsf{T}}\mathbf{P}\Gamma\mathbf{e}_j - c_d\sum_{i=1}^{N}\sum_{j=1}^{N} L_{ij}^d\mathbf{e}_i^{\mathsf{T}}\mathbf{P}\Gamma_d\text{sign}(\mathbf{e}_j - \mathbf{e}_i).$$

Adding and subtracting $\sum_{i=1}^{N} \mathbf{e}_i^{\mathsf{T}}\mathbf{P}\mathbf{f}_i(\tilde{\mathbf{x}})$, we get

$$\dot{V} = \sum_{i=1}^{N} \mathbf{e}_i^{\mathsf{T}}\mathbf{P}\left(\mathbf{f}_i(\mathbf{x}_i) - \mathbf{f}_i(\tilde{\mathbf{x}})\right) + \sum_{i=1}^{N} \mathbf{e}_i^{\mathsf{T}}\mathbf{P}\left(\mathbf{f}_i(\tilde{\mathbf{x}}) - \tilde{\mathbf{f}}(\tilde{\mathbf{x}})\right)$$

$$- c\sum_{i=1}^{N}\sum_{j=1}^{N} L_{ij}\mathbf{e}_i^{\mathsf{T}}\mathbf{P}\Gamma\mathbf{e}_j - c_d\sum_{(i,j)\in\mathcal{E}_d} (\mathbf{e}_i - \mathbf{e}_j)^{\mathsf{T}}\mathbf{P}\Gamma_d\text{sign}(\mathbf{e}_i - \mathbf{e}_j).$$

At this point, we exploit the hypothesis that the network is uniformly ultimately bounded. Therefore, there exists a finite time T such that for $t \geq T$, $\|\mathbf{x}(t)\| \in \mathcal{A}_r^c$. From now on, we assume that $t \geq T$. Then, using the assumption that $\mathbf{f}_i$ is QUAD($\mathbf{P}, \mathbf{Q}_i$), we get that

$$\mathbf{e}_i^\mathsf{T} \mathbf{P} \left(\mathbf{f}_i(\mathbf{x}_i) - \mathbf{f}_i(\tilde{\mathbf{x}}) \right) \leq \mathbf{e}_i^\mathsf{T} \mathbf{Q}_i \mathbf{e}_i.$$

We define the diagonal block matrix $\bar{\mathbf{Q}}$ having $\mathbf{Q}_1, \ldots, \mathbf{Q}_N$ on its diagonal, so that we can rewrite $\sum_{i=1}^N \left(\mathbf{e}_i^\mathsf{T} \mathbf{Q}_i \mathbf{e}_i \right) = \bar{\mathbf{e}}^\mathsf{T} \bar{\mathbf{Q}} \bar{\mathbf{e}}$.

It is immediate to verify that since all $\mathbf{f}_i$ are QUAD in the compact set $\mathcal{A}_r^c$, they are also bounded therein. Hence, there exists a vector $\mathbf{m} \in \mathbb{R}_{\geq 0}^n$, such that

$$\mathbf{m} \geq \left| \mathbf{f}_i(\tilde{\mathbf{x}}) - \tilde{\mathbf{f}}(\tilde{\mathbf{x}}) \right|, \qquad \forall i \in [1, \ldots, N], \ \forall \tilde{\mathbf{x}} \in \mathcal{A}_r^c.$$

Therefore, letting $M \triangleq \|(|\mathbf{P}|) \mathbf{m}\|_\infty$, it holds that

$$\sum_{i=1}^N \mathbf{e}_i^\mathsf{T} \mathbf{P} \left(\mathbf{f}_i(\tilde{\mathbf{x}}) - \tilde{\mathbf{f}}(\tilde{\mathbf{x}}) \right) \leq \sum_{i=1}^N \|\mathbf{e}_i\|_1 \left\| \mathbf{P} \left(\mathbf{f}_i(\tilde{\mathbf{x}}) - \tilde{\mathbf{f}}(\tilde{\mathbf{x}}) \right) \right\|_\infty \leq M \sum_{i=1}^N \|\mathbf{e}_i\|_1 = M \|\bar{\mathbf{e}}\|_1 .$$

Now, defining $\bar{\mathbf{y}} \triangleq \left(\mathbf{B}_{\mathrm{d}}^\mathsf{T} \otimes \mathbf{I}_n \right) \bar{\mathbf{e}}$, we can rewrite $\dot{V} \leq W_1 + W_2$, where

$$W_1 \triangleq \bar{\mathbf{e}}^\mathsf{T} \left(\bar{\mathbf{Q}} - c\mathbf{L} \otimes \mathbf{P}\mathbf{\Gamma} \right) \bar{\mathbf{e}},$$

$$W_2 \triangleq M \|\bar{\mathbf{e}}\|_1 - c_{\mathrm{d}} \bar{\mathbf{y}}^\mathsf{T} \left(\mathbf{I}_{N_{\mathcal{E}_{\mathrm{d}}}} \otimes \mathbf{P}\mathbf{\Gamma}_{\mathrm{d}} \right) \mathrm{sign}(\bar{\mathbf{y}}).$$

From here, one can follow the steps in Section 6.4.2 to find that $W_1 < 0$ if $c > c^*$, and $W_2 \leq 0$ if $c_{\mathrm{d}} \geq c_{\mathrm{d}}^*$, with c^*, c_{d}^* given in (C.3). Finally, since $W_1 < 0$ and $W_2 \leq 0$, $\dot{V} < 0$, which means that all $\mathbf{e}_i$ tend to zero. In turn, this means that all $\mathbf{x}_i$ tend to $\tilde{\mathbf{x}}$, whose dynamics is given in (C.2). □

We wish to make three important remarks.

1. In Theorem C.2, to satisfy the hypothesis that the network is uniformly ultimately bounded, it is possible adapt some results in [115], which employ *semipassivity*. Indeed, with some care to account for discontinuities, it can be shown that if a network of diffusively coupled systems is uniformly ultimately bounded, than it retains this property even if a discontinuous coupling is added (with $c_{\mathrm{d}}, \mathbf{\Gamma}_{\mathrm{d}} \geq 0$). We omit a formalisation of these results and their proof as they are far beyond the scope of this thesis.

2. To satisfy the hypothesis that the dynamics are QUAD, it is possible to use Proposition A.4.

3. Theorem C.2 can easily be adapted to account for the fact that the dynamics $\mathbf{f}_i$ are discontinuous. In that case, the agents are required to be σ-QUAD($\mathbf{P}, \mathbf{Q}_i, \mathbf{M}_i$) (rather than QUAD) and the critical threshold for the discontinuous coupling layer is given by

$$c_{\mathrm{d}}^* \triangleq \frac{\|(|\mathbf{P}|) \mathbf{m}\|_\infty + \|\bar{\mathbf{M}}\|_\infty}{\delta_{\mathcal{G}_{\mathrm{d}}} \mu_\infty^-(\mathbf{P}\mathbf{\Gamma}_{\mathrm{d}})}, \qquad \text{where } \bar{\mathbf{M}} \triangleq \mathrm{diag}([\mathbf{M}_1 \ \cdots \ \mathbf{M}_N]).$$

C.2 Example

We consider a modified van der Pol oscillator in the form

$$\dot{\mathbf{x}} = \mathbf{f}(\mathbf{x}) + \mathbf{u} = \begin{bmatrix} x_2 - \epsilon_1 x_1 \\ \mu(1 - x_1^2 - \epsilon_2 x_2^2)x_2 - x_1 \end{bmatrix} + \begin{bmatrix} u_1 \\ u_2 \end{bmatrix},$$

where $\epsilon_1, \epsilon_2 > 0$. For small values of ϵ_1, ϵ_2, the phase portrait is topologically equivalent to that of a van der Pol oscillator. We then consider a complete network of three oscillators, all having $\epsilon_1 = 0.01$ and $\epsilon_2 = 0.001$ and with $\mu_1 = 1$, $\mu_2 = 2$, $\mu_3 = 3$, respectively. The agents are coupled with the diffusive and discontinuous coupling law in (C.1), with $\mathbf{\Gamma} = \mathbf{\Gamma}_d = \mathbf{I}_2$.

It is possible to show that the network is uniformly ultimately bounded to a ball $\mathcal{A}_r^c$ if the agents are strictly semipassive. In turn, semipassivity of any of the agents can be shown [115] by selecting $V = \frac{1}{2}(x_1^2 + x_2^2)$ as a storage function. Indeed,

$$\begin{aligned}
\dot{V} &= x_1\dot{x}_1 + x_2\dot{x}_2 = x_1 x_2 - \epsilon_1 x_1^2 + x_1 u_1 + \mu x_2^2(1 - x_1^2 - \epsilon_2 x_2^2) - x_1 x_2 + x_2 u_2 \\
&= -\epsilon_1 x_1^2 + \mu x_2^2(1 - x_1^2 - \epsilon_2 x_2^2) + \mathbf{x}^\mathsf{T}\mathbf{u} = \mathbf{y}^\mathsf{T}\mathbf{u} - h(\mathbf{x}),
\end{aligned} \tag{C.5}$$

where clearly $\mathbf{y} = \mathbf{x}$ is the output of the oscillator and $h(\mathbf{x}) \triangleq \epsilon_1 x_1^2 + \mu x_2^2(x_1^2 + \epsilon_2 x_2^2 - 1)$. Since all $\mathbf{f}_i$ are continuous, their Jacobian matrices are bounded in $\mathcal{A}_r^c$, therefore the three agents are QUAD($\mathbf{I}, \mathbf{Q}_i$), $i = 1, \ldots, n$, therein (see Proposition A.4). For simplicity we shall not determine the matrices $\mathbf{Q}_i$.

Theorem C.2 can be used to assert that some critical values c^* and c_d^* exist that guarantee asymptotic synchronization. In Figure C.1a, where $c = 0.1$ and the discontinuous coupling is absent, we show that the network does not achieve synchronization. When the discontinuous action is turned on with strength $c_d = 2$, as portrayed in Figure C.1b, convergence is attained. Note that even if c is large, as in Figure C.1c with $c = 10$, the diffusive coupling alone is not able to bring the synchronization error to zero.
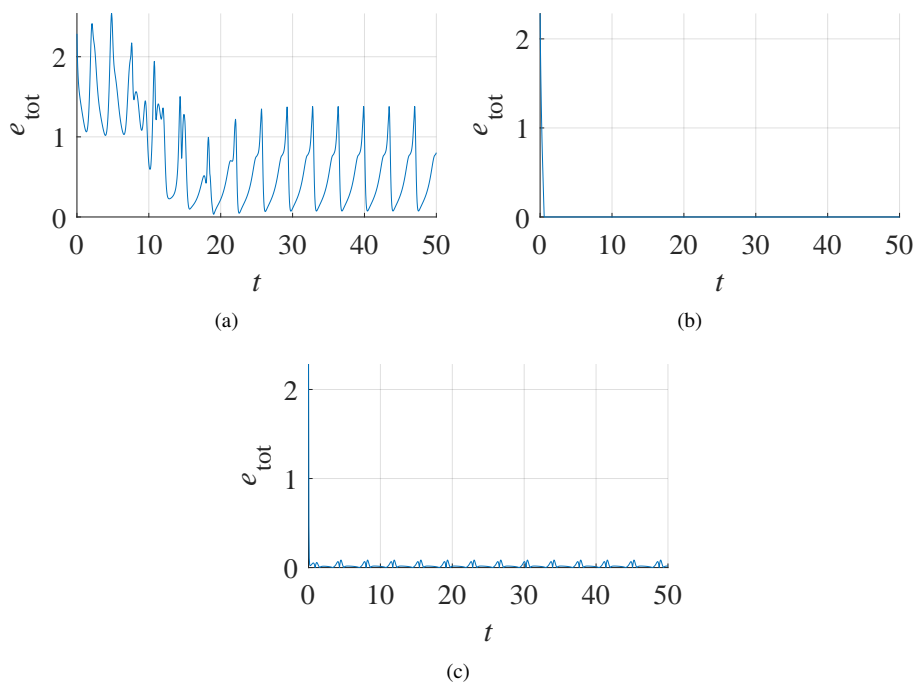
Figure C.1: Total synchronization error in a network of three modified van der Pol oscillators. In (a), $c = 0.1$, $c_d = 0$; in (b), $c = 0.1$, $c_d = 2$; in (c), $c = 10$, $c_d = 0$; The initial conditions are $\bar{\mathbf{x}}(t = 0) = [1.5 \ 1.5 \ 1.75 \ 1.75 \ 2 \ 2]^\mathsf{T}$.

Bibliography

[1] Ricardo Alzate, Petri Piiroinen, and Mario di Bernardo. From complete to incomplete chattering: a novel route to chaos in impacting cam-follower systems. *International Journal of Bifurcation and Chaos*, 22(5):1250102, 2012.

[2] Zahra Aminzare and Eduardo D. Sontag. Contraction methods for nonlinear systems: a brief introduction and some open problems. In *Proc. of IEEE Conference on Decision and Control*, pages 3835–3847, 2014.

[3] David Angeli. A Lyapunov approach to incremental stability properties. *IEEE Transactions on Automatic Control*, 47(3):410–421, 2002.

[4] Fabiola Angulo, Enric Fossas, and Gerard Olivar. Transition from periodicity to chaos in a PWM-controlled buck converter with ZAD strategy. *International Journal of Bifurcation and Chaos*, 15(10):3245–3264, 2005.

[5] M. Arcak and P. Kokotovic. Observer-based control of systems with slope-restricted nonlinearities. *IEEE Transactions on Automatic Control*, 46(7):1146–1150, 2001.

[6] Alex Arenas, Albert Díaz-Guilera, Jurgen Kurths, Yamir Moreno, and Changsong Zhou. Synchronization in complex networks. *Physics Reports*, 469(3):93–153, 2008.

[7] Sanjeev Arora, Elad Hazan, and Satyen Kale. $o(\sqrt{\log n})$ approximation to sparsest cut in $\tilde{O}(n^2)$ time. *SIAM Journal on Computing*, 39(5):1748–1771, 2010.

[8] Sanjeev Arora, Satish Rao, and Umesh Vazirani. Geometry, flows, and graph-partitioning algorithms. *Communications of the ACM*, 51(10):96–105, 2008.

[9] Carolyn M. Berger, Xiaopeng Zhao, David G. Schaeffer, Hana M. Dobrovolny, Wanda Krassowska, and Daniel J. Gauthier. Period-doubling bifurcation to alternans in paced cardiac tissue: crossover from smooth to border-collision characteristics. *Physical Review Letters*, 99(5):058101, 2007.

[10] Andre Bergner, Mattia Frasca, Gregorio Sciuto, Arturo Buscarino, Eulalie Joelle Ngamga, Luigi Fortuna, and Jürgen Kurths. Remote synchronization in star networks. *Physical Review E*, 85(2):026208, 2012.

[11] Ignatius Jozef Maria Besselink. *Shimmy of aircraft main landing gears*. PhD thesis, Delft University of Technology, 2000.

[12] Aldo Boglietti, Andrea Cavagnino, Alberto Tenconi, and Silvio Vaschetto. The safety critical electric machines and drives in the more electric aircraft: a survey. In *IECON, Industrial Electronics Conference*, pages 2587–2594. IEEE, 2009.

[13] Marcello Bonfé. Discussion on: "state feedback fuzzy adaptive control for active shimmy damping". *European Journal of Control*, 17(4):394–396, 2011.

[14] Silvere Bonnabel, Alessandro Astolfi, and Rodolphe Sepulchre. Contraction and observer design on cones. In *Proc. of IEEE Conference on Decidion and Control*, pages 7147–7151, 2011.

[15] Bernard Brogliato and W. P. M. H. Heemels. Observer design for Lur'e systems with multivalued mappings: a passivity approach. *IEEE Transactions on Automatic Control*, 54(8):1996–2001, 2009.

[16] Winfried Bruns and Joseph Gubeladze. *Polytopes, rings, and K-theory*. Springer, 2009.

[17] Francesco Bullo. *Lectures on Network Systems*. Kindle Direct Publishing, 1.3 edition, 2019. With contributions by J. Cortes, F. Dorfler, and S. Martinez.

[18] Aydın Buluç, Henning Meyerhenke, Ilya Safro, Peter Sanders, and Christian Schulz. Recent advances in graph partitioning. In *Algorithm Engineering*, pages 117–158. Springer, 2016.

[19] Daniel A. Burbano-L, Marco Coraggio, Mario di Bernardo, Franco Garofalo, and Michele Pugliese. Adaptive and quasi-sliding control of shimmy in landing gears. In *2018th European Control Conference (ECC)*, pages 563–568. IEEE, 2018.

[20] Daniel Alberto Burbano Lombana and Mario di Bernardo. Multiplex PI control for consensus in networks of heterogeneous linear agents. *Automatica*, 67:310–320, 2016.

[21] Shane Burns and Petri Piiroinen. Numerical location of Painlevé paradox-associated jam and lift-off in a double-pendulum mechanism. *Journal of Computational and Nonlinear Dynamics*, 12, 2017.

[22] Robert Burridge and Leon Knopoff. Model and theoretical seismicity. *Bulletin of the Seismological Society of America*, 57(3):341–371, 1967.

[23] Richard Casey, Hidde De Jong, and Jean-Luc Gouzé. Piecewise-linear models of genetic regulatory networks: equilibria and their stability. *Journal of Mathematical Biology*, 52(1):27–56, 2006.

[24] Alan R. Champneys and P. L. Várkonyi. The Painlevé paradox in contact mechanics. *IMA Journal of Applied Mathematics*, 81(3):538–588, 2016.

[25] Heping Chen, George Zhang, William Eakins, and Thomas Fuhlbrigge. Assembly on moving production line based on sensor fusion. *Assembly Automation*, 29(3):257–262, 2009.

[26] Soon-Jo Chung and Jean-Jacques E. Slotine. Cooperative robot control and concurrent synchronization of Lagrangian systems. *IEEE transactions on Robotics*, 25(3):686–700, 2009.

[27] Nadav Cohen and Izhak Bucher. On the dynamics and optimization of a non-smooth bistable oscillator — application to energy harvesting. *Journal of Sound and Vibration*, 333(19):4653–4667, sep 2014.

[28] Steve Collins, Andy Ruina, Russ Tedrake, and Martijn Wisse. Efficient bipedal robots based on passive-dynamic walkers. *Science*, 307(5712):1082–1085, 2005.

[29] Alessandro Colombo, Mario di Bernardo, S. John Hogan, and Mike R. Jeffrey. Bifurcations of piecewise smooth flows: perspectives, methodologies and open problems. *Physica D: Nonlinear Phenomena*, 241(22):1845–1860, 2012.

[30] Stephen Coombes, Yi Ming Lai, Mustafa Şayli, and Ruediger Thul. Networks of piecewise linear neural mass models. *European Journal of Applied Mathematics*, pages 1–22, 2018.

[31] Stephen Coombes and Rüdiger Thul. Synchrony in networks of coupled non-smooth dynamical systems: Extending the master stability function. *European Journal of Applied Mathematics*, 27(06):904–922, dec 2016.

[32] Marco Coraggio, Pietro DeLellis, and Mario di Bernardo. Achieving convergence and synchronization in networks of piecewise-smooth systems via distributed discontinuous coupling. *Submitted to Automatica (arxiv:1905.05863)*, 2019.

[33] Marco Coraggio, Pietro DeLellis, S. John Hogan, and Mario di Bernardo. Synchronization of networks of piecewise-smooth systems. *IEEE Control Systems Letters*, 2:653–658, 2018.

[34] Jorge Cortés. Discontinuous dynamical systems. *IEEE Control Systems Magazine*, 28(3):36–73, 2008.

[35] Gábor Csernák and Gábor Stépán. On the periodic response of a harmonically excited dry friction oscillator. *Journal of Sound and Vibration*, 295(3):649–658, 2006.

[36] Germund Dahlquist. *Stability and error bounds in the numerical integration of ordinary differential equations*. PhD thesis, 1958.

[37] Marius F. Danca. Synchronization of switch dynamical systems. *International Journal of Bifurcation and Chaos*, 12(8):1813–1826, 2002.

[38] Pietro DeLellis, Mario di Bernardo, and Davide Liuzza. Convergence and synchronization in heterogeneous networks of smooth and piecewise smooth systems. *Automatica*, 56:1–11, 2015.

[39] Pietro DeLellis, Mario di Bernardo, and Giovanni Russo. On QUAD, Lipschitz, and contracting vector fields for consensus and synchronization of networks. *IEEE Transactions on Circuits and Systems I: Regular Papers*, 58(3):576–583, 2011.

[40] Pietro DeLellis, Franco Garofalo, and Francesco Lo Iudice. The partial pinning control strategy for large complex networks. *Automatica*, 89:111–116, 2018.

[41] Fabio Dercole, Alessandra Gragnani, and Sergio Rinaldi. Bifurcation analysis of piecewise smooth ecological models. *Theoretical Population Biology*, 72(2):197–213, 2007.

[42] Charles Desoer and Hiromasa Haneda. The measure of a matrix as a tool to analyze computer algorithms for circuit analysis. *IEEE Transactions on Circuit Theory*, 19(5):480–486, 1972.

[43] Mario di Bernardo, Chris Budd, Alan Richard Champneys, and Piotr Kowalczyk. *Piecewise-smooth dynamical systems: theory and applications*. Springer, 2008.

[44] Mario di Bernardo and Davide Fiore. Incremental stability of bimodal Filippov systems in $\mathbb{R}^n$. In *Proc. of IEEE Conference on Decision and Control*, pages 4679–4684, 2014.

[45] Mario di Bernardo and Davide Fiore. Switching control for incremental stabilization of nonlinear systems via contraction theory. In *Proc. of European Control Conference*, pages 2054–2059, 2016.

[46] Mario di Bernardo and Davide Liuzza. Incremental stability of planar Filippov systems. In *Proc. of European Control Conference*, pages 3706–3711, 2013.

[47] Mario di Bernardo, Davide Liuzza, and Giovanni Russo. Contraction analysis for a class of nondifferentiable systems with applications to stability and network synchronization. *SIAM Journal on Control and Optimization*, 52(5):3203–3227, 2014.

[48] Thach N. Dinh, Silvere Bonnabel, and Rodolphe Sepulchre. Contraction-based design of positive observers. In *Proc. of IEEE Conference on Decision and Control*, pages 6574–6579, 2013.

[49] Tzanko Donchev and Elza Farkhi. Stability and Euler approximation of one-sided Lipschitz differential inclusions. *SIAM journal on control and optimization*, 36(2):780–796, 1998.

[50] Apostolos Doris, Aleksandar Lj Juloski, Nenad Mihajlovic, W. P. M. H. Heemels, Nathan van de Wouw, and Henk Nijmeijer. Observer designs for experimental non-smooth and discontinuous systems. *IEEE Transactions on Control Systems Technology*, 16(6):1323–1332, 2008.

[51] Hesham A. Elkaranshawy, Khaled T. Mohamed, Ahmed S. Ashour, and Hassan M. Alkomy. Solving Painlevé paradox: (P–R) sliding robot case. *Nonlinear Dynamics*, 88(3):1691–1705, 2017.

[52] Andreas K. Engel, Pascal Fries, Peter König, Michael Brecht, and Wolf Singer. Temporal binding, binocular rivalry, and consciousness. *Consciousness and Cognition*, 8(2):128–151, 1999.

[53] Paul Erdős and Alfréd Rényi. On the evolution of random graphs. *Publications of the Mathematical Institute of the Hungarian Academy of Sciences*, 5(1):17–60, 1960.

[54] Paul Erdös and Alfréd Rényi. On random graphs, I. *Publ. Math.-Debrecen*, 6:290–297, 1959.

[55] Miroslav Fiedler. Absolute algebraic connectivity of trees. *Linear and Multilinear Algebra*, 26(1-2):85–106, 1990.

[56] Alekseĭ Fedorovich Filippov. *Differential equations with discontinuous righthand sides*. Kluwer, 1988.

[57] Davide Fiore, Marco Coraggio, and Mario di Bernardo. Observer design for piecewise smooth and switched systems via contraction theory. *IFAC-PapersOnLine*, 50(1):2959–2964, 2017.

[58] Davide Fiore, S. John Hogan, and Mario di Bernardo. Contraction analysis of switched systems via regularization. *Automatica*, 73:279–288, 2016.

[59] Gianfranco Fiore, Giansimone Perrino, Mario di Bernardo, and Diego di Bernardo. In vivo real-time control of gene expression: a comparative analysis of feedback control strategies in yeast. *ACS synthetic biology*, 5(2):154–162, 2015.

[60] Fulvio Forni and Rodolphe Sepulchre. A differential Lyapunov framework for contraction analysis. *IEEE Transactions on Automatic Control*, 59(3):614–628, 2014.

[61] Fulvio Forni, Andrew R. Teel, and Luca Zaccarian. Follow the bouncing ball: global results on tracking and state estimation with impacts. *IEEE Transactions on Automatic Control*, 58(6):1470–1485, 2013.

[62] Enric Fossas, Robert Grino, and Domingo Biel. Quasi-sliding control based on pulse width modulation, zero averaged dynamics and the L2 norm. *Advances in Variable Structure System, Analysis, Integration and Applications*, pages 335–344, 2000.

[63] Xinchu Fu, Michael Small, David M. Walker, and Haifeng Zhang. Epidemic dynamics on scale-free networks with piecewise linear infectivity and immunization. *Physical Review E*, 77(3):036113, 2008.

[64] Ugo Galvanetto. Bifurcations and chaos in a four-dimensional mechanical system with dry friction. *Journal of Sound and Vibration*, 204(4):690–695, 1997.

[65] Ugo Galvanetto. Non-linear dynamics of multiple friction oscillators. *Computer methods in applied mechanics and engineering*, 178(3-4):291–306, 1999.

[66] Ugo Galvanetto. Sliding bifurcations in the dynamics of mechanical systems with dry friction—remarks for engineers and applied scientists. *Journal of Sound and Vibration*, 276(1-2):121–139, 2004.

[67] F. Génot and B. Brogliato. New results on Painlevé paradoxes. *European Journal of Mechanics - A/Solids*, 18(4):653–677, 1999.

[68] Chris Godsil and Gordon F. Royle. *Algebraic graph theory*. Springer, 2013.

[69] Bill Goodwine and Gábor Stépán. Controlling unstable rolling phenomena. *Journal of Vibration and Control*, 6(1):137–158, 2000.

[70] A. Hajiloo and W. F. Xie. The stochastic robust model predictive control of shimmy vibration in aircraft landing gears. *Asian Journal of Control*, 17(2):476–485, 2015.

[71] W. P. M. H. Heemels, M. K. Camlibel, J. M. Schumacher, and B. Brogliato. Observer-based control of linear complementarity systems. *International Journal of Robust and Nonlinear Control*, 21(10):1193–1218, 2011.

[72] C. Howcroft, M. Lowenberg, S. Neild, B. Krauskopf, and E. Coetzee. Shimmy of an aircraft main landing gear with geometric coupling and mechanical freeplay. *Journal of Computational and Nonlinear Dynamics*, 10(5):051011–1–051011–14, 2015.

[73] R. A. Ibrahim. Friction-induced vibration, chatter, squeal, and chaos—part I: Mechanics of contact and friction. *Applied Mechanics Reviews*, 47(7):209–226, 1994.

[74] David A. N. Jacobson, Peter W. Lehn, and Robert W. Menzies. Stability domain calculations of period-1 ferroresonance in a nonlinear resonant circuit. *IEEE Transactions on Power Delivery*, 17(3):865–871, 2002.

[75] Jerome Jouffroy. Some ancestors of contraction analysis. In *Proc. of IEEE Conference on Decision and Control and European Control Conference*, pages 5450–5455, 2005.

[76] Aleksandar Lj. Juloski, W. P. M. H. Heemels, and S. Weiland. Observer design for a class of piecewise linear systems. *International Journal of Robust and Nonlinear Control*, 17(15):1387–1404, 2007.

[77] George Karypis and Vipin Kumar. A fast and high quality multilevel scheme for partitioning irregular graphs. *SIAM Journal on Scientific Computing*, 20(1):359–392, 1998.

[78] Olga Kiuila and Thomas F. Rutherford. Piecewise smooth approximation of bottom–up abatement cost curves. *Energy Economics*, 40:734–742, 2013.

[79] Ulrich Krause. A discrete nonlinear and non-autonomous model of consensus formation. *Communications in difference equations*, 2000:227–236, 2000.

[80] Yi Ming Lai, Rüdiger Thul, and Stephen Coombes. Analysis of networks where discontinuities and nonsmooth dynamics collide: understanding synchrony. *The European Physical Journal Special Topics*, 227(10-11):1251–1265, 2018.

[81] G. Lancioni, S. Lenci, and Ugo Galvanetto. Non-linear dynamics of a mechanical system with a frictional unilateral constraint. *International Journal of Non-Linear Mechanics*, 44(6):658–674, 2009.

[82] Julie Leifeld, Kaitlin Hill, and Andrew Roberts. Persistence of saddle behavior in the nonsmooth limit of smooth dynamical systems. *arXiv preprint arXiv:1504.04671*, 2015.

[83] R. Leine, Bernard Brogliato, and H. Nijmeijer. Periodic motion and bifurcations induced by the Painlevé paradox. *European Journal of Mechanics - A/Solids*, 21(5):869–896, 2002.

[84] Remco I. Leine, Bernard Brogliato, and Henk Nijmeijer. Periodic motion and bifurcations induced by the Painlevé paradox. *European Journal of Mechanics-A/Solids*, 2002.

[85] Remco I. Leine and Henk Nijmeijer. *Dynamics and bifurcations of non-smooth mechanical systems*. Springer, 2013.

[86] Jianxun Liang, Ou Ma, and Caishan Liu. Relative contact dynamics and its application on manipulator's contact stability problem. In *ASME 2012 International Design Engineering Technical Conferences and Computers and Information in Engineering Conference*, pages 1473–1480. American Society of Mechanical Engineers, 2012.

[87] Daniel Liberzon. *Switching in systems and control*. Springer, 2012.

[88] David J. N. Limebeer and Robin S. Sharp. Bicycles, motorcycles, and models. *IEEE Control Systems Magazine*, 26(5):34–61, 2006.

[89] J. Liscouët, J. C. Maré, and M. Budinger. An integrated methodology for the preliminary design of highly reliable electromechanical actuators: search for architecture solutions. *Aerospace Science and Technology*, 22(1):9–18, 2012.

[90] Bo Liu, Wenlian Lu, and Tianping Chen. New conditions on synchronization of networks of linearly coupled dynamical systems with non-Lipschitz right-hand sides. *Neural Networks*, 25:5–13, 2012.

[91] Mingjian Liu, Alfredo Marciello, Mario di Bernardo, and Ljiljana Trajkovic. Discontinuity-induced bifurcations in TCP/RED communication algorithms. In *IEEE International Symposium on Circuits and Systems, ISCAS 2006*, 2006.

[92] Xiaoyang Liu, Jinde Cao, and Wenwu Yu. Filippov systems and quasi-synchronization control for switched networks. *Chaos: An Interdisciplinary Journal of Nonlinear Science*, 22(3):033110, 2012.

[93] Xiaoyang Liu, Tianping Chen, Jinde Cao, and Wenlian Lu. Dissipativity and quasi-synchronization for neural networks with discontinuous activations and parameter mismatches. *Neural Networks*, 24(10):1013–1021, 2011.

[94] Winfried Lohmiller and Jean-Jacques E. Slotine. On contraction analysis for non-linear systems. *Automatica*, 34(6):683–696, 1998.

[95] Winfried Lohmiller and Jean-Jacques E. Slotine. Nonlinear process control using contraction theory. *AIChE Journal*, 46(3):588–596, 2000.

[96] Emanuele Lorenzano and Michele Dragoni. Complex interplay between stress perturbations and viscoelastic relaxation in a two-asperity fault model. *Nonlinear Processes in Geophysics*, 25(1):251–265, 2018.

[97] P. Lötstedt. Mechanical systems of rigid bodies subject to unilateral constraints. *SIAM Journal on Applied Mathematics*, 42(2):281–296, 1982.

[98] Jinhu Lü, Xinghuo Yu, Guanrong Chen, and Wenwu Yu. *Complex Systems and Networks: Dynamics, Control and Applications*. Springer, 2016.

[99] Wenlian Lu and Mario di Bernardo. Contraction and incremental stability of switched Carathéodory systems using multiple norms. *Automatica*, 70:1–8, 2016.

[100] I. R. Manchester and Jean-Jacques E. Slotine. Output-feedback control of nonlinear systems using control contraction metrics and convex optimization. In *Proc. of Australian Control Conference*, pages 215–220, 2014.

[101] Ian R. Manchester and Jean-Jacques E. Slotine. Control contraction metrics and universal stabilizability. *IFAC Proceedings Volumes*, 47(3):8223–8228, 2014.

[102] Davide Marchese, Marco Coraggio, S. John Hogan, and Mario di Bernardo. Control of Painlevé paradox in a robotic system. In *2019 18th European Control Conference (ECC)*, pages 2620–2625. IEEE, 2019.

[103] Michał Marszal, Ashesh Saha, Krzysztof Jankowski, and Andrzej Stefański. Synchronization in arrays of coupled self-induced friction oscillators. *The European Physical Journal Special Topics*, 225(13-14):2669–2678, nov 2016.

[104] Michał Marszal and Andrzej Stefański. Parameter study of global and cluster synchronization in arrays of dry friction oscillators. *Physics Letters A*, 381(15):1286–1301, apr 2017.

[105] David W. Matula and Farhad Shahrokhi. Sparsest cuts and bottlenecks in graphs. *Discrete Applied Mathematics*, 27(1-2):113–123, 1990.

[106] Yizhar Or. Painlevé's paradox and dynamic jamming in simple models of passive dynamic walking. *Regular and Chaotic Dynamics*, 19(1):64–80, 2014.

[107] Calogero Orlando and Andrea Alaimo. A robust active control system for shimmy damping in the presence of free play and uncertainties. *Mechanical Systems and Signal Processing*, 84:551–569, 2017.

[108] Paul Painlevé. Sur les loi du frottement de glissement. *Comptes Rendus Hebdomadaires des Séances de l'Académie des Science*, 141:401–405, 1905.

[109] Elena Panteley and Antonio Loría. Synchronization and dynamic consensus of heterogeneous networked systems. *IEEE Transactions on Automatic Control*, 62(8):3758–3773, 2017.

[110] Alexey Pavlov, Alexander Pogromsky, Nathan van de Wouw, and Henk Nijmeijer. On convergence properties of piecewise affine systems. *International Journal of Control*, 80(8):1233–1247, 2007.

[111] Alexey Pavlov, Alexander Pogromsky, Nathan van de Wouw, Henk Nijmeijer, and K. Rooda. Convergent dynamics, a tribute to Boris Pavlovich Demidovich. *Systems & Control Letters*, 52(3):257–261, 2004.

[112] Louis M. Pecora and Thomas L. Carroll. Synchronization in chaotic systems. *Physical Review Letters*, 64(8):821, 1990.

[113] Louis M. Pecora and Thomas L. Carroll. Master stability functions for synchronized coupled systems. *Physical Review Letters*, 80(10):2109, 1998.

[114] Petri T. Piiroinen and Yuri A. Kuznetsov. An event-driven method to simulate Filippov systems with accurate computing of sliding motions. *ACM Transactions on Mathematical Software*, 34(3):13:1–13:24, 2008.

[115] Alexander Pogromsky, Torkel Glad, and Henk Nijmeijer. On diffusion driven oscillations in coupled dynamical systems. *International Journal of Bifurcation and Chaos*, 9(04):629–644, 1999.

[116] Athanasios Polynikis, Mario di Bernardo, and S. John Hogan. Synchronizability of coupled PWL maps. *Chaos, Solitons & Fractals*, 41(3):1353–1367, 2009.

[117] Maurizio Porfiri and Mario di Bernardo. Criteria for global pinning-controllability of complex networks. *Automatica*, 44(12):3100–3106, 2008.

[118] Gaétan Pouly, Thai-Hoang Huynh, Jean-Philippe Lauffenburger, and Michel Basset. State feedback fuzzy adaptive control for active shimmy damping. *European Journal of Control*, 17(4):370–393, 2011.

[119] Rajesh Rajamani. Observers for Lipschitz nonlinear systems. *IEEE Transactions on Automatic Control*, 43(3):397–401, 1998.

[120] Shenhai Ran. *Tyre models for shimmy analysis: from linear to nonlinear*. PhD thesis, Technische Universiteit Eindhoven, 2016.

[121] Priya Ranjan, Eyad H. Abed, and Richard J. La. Nonlinear instabilities in TCP-RED. *IEEE/ACM Transactions on Networking*, 12(6):1079–1092, 2004.

[122] Giovanni Russo, Mario di Bernardo, and Eduardo D. Sontag. Global entrainment of transcriptional systems to periodic inputs. *PLoS Computational Biology*, 6(4):e1000739, 2010.

[123] Mustafa Şayli, Yi Ming Lai, Rüdiger Thul, and Stephen Coombes. Synchrony in networks of franklin bells. *IMA Journal of Applied Mathematics*, 84(5):1001–1021, 2019.

[124] Luca Scardovi and Rodolphe Sepulchre. Synchronization in networks of identical linear systems. *Automatica*, 45(11):2557–2562, nov 2009.

[125] Bruno Siciliano, Lorenzo Sciavicco, Luigi Villani, and Giuseppe Oriolo. *Robotics: Modelling, Planning and Control*. Springer Publishing Company, 1st edition, 2008.

[126] Houshang H Sohrab. *Basic real analysis*, volume 231. Springer, 2003.

[127] Gerhard Somieski. Shimmy analysis of a simple aircraft nose landing gear model using different mathematical methods. *Aerospace Science and Technology*, 1(8):545–555, 1997.

[128] J. Sotomayor and M. A. Teixeira. Regularization of discontinuous vector fields. In *Proc. of International Conference on Differential Equations, Lisbon*, pages 207–223, 1996.

[129] David Paul Stoten and Hacine Benchoubane. Robustness of a minimal controller synthesis algorithm. *International Journal of Control*, 51(4):851–861, 1990.

[130] Steven H. Strogatz. Exploring complex networks. *Nature*, 410(6825):268–276, 2001.

[131] Housheng Su and Wang Xiaofan. *Pinning control of complex networked systems: Synchronization, consensus and flocking of networked systems via pinning*. Springer, 2013.

[132] Dénes Takács and Gábor Stépán. Comparison of time delayed tyre models. *IFAC Proceedings Volumes (9th IFAC Workshop on Time Delay Systems)*, 43(2):114–119, 2010.

[133] H. Tourajizadeh and S. Zare. Robust and optimal control of shimmy vibration in aircraft nose landing gear. *Aerospace Science and Technology*, 50:1–14, 2016.

[134] Matthew C. Tresch and Ole Kiehn. Synchronization of motor neurons during loco-motion in the neonatal rat: predictors and mechanisms. *Journal of Neuroscience*, 22(22):9997–10008, 2002.

[135] Chi Kong Tse. *Complex behavior of switching power converters*. CRC Press, 2003.

[136] Iakov Zalmanovich Tsypkin. *Relay control systems*. Cambridge University Press, 1984.

[137] Vadim I. Utkin. *Sliding modes in control and optimization*. Springer, 1992.

[138] Nathan van de Wouw and Alexey Pavlov. Tracking and synchronisation for a class of PWA systems. *Automatica*, 44(11):2909–2915, 2008.

[139] Mathukumalli Vidyasagar. *Nonlinear systems analysis*. SIAM, 2nd edition, 2002.

[140] Xiao Fan Wang and Guanrong Chen. Complex networks: small-world, scale-free and beyond. *IEEE Circuits and Systems Magazine*, 3(1):6–20, 2003.

[141] Duncan J. Watts and Steven H. Strogatz. Collective dynamics of 'small-world' networks. *Nature*, 393(6684):440–442, 1998.

[142] Jieqiang Wei, Xinlei Yi, Henrik Sandberg, and Karl Henrik Johansson. Nonlinear consensus protocols with applications to quantized systems. In *IFAC-PapersOnLine*, volume 50, pages 15440–15445, 2017.

[143] Gérard Weisbuch, Guillaume Deffuant, Frédéric Amblard, and Jean-Pierre Nadal. Meet, discuss, and segregate! *Complexity*, 7(3):55–63, 2002.

[144] Chao Yang and Lihong Huang. Finite-time synchronization of coupled time-delayed neural networks with discontinuous activations. *Neurocomputing*, 249:64–71, 2017.

[145] Xinsong Yang and Jinde Cao. Exponential synchronization of delayed neural networks with discontinuous activations. *IEEE Transactions on Circuits and Systems I: Regular Papers*, 60(9):2431–2439, 2013.

[146] Xinsong Yang, Zhiyou Wu, and Jinde Cao. Finite-time synchronization of complex networks with nonidentical discontinuous nodes. *Nonlinear Dynamics*, 73(4):2313–2327, 2013.

[147] Or Yizhar and Elon Rimon. Investigation of Painlevé's paradox and dynamic jamming during mechanism sliding motion. *Nonlinear Dynamics*, 67(2):1647–1668, 2012.

[148] Ziad Zahreddine. Matrix measure and application to stability of matrices and interval dynamical systems. *International Journal of Mathematics and Mathematical Sciences*, 2003(2):75–85, 2003.

[149] Ali Zemouche and Mohamed Boutayeb. On LMI conditions to design observers for Lipschitz nonlinear systems. *Automatica*, 49(2):585–591, 2013.

[150] Ali Zemouche and Mohamed Boutayeb. On lmi conditions to design observers for Lipschitz nonlinear systems. *Automatica*, 49(2):585–591, 2013.

[151] Wei Zhang, Housheng Su, Hongwei Wang, and Zhengzhi Han. Full-order and reduced-order observers for one-sided Lipschitz nonlinear systems using Riccati equations. *Communications in Nonlinear Science and Numerical Simulation*, 17(12):4968–4977, 2012.

[152] Jun Zhao and David J. Hill. Passivity and stability of switched systems: a multiple storage function method. *Systems & Control Letters*, 57(2):158–164, 2008.

[153] Zhen Zhao, Caishan Liu, Wei Ma, and Bin Chen. Experimental investigation of the Painlevé paradox in a robotic system. *Journal of Applied Mechanics*, 75(4):041006, 2008.

[154] Viktor Filippovich Zhuravlev, Dmitrii Mihailovich Klimov, and Petr Kolestra-tovich Plotnikov. A new shimmy model. *Proceedings of the Steklov Institute of Mathematics*, 281(1):27–36, 2013.